Stony Brook University

Synthesis and Structural Characterization of Main-Group Metal Coordination Networks

A Dissertation Presented

By

Debasis Banerjee

To

The Graduate School

in Partial Fulfillment of the Requirements

for the Degree of

Doctor of Philosophy

in

Chemistry

Stony Brook University

May 2012

Stony Brook University

The Graduate School

Debasis Banerjee

We, the dissertation committee for the above candidate for the

Doctor of Philosophy degree

Hereby recommend acceptance of this dissertation.

(John B. Parise, Ph. D., Advisor)

Distinguished Professor, Department of Chemistry & Geosciences, Stony Brook University

(Andreas Mayr, Ph. D, Chairperson)

Professor, Department of Chemistry, Stony Brook University

(Peter Khalifah, Ph. D., Third Member)

Professor, Department of Chemistry, Stony Brook University

(Christopher L. Cahill, Ph. D., Outside Member)

Professor, Department of Chemistry, George Washington University

This Dissertation is accepted by the Graduate School.

Charles Taber
Interim Dean of the Graduate School

Abstract of the Dissertation

Synthesis and Structural Characterization of Main-Group Metal Coordination Networks

By

Debasis Banerjee

Doctor of Philosophy in Chemistry

Stony Brook University

2012

Coordination Networks (CNs) or Metal-Organic Frameworks (MOFs) are crystalline materials, composed of infinite arrays of metal ions, connected by functionalized organic linkers, forming chains, layers or 3-D networks. The exploratory synthesis and characterization of novel MOFs or CNs is of current interest, because of their potential applications across a broad range of technologies, including gas storage, separation, catalysis, and luminescence.

A wide range of metal centers and functionalized organic linkers are used to form CNs or MOFs under different synthetic conditions, giving rise to unprecedented structural diversity. First row transition metal centers are often chosen because of their well-known coordination behavior with carboxylate groups under hydro- and solvothermal conditions. On the other hand, CNs/MOFs based on s-block metal centers are relatively less studied. The ionic nature of M-O bonding in s-block CNs provides little room for prediction and control over coordination geometry. Despite difficulties in predicting the coordination geometry, the incorporation of s - block metal centers into CNs offers several advantages. The relatively high charge density and ionic nature of these metal ions leads to strong bonding interaction with carboxylate oxygen atoms. Porous networks prepared from early members of the s - block metal series could further provide gravimetric advantages for gas storage applications due to their low-atomic weight.

Our aim was to understand the chemistry of s-block CNs using synthetic variables like temperature and solvents. To accomplish this, lithium based CNs were synthesized using a diverse range of aliphatic and aromatic polycarboxylates. Our study showed that the mutual orientation of the functional groups plays a pivotal role in determining the topologies of the

networks. Electrochemical studies reveal the potential of these networks as Li-ion battery electrode. Solid state ^{6}Li NMR was further applied to understand the desolvation-resolvation behavior of a Li-CN, which indicate rearrangement of the metal coordination sphere after solvent removal.

The s-block metals CNs were further explored using magnesium and calcium as metal centers. These metal centers are inexpensive, non-toxic and essential in many biological processes. The structural chemistry of Mg^{2+} is similar to that of Zn^{2+}, which forms many porous MOFs. A series of magnesium-3,5-pyridinedicarboxylates networks were synthesized, using common organic solvents in both pure and mixture forms as the synthetic variable. Networks of different dimensionalities were formed due to the variable coordination ability of solvent molecules with the metal center. Physical properties, such as thermal stability and gas-adsorption behavior of the synthesized networks, vary with the incorporation of different solvent molecules. Water molecules coordinate with the magnesium metal centers preferably over other polar solvents. A similar synthetic strategy was adopted to synthesize calcium based CNs using different solvent mixtures. The larger size of Ca^{2+} compared to Mg^{2+} leads to higher coordination numbers for the former, while the structural topologies of the networks formed are equally dependent on the chemical nature and geometry of the ligands and the synthetic variables.

Table of Contents

List of Abbreviations

BDC	terephthalate
BPDC	biphenyldicarboxylate
BTC	benzenetricarboxylate
BET	Brunauer-Emmett-Teller
BTB	benzenetribenzoate
CN	Coordination Network
DMA	Dimethylamine
DMF	N,N-dimethylformamide
dhtp	2,5-dihydroxoterephthalate
INA	isonicotinate
MOF	Metal-Organic Framework
NMR	Nuclear Magnetic Resonance
NDC	naphthalenedicarboxylate
PDC	pyridinedicarboxylate
PC	pyridinecarboxylate
SDB	sulfonyldibenzoate
TGA	Thermogravimetric Analysis
XRD	X-ray diffraction
ICP	Inductive Coupled Plasma

List of Structures

List of Figures

List of Tables

Acknowledgements

This thesis is a result of five years of work that would not have been possible without the support of various individual and organizations. Firstly, I would like to acknowledge my advisor, Prof. John B. Parise for his constant guidance and helpful suggestions. I am influenced by his vision of science and hopefully I will carry that out in my future scientific career. I would like to thank Prof. Clare P. Grey, Prof. Andreas Mayr and Prof. Peter Khalifah for all their help and support as members of my dissertation committee. I also would like to thank external member of the committee Prof. Christopher L. Cahill for his time.

My sincere thanks go to Dr. Sun Jin Kim (Korea Advanced Institute of Technology) for teaching me the basics of exploratory synthesis. I learned a great deal of synthetic strategies working with Sun-Jin over a summer. Much work would not have been possible without the active contribution of many collaborators and beamline scientists: Yu-Sheng Chen (Advanced Photon Source, Argonne National Laboratory), Simon Teat (Advanced Light Source, Lawrence Berkeley National Laboratory), Paul M. Forster (University of Nevada-Las Vegas), Haohan Wu (Rutgers University) and Jing Li (Rutgers University).

Many thanks to the past and present Parise group members: Lauren Borkowski, Richard Harrington, Wenqian Xu, Anna Plonka, William Woerner, Lena Lazarova, Xianyin Chen and Paul Calderone, particularly Paul Calderone and Anna Plonka, with whom, I collaborated extensively over the past years.

I am thankful for the financial support provided by the National Science Foundation (DMR-0800415) and Department of Energy (DE-FG02-09ER46650). I am also thankful to American Crystallographic Association and Advanced Photon Source for providing me travel fellowships.

Finally I would like to thank my friends and my parents, for their constant support and encouragement throughout the year. Without their moral input, this work could not have been accomplished.

List of Publications

1. Lithium Based Metal−Organic Framework with Exceptional Stability. **Banerjee, D**.; Kim, S. J.; Parise, J. B., *Cryst. Growth Des.* **2009,** 9 (5), 2500-2503.

2. Synthesis and Structural Characterization of Lithium-Based Metal-Organic Frameworks. **Banerjee, D**.; Borkowski, L. A.; Kim, S. J.; Parise, J. B., *Cryst. Growth Des.* **2009,** 9 (11), 4922-4926.

3. Solvothermal Synthesis and Structural Characterization of Ultralight Metal Coordination Networks. **Banerjee, D**.; Kim, S. J.; Borkowski, L. A.; Xu, W. Q.; Parise, J. B., *Cryst. Growth Des.* **2010,** 10 (2), 709-715.

4. Synthesis and Structural Characterization of a 3-D Lithium Based Metal-Organic Framework Showing Dynamic Structural Behavior. **Banerjee, D**.; Kim, S. J.; Li, W.; Wu, H. H.; Li, J.; Borkowski, L. A.; Philips, B. L.; Parise, J. B., *Cryst. Growth Des.* **2010,** 10 (6), 2801-2805.

5.Poly[bis(N,N-dimethylformamide-kappaO)(mu(4)-naphthalene-1,disulfonato)magnesium(II)]. Borkowski, L. A.; **Banerjee, D**.; Parise, J. B., *Acta Crystallogr E* **2010,** 66, M691-U924.

6. An Anionic Gallium Based Metal Organic Framework and its Sorption and Ion Exchange Properties**. Banerjee D**., Kim, S. J.; Wu H.; Xu W. Q.; Borkowski L. A.; Li, J.; Parise, J.B;. *Inorg. Chem.* **2011**, 50 (1), 208-212

7. A magnesium-lithium heterometallic coordination network. Calderone, P. J.; ***Banerjee, D**., Borkowski L. A.; Parise, J. B.; *Inorg.Chem. Commun*, **2011**, 14 (5), 741-744

8. Synthesis and Structural Characterization of Magnesium Based Coordination Networks in Different Solvents. **Banerjee D**., Finkelstein, J., Smirnov, A., Forster, P. M., Borkowski, L. A., Teat, S. J., Parise, J. B., *Cryst. Growth. Des.* **2011**, 11 (6), 2572-2579

9. Recent Advances in s- Block Metal Carboxylate Networks. ***Banerjee, D**., Parise, J. B., *Cryst. Growth Des.* **2011,** 11(11), 4704 - 4720.

10. Synthesis, Characterization, and Luminescence Properties of Magnesium Coordination networks Using Thiophene based linker. Calderone, P. J.; ***Banerjee, D**., Santulli, A, C., Wong, S. S., Parise, J. B., *Inorg. Chim. Acta*. **2011**, 378, 109–114

11.Poly[(μ_4-adamantane-1,3-dicarboxylato-$^5O^1$:$O^{1'}$:O^3,$O^{3'}$:$O^{3'}$)(μ_3-adamantane-1,3-dicarboxylato-$^5O^1$,$O^{1'}$:O^3,$O^{3'}$:$O^{3'}$)dimagnesium]: a layered coordination polymer. Plonka, A. M., ***Banerjee, D**., Parise, J. B., *Acta Crystallogr C*. **2011,** 67, m335-m337.

12. Synthesis, Characterization, and Luminescence Properties of Magnesium Isophthalate Coordination Networks Using Isophthalate Linker. Calderone, P. J.; ***Banerjee, D**., Nizami, Q., Parise, J. B., *Polyhedron*. **2012**, 37, 42-47.

13. A Calcium Coordination Framework Having Permanent Porosity and High CO_2/N_2 Selectivity. *__Banerjee, D__., Zhang, Z., Plonka, A. M., Li, J., Parise, J. B., *Cryst. Growth Des*. **2012,** 12(5), 2162 - 2165.

14. Effect of Ligand Structural Isomerism in Formation of Calcium Coordination Networks. Plonka, A. M., *__Banerjee D__., Parise J. B., *Cryst. Growth Des*. **2012,** 12(5), 2460 - 2467.

Chapter 1

Recent Advances in s-block Metal Carboxylates

The content of this chapter is published in

Recent Advances in s- Block Metal Carboxylate Networks. Banerjee, D., Parise, J. B., *Cryst. Growth Des.* **2011**, 11(11), 4704 - 4720.

Coordination Networks (CNs) or metal-organic frameworks (MOFs)[1,2] are crystalline materials composed of infinite arrays of metal ions, connected by functionalized organic linkers, forming chains, layers, or 3-D networks. The exploratory synthesis and characterization of novel MOFs or CNs is of current interest, because of their potential applications across a broad range of technologies, including gas storage,[3] separation,[4] catalysis,[5] and luminescence.[6] A wide variety of metal centers and functionalized organic linkers are used to form CNs or MOFs under different synthetic conditions, giving rise to unprecedented structural diversity tailored for specific applications.[7-9] The most commonly used organic linkers are aromatic polycarboxylates, due to their structural rigidity and strong bonding interactions between metal centers and carboxylate oxygen atoms.[10] First row transition metal centers are often chosen because of their well-known coordination behaviors with carboxylate groups under hydro/solvothermal conditions. On the other hand, CNs/MOFs based on s-block metal centers are relatively less studied. The bonding interaction of s-block metal centers with carboxylate oxygen atoms is mainly ionic in nature due to large differences in electronegativity, which provides little room for prediction and control over coordination geometry. The mutual orientation of the functional groups plays a bigger role in determining the coordination nature of the metal centers within the network. The lack of predictive coordination behavior and the dominance of steric considerations are challenges in carrying out systematic studies of CNs based on s-block metal ions. Despite

difficulties in predicting coordination geometry and carrying out systematic investigations, the incorporation of s-block metal centers into CNs offers several advantages. The relatively high charge density and ionic nature of these metal ions leads to strong bonding interactions with carboxylate oxygen atoms. Porous networks prepared from early members of the s-block metal series could further provide gravimetric advantages for gas-storage applications due to their low-atomic weight. The alkali (Na, K) and alkaline earth metals (Mg, Ca) are among the 10 most abundant elements on the planet; they are inexpensive, nontoxic, and essential in many biological processes.[11] The atomic properties and metal-oxygen bond distances of s-block metals are listed in tables 1.1-1.3 at the end of the chapter.

The research directed towards the synthesis of s-block metal- based CNs has produced a number of novel materials with unique physical properties. Robson and co-workers[12] reported the synthesis of a Li(INA) 0.5DMF network under solvothermal conditions (Fig. 1.1). The structure is comprised of Li(INA) chains, which are linked by Li-N bonding interactions to form layers, linked together to construct the 3-D network. Solvent DMF resides in the rectangular shaped channels of average dimension 4 Å × 5.5 Å. N-Methylpyrrolidine and morpholine were used as synthesis solvents to obtain networks of similar topology. Activated network demonstrates H_2, N_2, CO_2, and CH_4 adsorption, indicating robustness and permanent porosity of the network after solvent removal. The unusually high heat of adsorption for H_2 (9.9 kJ mol^{-1}) or CO_2 (34 kJ mol^{-1}) was attributed to strong interactions between the pore surface and adsorbed gas molecules.

The first example of a beryllium based network, reported by Matzger and co-workers,[13] was synthesized using a terephthalate linker under solvothermal conditions. The similarities in the PXRD pattern of the as-synthesized material with the zinc based MOF-5 suggest comparable

structural topologies of the two. However, the elemental microanalysis of the as-synthesized Be-MOF was found to be inconsistent with a MOF-5 type stoichiometry. The material further shows a BET surface area of 3500 m^2/g with a H_2 storage capacity of 5.0 wt % at 77 K and 24 bar, comparable to that of MOF-5. A second synthetic approach to form a MOF-5 type beryllium homolog was reported by Mertens and co-workers[14] using a "control SBU approach"(CSA) originally developed by Férey and his group.[15] A presynthesized $[M_4O]^{6+}$ based tetraberyllium oxohexaacetate, commonly known as basic beryllium acetate, was used as the precursor to form the MOF-5(Be). The structural model (space group *Fm3m*, a = 23.73 Å) was developed on the basis of the MOF-5(Zn) network topology with the assumption that the deviation in the cell parameter from MOF-5 [a = 25.76 Å] is due to the formation of a smaller secondary building unit (SBU). The activated material shows a BET surface area of 3289 m^2/g, consistent with a MOF-5(Zn) type framework. The first nonisomorphous crystal structure of a beryllium based MOF was reported by Long and co-workers[16] using BTB as the organic linker (Fig. 1.2). The $Be_{12}(OH)_{12}(BTB)_4$ framework was constructed by a combination of tetrahedrally coordinated Be forming $[Be_{12}(OH)_{12}]^{12+}$ rings, linked by BTB to form a 3,12-network topology. The framework contains large diamond shaped channels with ~27 Å diameters and shows a BET surface area of 4030 m^2/g and a H_2 storage capacity of 9.2 wt % at 77 K and 100 bar.

The first example of a microporous magnesium based network, $Mg_3(2,6\text{-}NDC)_3(DEF)_4$, was reported by Long and co-workers.[17] It contains octahedrally coordinated Mg_3 trimers, connected by the organic linkers, forming a 3-D neutral network (Fig.1.3). The central magnesium metal of the Mg_3 trimer is octahedrally coordinated with six carboxylate oxygen atoms, whereas the two terminal magnesium centers coordinate with two solvent molecules and four carboxylate-oxygen atoms. The coordinated DEF molecules are present within the 1D -

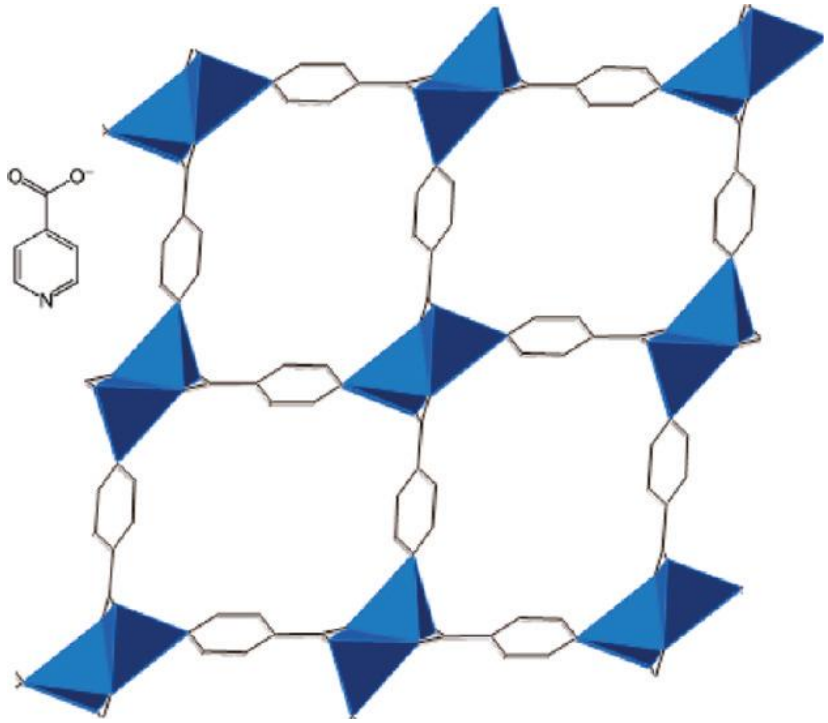

Figure. 1.1. Structure of Li(INA) 0.5DMF. DMF molecules, situated within the channel, were omitted for clarity.

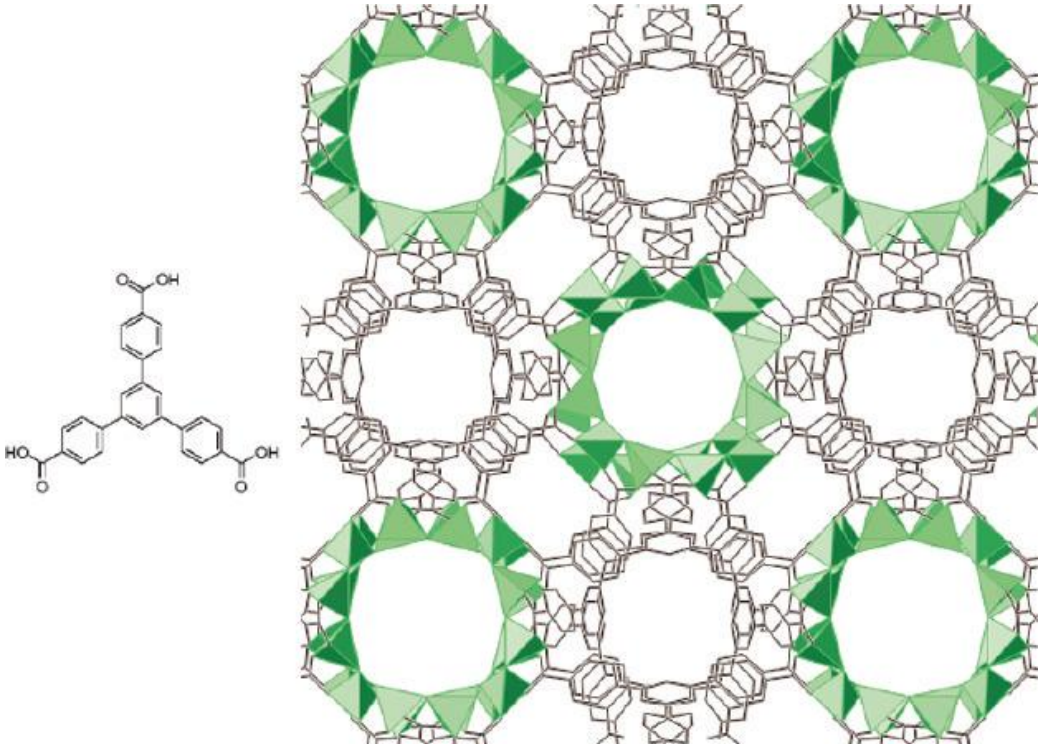

Figure. 1.2. Packing of beryllium based $Be_{12}(OH)_{12}(BTB)_4$ along the crystallographic [001] direction

channel. The desolvated material has a different structure than the parent network, as evident from the PXRD pattern. It reverts to its original form upon exposure to DEF, indicating the dynamic nature of the network. $Mg_3(2,6\text{-}NDC)_3(DEF)_4$ shows preferential adsorption of O_2 and H_2 over N_2 due to the smaller pore opening of the desolvated material. The high enthalpy of adsorption of H_2 was attributed to the presence of open magnesium sites. Further, Dietzel and co-workers, [18] using H_4dhtp as an organic linker, synthesized a nanoporous network $[Mg_2(dhtp)(H_2O)_2]\cdot 8H_2O$ (CPO-27-Mg), which contains 1-D helical chains of edge sharing magnesium octahedra (Fig. 1.4). Both the hydroxyl groups of the linker are deprotonated under the synthesis conditions used. The connectivity of the helical metal octahedral chains with organic linkers forms a honeycomb-like pattern, with 1-D channels of diameter close to 12 Å. The compound displays microporosity upon desolvation, with a Langmuir surface area of 1030 m^2/g. Caskey and co-workers[19] later reported a Langmuir surface area of 1905 m^2/g for the same compound with a CO_2 uptake of 35.2 wt % under 1 atm of pressure. The high CO_2 uptake was postulated to be due to the ionic nature of the Mg-O bonding. Neutron diffraction studies[20,21] on CPO-Mg-27 identified coordinatively unsaturated magnesium centers as the primary binding site for adsorbed CO_2, CH_4, and H_2 molecules. CPO-Mg-27 also shows excellent selectivity for toxic gas separation (NH_3, SO_2) and CO_2 capture under dynamic conditions due to the presence of unsaturated metal sites.[22] The activated network shows record high CO_2 uptake (20.6 wt %) under 0.15atm of CO_2 pressure ideal for commercial flue gas conditions.[23] However, a recent CO_2 adsorption study under dynamic flow through conditions by Kizzie and co-workers[24] reveals that such capture process is strongly dependent on the presence of moisture in the flue gas. The moisture dependent adsorption behavior of activated CPO-27-Mg makes it a poor choice for industrial-scale adsorption operations.

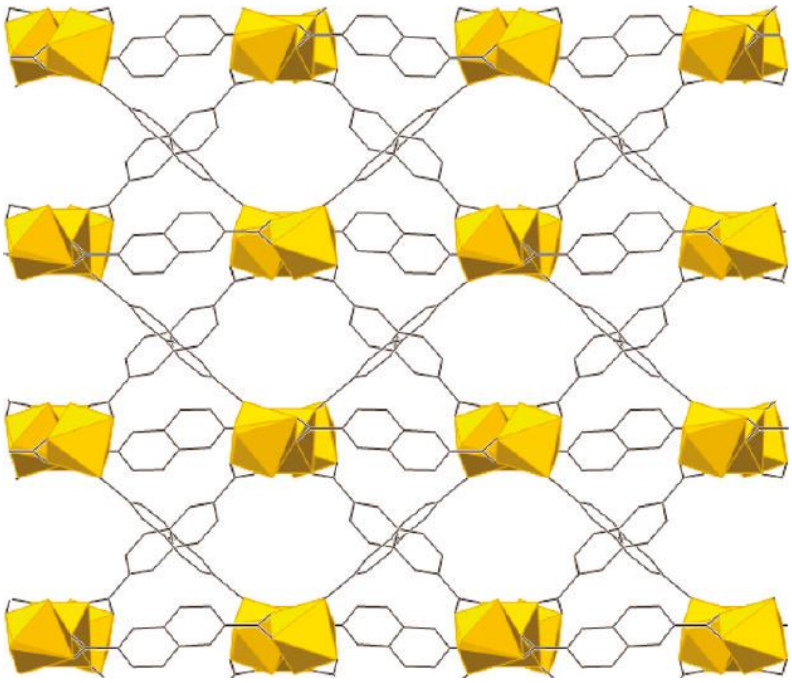

Figure 1.3. Arrangement of channels in $Mg_3(NDC)_3(DEF)_4$ along the crystallographic [100] direction. The DEF molecules were omitted for clarity.

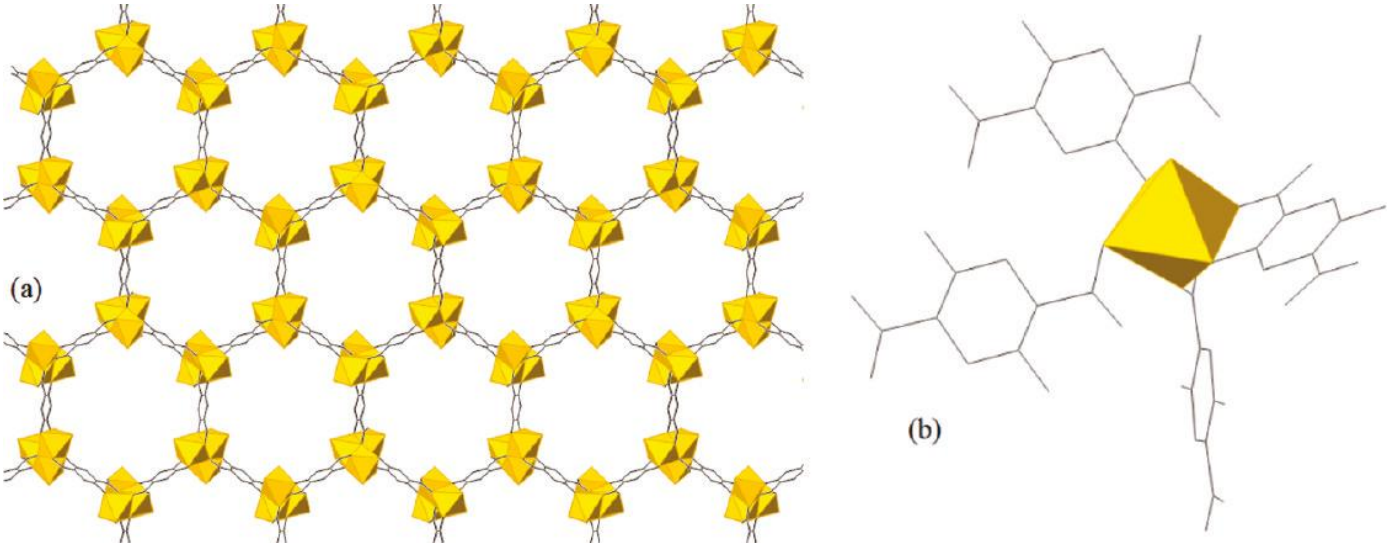

Figure.1.4. (a) Crystal packing of $[Mg_2(dhtp)(H_2O)_2]\ 8H_2O$. (b) The local environment of the magnesium metal center

The topological trend in s-block coordination networks depends on a number of factors, including metal centers, organic linkers, and synthetic parameters, such as temperature, pH, and solvents. For lithium CNs, targeted for their potential advantages for energy storage applications, crystal packing forces determine the denticity (μ) of the donor carboxylate oxygen atoms, which is generally present in bidented (μ2) coordination. Polar solvents, particularly water and DMF used to increase precursor's solubility, tend to coordinate with the metal sites; their removal often leads to network collapse. Lithium CNs exhibit diverse forms of connectivity for the LiO_4 unit, ranging from isolated to layered edge linked tetrahedra. The network topologies of late alkali metal (Na-Cs) CNs are dominated by closed packed MOn [n = 6.10] polyhedra, forming chains or layers, interconnected by organic linkers. Such separation of the hydrophilic inorganic units from the hydrophobic core of the linkers is one of the structural characteristics of late alkali metal based CNs. Alkaline earth metal centers are chemically less reactive than their alkali-metal counterparts, and they are more amenable as metal nodes in the formation of 3-D CNs. Mg-CNs contain ^{VI}Mg metal centers, occurring as units of isolated octahedra, dimers, and more extended chains depending on solvent, synthesis temperature, and the linker geometry. The latter members of the group show irregular coordination geometry, forming either edge/corner sharing chains or layers of $^{VI-XI}MO_n$ polyhedra. Synthesis solvents are often found in the coordination sphere of the metal center, and structural changes are common after solvent removal.

An increase in the cation ionic radius generally leads to an increase in the inorganic M-O-M connectivity within the networks. For example, Clegg and Russo[25] reported a series of alkali metal-isophthalate CNs with diverse types of inorganic connectivity. The formation of edge and face sharing dimeric polyhedra is observed for lithium and sodium networks while the cesium and rubidium networks form face sharing infinite polyhedral chains as the primary structural

motif. A study of alkaline earth (Mg - Ba) thiazoledicarboxylate networks by Cheetham and co-workers[26] showed similar structural trends. The formation of isolated, edge sharing dimers, edge sharing chains, and face sharing layers of polyhedra as inorganic motifs was observed with increasing cation size. Identical trends are observed with alkaline-earth tartarate systems reported by the same group.[27,28] The sheer diversity in shape and functionalities of the organic linkers makes the cataloguing of structural trends based on linkers a difficult task. The s-block metal centers favor coordination with oxygen based functionalities such as carboxylates groups, as predicted by the HSAB principle; however, the mutual angular distribution of the functional groups, and not just the preferred coordination geometry of the metal centers, plays an important role, as reported in lithium[29,30] and magnesium[31] based pyridinedicarboxylate networks.

As for the temperature, the general trend is that the dimensionality of the networks increases with increase in synthetic temperature,[27,32] similar to the case of transitional metal based MOFs or coordination polymers.[33] The influence of pH on the network topologies depends on the nature of linker functional groups and their pK_a values. Maji[32] and Li[34] reported the formation of higher dimensional alkaline earth- pyrazole/imidazoledicarboxylate based networks with increase in pH of the solvent. The role of the pH was further explored by Dietzel and co-workers[18] in the synthesis of Mg-coordination networks (CPO-26/27-Mg) using 2,5-dihydroxyteraphthalic acid as the linker. The differences in the pK_a values of the carboxylic and hydroxyl groups were used to tune the coordinating ability of the functional groups. At lower pH only the carboxylic acid groups are deprotonated, while at higher pH all four functional groups are deprotonated, which leads to the formation of completely different structural topologies and properties. The solvents used to synthesize CNs are mainly polar and protic in nature. The study of the formation of the Mg-3,5-pyridinedicarboxylate system[31] using different solvents shows

that the coordinating ability of the solvents with the metal center determines the network topologies. Water shows the ability to coordinate with the metal center over all other solvents used in the study (DMF, ethanol, methanol), as expected from its polar nature. Further, the amount of water in the solvent mixture determines the number of water molecules in the metal coordination sphere, thus directly influencing the dimensionality of the networks.

The dominance of ionic forces makes directed synthesis of s-block CNs difficult; there is a lack of preformed secondary building units (SBUs), and solvent incorporation to the metal center often leads to low dimensional networks. Synthetic approaches applied to overcome these challenges include (1) formation of s-block heterobimetallic MOFs using 3-D transition,[35-37] Zn,[38] Bi,[39] or lightweight (B,[40,41] Mg[42]) metal centers; (2) the synthesis of porous lithium imidazolate[43] networks using multifunctional coordinating neutral linkers such as 4,4'-bipyridine, which serves the purpose of neutralizing local charge without trading off the dimensionality of the network and (3) incorporation of alkali metal ions, either by ion exchange into anionic frameworks[44,45] or by redox reactions involving aromatic linkers[46-48] in neutral frameworks. One important underexplored parameter in the field of s-block metal carboxylates may prove crucial for their future practical application: the effect of moisture. Kizzie and co-workers[24] recently reported that the presence of moisture drastically reduces the CO_2 capture ability of activated CPO-27-Mg under dynamic flow-through conditions. The less polarizable pre-transition metal cations are prone to hydrolysis because of the formation of predominantly ionic bonds, and thus, s-block metal carboxylates are more sensitive to moisture than the transition metal based MOFs.[49] Approaches to form moisture resistive porous networks include the introduction of hydrophobic groups in the pore surface by (a) postsynthetic modifications,[50] (b) organic linkers with hydrophobic side chains,[51,52] or the use of hydrophobic surfactant coating over the as-

synthesized materials,[53] though such methods have not been applied on s-block CNs systems thus far. Other potential applications for s-block based CNs are expanding into areas such as battery technology, where thermally stable lithium carboxylates are explored as anode materials, and into drug delivery using alkali and alkaline earth metal based bimolecular CNs (BioCNs),[54] such as a recently reported porous K-carbohydrate CN.[55] The exploratory synthesis and characterization of novel biocompatible porous s-block CNs will likely yield further fundamental and applied results.

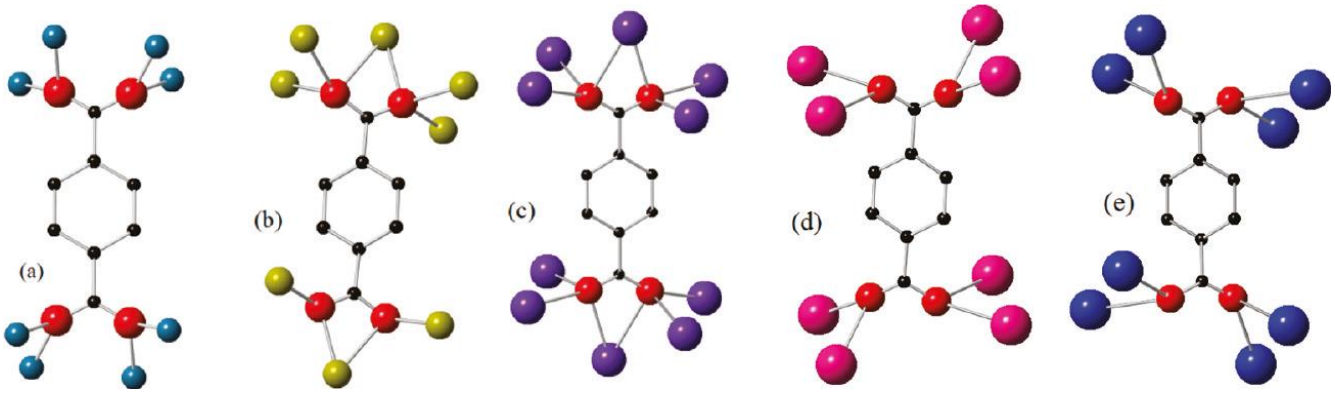

Figure.1.5. Change in bonding pattern from (a) Li (b) Na (c) K (d) Rb (e) Cs with BDC as linker under similar reaction conditions. [56]

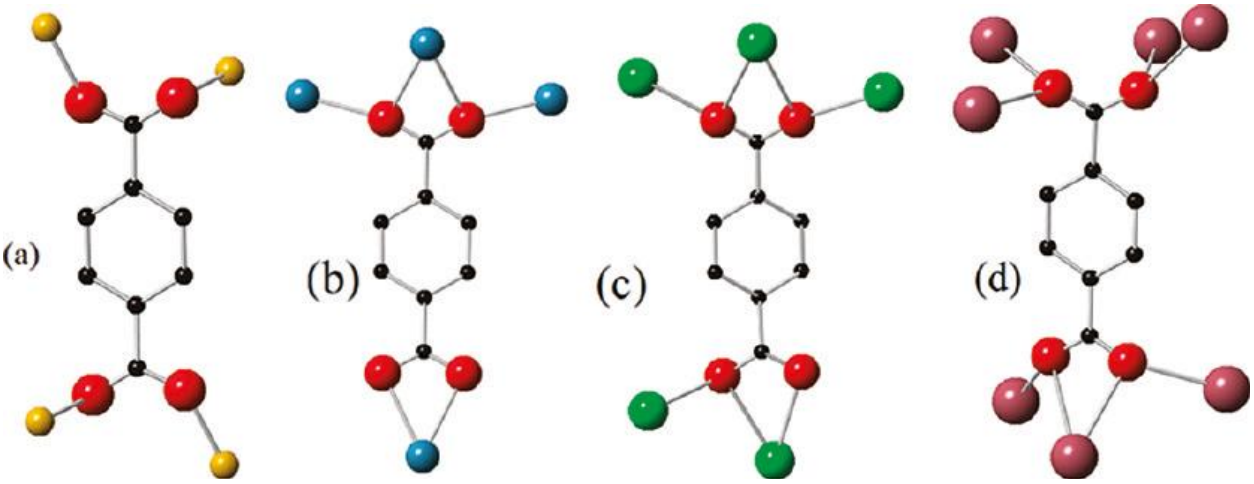

Figure. 1.6. Change in bonding pattern from (a) Mg (b) Ca (c) Sr (d) Ba with BDC as linker under similar reaction conditions. [56]

Table 1.1. Properties of Alkali Metal Cations [11]

Alkali Metal	Atomic Radius (Å)	Ionic Radius (Å)	Ionization Energy	Electronegativity (Pauling)
Li	1.52	0.76	520.1	1.0
Na	1.86	1.02	495.7	0.9
K	2.27	1.38	418.6	0.8
Rb	2.48	1.52	402.9	0.8
Cs	2.65	1.67	375.6	0.7

Table 1.2. Properties of Alkali Earth Metal cations [11]

Alkaline Earth Metal	Atomic Radius (Å)	Ionic Radius/M^{2+}(Å)	Ionization Energy ($KJmol^{-1}$)	Electronegativity (Pauling)
Be	1.13	0.31	1757	1.5
Mg	1.60	0.72	1450	1.2
Ca	1.97	1.00	1145	1.0
Sr	2.15	1.18	1064	1.0
Ba	2.12	1.35	965	0.9

Table 1.3. Average bond distance variation in s-block metal carboxylate bonds [a]

Metal-$O_{carboxylate}$	Distance(Å)	Metal-$O_{carboxylate}$	Distance(Å)
Li-O	1.976 (0.09)	Be-O	1.636(0.005)
Na-O	2.431(0.004)	Mg-O	2.066(0.02)
K-O	2.802(0.006)	Ca-O	2.428(0.006)
Rb-O	2.997(0.016)	Sr-O	2.622(0.006)
Cs-O	3.185(0.015)	Ba-O	2.816(0.005)

[a] Cambridge Structural Database (CSD)

Chapter 2

Experimental Methods

2.1. Synthesis Techniques for Coordination Networks

Metal-Organic Frameworks (MOFs) or Coordination Networks (CNs)[56] are generally synthesized using hydrothermal or solvothermal conditions. As the name implies, water is the sole solvent in hydrothermal synthesis, while organic solvents are used during solvothermal syntheses. Mixture of solvents are also used, particularly when the reactants have different solublities.[57] Often, the metal salts are soluble in water while the organic linkers are soluble in organic solvents. The uses of water/organic solvent mixture thus can facilitate the solubility of both the constituents. Solvents in such biphasic mixtures are sometimes not miscible. It is postulated that such situation is advantageous for single crystal growth at the contact surface.[57] The use of different fluoride based mineralizer (HF, NaF, NH_4F) alongside the reactants also increase the solubility of the otherwise insoluble reactants in particular solvents.[56,58] For s-block metal based CNs, the higher hydration energy of the metal centers make hydrothermal synthesis an unlikely choice.[56] The coordination sites of the metal centers are mostly occupied by the water molecules, leading to the formation of low dimensional networks. The solvothermal synthesis is normally carried out using Teflon-lined stainless steel Parr Autoclaves. The autoclaves can be used for synthesis upto 250°C and ~ 150 bar. The use of the autoclaves as 'pressure vessel' is necessary, as the temperature to synthesize a particular phase is often over the boiling point of the synthesis solvent. In a number of cases, where crystallization is facilitated by mild temperature (< 100°C), capped glass vials are used. A relatively new synthesis technique involves the use of ionic liquids (ILs) as the synthesis solvents. Synthesis of microporous solids

using ionic liquids is termed as 'ionothermal synthesis'.[59] Ionothermal synthesis offer many distinct advantages over traditional solvothermal synthesis, such as negligible vapor pressures, good thermal stability, high ionic conductivity, broad electrochemical potential windows, and high synthetic flexibility.[60,61] In particular, the negligible vapor pressures of ionic liquids are important for minimizing the exposure to toxic volatile vapors in industrial scale production. Further, their low melting points (as low as -80°C) and high thermal stability (stable upto 300°C) provide a wide range for synthesis of microporous compounds.[60-63]

Temperature and solvents are often popular synthetic variations used to form networks with different topologies and properties for a given set of metal salt and organic linkers. As for temperature, the general trend is that with an increase in temperature, the dimensionality of the network increases.[64] The trend with the variation of solvents is generally much more complex and depends on factors like pH and molar ratio among others. In case of s-block metal based CNs, the presence of water as one of the co-solvents always favor the formation of hydrated phases.[31]

In the current work, appropriate metal salts and organic linkers were mixed in molar ratio with either pure or mixture of solvents. The solution was stirred for 2-4 hours to achieve homogeneity. The solution was then heated in a Teflon lined Parr autoclave for 3-5 days at a temperature range of 100°-180°C. Polar protic (water, methanol, ethanol) or polar aprotic (DMF, DEF) solvents were used to synthesize the networks. The as-synthesized materials were filtered and washed with ethanol and DMF.

2.2. Powder X-ray diffraction

A crystalline sample contains a large number of microcrystalline particles in random orientation. The diffraction condition is met when the orientation satisfy the Bragg' law, $\lambda = 2d\sin\theta$. Powder diffraction data is collected as a diffractrogram where the intensity of diffraction (I) is plotted against the scattering angle 2θ.

In this work, powder X-ray diffraction was carried out for as-synthesized compounds to confirm phase purity and crystallinity. Data were collected using a Scintag PAD-X or a Rigaku® Ultima-IV diffractometer equipped with Cu Kα (λ = 1.5405 Å) radiation within a range of $5° \leq 2\theta \leq 40°$(counting time : 1s/step; stepsize : 0.02°). The diffractometers use Bragg-Brentano parfocusing geometry where the incident beam and take-off geometry are fixed at θ/θ configuration. X-rays were generated at 40 kV and 25 mA for the Scintag and 40KV and 44mA for the Rigaku Ultima diffractometer. The diffraction patterns so obtained were compared with the simulated diffraction pattern based on single-crystal data for phase purity confirmation.

2.3. X-ray Single Crystal diffraction

The growth of good quality single crystals is essential for structure determination of synthesized MOFs or CNs with complex structural topologies. Powder X-ray diffraction is generally not suitable to provide data of good resolution and accuracy for detailed structural information. Single crystal X-ray diffraction is thus a valuable tool.

The laboratory single crystal data were collected using a Bruker four circle P4 diffractometer equipped with a smart 1K CCD area detector. X-ray was generated at 50 KV and 30 mA using a normal focus X-ray tube with Mo as the target metal (λ = 0.71073 Å). The raw intensity data were collected using software SMART.[65] The data were further integrated and corrected for Lorentz and polarization effects using SAINT.[66] Adsorption corrections were

applied with SADABS.[67] The single crystal data for compound [6.1] were collected using newly acquired four-circle kappa Oxford Gemini diffractometer equipped with an Atlas detector (λ = 0.71073 Å) with 1° scans. The raw intensity data were collected, integrated and corrected for absorption effects using CrysAlis PRO software.[68] The structure solution and least-squares refinements were carried out using direct methods.[67] The heaviest atoms were located first, followed by determination of other atom positions (C, N, H) from the Fourier difference map and were refined anisotropically. Hydrogen atoms were placed in the appropriate positions using geometrical constraint.

It is sometimes difficult to obtain the desired materials in the form of good quality single crystals under applied synthetic conditions. If the as-synthesized materials are microcrystalline in nature (10-100μm in dimension), it is not possible to characterize the crystal structure in details using the in-house single crystal diffractometer. In these particular cases, X-ray diffraction setups at different synchrotron sources were used for structure determination purposes. The increased brightness, tunability and low divergence of X-ray beams at a synchrotron source can render the structural studies of microcrystals (~ 5μm) possible. The synchrotron radiation is ten orders of magnitude brighter and has a spectral distribution of energy in the range of 5-40KeV.

The single crystal data of compounds [3.2], [5-1] and [7.1], described in details later, were collected at 15-ID ChemMatCARS beamline, Advanced Photon Source, Argonne National Laboratory. The beamline is equipped with a Bruker D8 diffractometer with a Bruker APEXII detector.[69] Monochromatic X-ray radiation is achieved using a diamond (111) crystal (λ = 0.41328 Å). Data collection was performed at 100K using a N_2 cryostat. The single crystal data for compound [5-2] were collected at 11.3.1 beamline at Advanced Light Source, Lawrence Berkeley National Laboratory using a similar experimental setup but a different X-ray

wavelength (λ =0.7749 Å). The data were integrated using APEXII suite of software.[69] The data were processed using SHELXTL[67] in the same manner as the laboratory diffractometer data.

2.4. Thermogravimetric Analysis

Thermogravimetric analysis (TGA) is an important technique, which gives us valuable information about the thermal stability of the synthesized material, crucial for many advanced applications. The shape of the TGA curve further is immensely informative about the type of interaction of the guest molecules with the parent network. The thermal profile is also used to confirm the purity of the material, and for choosing a suitable activation temperature for porosity measurement purposes. The thermal data of the synthesized materials described herein was collected using a Netzsch 449C Jupiter instrument. The instrument is equipped with a SiC furnace with a temperature range of RT to 1500°C and a microbalance with an accuracy of ± 0.01mg. In a typical experiment, a correction curve with an empty alumina crucible is collected first. Following this step, the as-synthesized sample (5-10 mg) was placed in an alumina crucible and heated between RT and 750°C under N_2 atmosphere, at a rate of 10°C/min. Data for compounds [3.2] and [3.3] were collected in air as well, to compare the thermal stability in different atmospheres. Networks, without the presence of any solvent molecules generally show higher thermal stabilities because of their dense packing. The materials with either coordinated or free solvent molecules show multistep weight-loss. The first weight-losses are due to the evacuation of the solvent molecules. The evacuation temperature depends on multiple factors, including the nature of the solvent and network topologies. The final weight-loss step corresponds to the removal of the organic linker, leading to the destruction of the network. The recovered material was further characterized using powder X-ray diffraction.

2.5. Gas-Adsorption Techniques

Gas-adsorption is a common technique to measure the surface area and pore size of the synthesized materials. Permanently porous networks have a wide range of applicability, and such measurement using different types of gases gives us molecular level insight about the pore surface characteristics of the porous material. Adsorption is defined as the addition of a component (gas-molecule) to a solid/fluid surface.[70] Depending on the type of "addition" interaction, adsorption processes are divided in two categories - chemisorption and physisorption. As the name suggests, in chemisorption the adsorbed gas molecules form chemical bonding with the adsorbate. Physisorption process is dominated by the weak non-bonding interaction between the adsorbed gas molecules and pore surface of the activated framework.[70]

The measurement of surface area is usually carried out using N_2 as the adsorbate gas, applying the Brunauer-Emmett-Teller (BET) theory.[71] The BET theory is an extension of Langmuir theory of monolayer molecular adsorption to multilayer adsorption and is based on the hypothesis that the uppermost molecules of the adsorbed layers are in dynamic equilibrium with gas vapor. The Langmuir equation can be applied to each of the adsorbed layers independently.[72] Based on the adsorption characteristics and pore size, porous materials are divided in three categories - microporous (pore diameter < 2nm, e.g. Metal-Organic Frameworks or Coordination Polymers), mesosporous (pore diameter 2-50 nm, e.g. silica and alumina) and macroporous (pore diameter > 50 nm).

In the current context, several lithium, magnesium, calcium and gallium based porous networks were characterized using N_2 as an adsorbate, using Quantochrome Nova 2200e surface Area Analyzer instrument. Prior to the measurement, the materials were outgassed under vacuum

between 100°C-300°C overnight, in order to remove the guest solvent molecules. The appropriate heating temperatures were judged based on the thermogravimetric profile of the respective compounds. The activated materials were then weighed to confirm complete removal of the solvent molecules. Afterwards the samples were cooled to liquid N_2 temperature and N_2 gas was introduced to the sample tube with a known reference pressure. The pore volume and surface area were calculated from the extent of decrease in pressure due to the expansion of N_2 within the void space.

The H_2 and CO_2 adsorption studies were performed on a volumetric gas sorption analyzer (Autosorb-1-MP, Quantachrome Instruments). Liquid nitrogen and liquid argon were used as coolants to achieve cryogenic temperatures (77 and 87 K). Ultra high purity H_2 and CO_2 (99.999%) were used. The hydrogen adsorption-desorption isotherms were collected in the pressure range from 10^{-4} to 1 atm at 87 and 77 K, respectively. Temperature-dependent adsorption-desorption isotherms of CO_2 and N_2 (273, 288 and 298 K) were collected from 10^{-3} to 1 atm.

Chapter 3

Synthesis and Structural Characterization of Lithium based Coordination Networks using Aromatic Polycarboxylates

The content of this chapter is published in

(a) Lithium Based Metal−Organic Framework with Exceptional Stability. Banerjee, D.; Kim, S. J.; Parise, J. B., Cryst. Growth Des. **2009,** 9 (5), 2500-2503 & *(b)* Synthesis and Structural Characterization of Lithium-Based Metal-Organic Frameworks. Banerjee, D.; Borkowski, L. A.; Kim, S. J.; Parise, J. B., Cryst. Growth Des. **2009,** 9 (11), 4922-4926.

3.1. Abstract

Three lithium based coordination networks, $Li_2(C_{12}H_8O_4)$ [Li_2(2,6-NDC) [3.1]: UL-MOF-1, UL = Ultra-Light; space group $P2_1/c$, a = 10.302(5) Å, b = 5.345(2) Å, c = 8.663(4) Å, β = 98.659(9)°, V= 471.6(4) $Å^3$] $Li_2(C_{14}H_8O_4)$ [Li_2(4,4'-BPDC) **[**3.2**]:** ULMOF-2, space group $P2_1/c$, a=12.758(2) Å, b=5.142(4) Å, c= 8.00(2) Å, β= 97.23°, V= 520.6(14) $Å^3$] and $Li_2(C_{14}H_8O_6S)$ [Li_2(4,4'-SDB) **[**3.3**]**: ULMOF-3, space group $P2_1/n$, a= 5.5480(11) Å, b= 23.450(5) Å, c= 10.320(2) Å, β= 96.47(3)°, V= 1334.1(5) $Å^3$] were synthesized. Compounds [3.1] – [3.3] were synthesized by solvothermal methods and were characterized using single crystal X-ray diffraction. Compounds [3.1] and [3.2] are isostructural, formed by layers of antifluorite related LiO motif connected by organic linker, whereas compound [3.3] is constructed by a combination of tetrameric lithium polyhedral clusters, connected by the sulfonyldibenzoate linker. All the networks are stable over 500°C under N_2 atmosphere, with compound [3.1] exhibiting the highest thermal stability till date of any organic-inorganic hybrid materials.

3.2. Introduction

A wide range of metal-centers form metal-organic frameworks (MOFs) or Coordination Networks (CNs) through linkages with multifunctional ligands.[7,73,74] The variety of possible geometries thus formed inspire researchers to test potential uses of these networks in gas storage,[10,17,73,75-84] ion exchange,[85-87] catalysis[88-91] and separation,[52,92,93] and to expand exploratory synthetic efforts aimed at uncovering further novel materials tailored for specific uses.

The network topology primarily depends on the metal centers, geometry of the functionalized organic linkers and synthetic conditions (e.g. temperature, [33] solvent[94]). Aromatic polycarboxylates linkers [10,95-97] are commonly used as linker molecules due to their structural rigidity and diversity of possible coordination geometries with metal centers. First row transition metals[76,77,79,82,98] are popular choice in constructing such networks, because of their well-known coordination preference with polycarboxylates. On the other hand, exploratory synthesis directed towards constructing networks with lightweight metals (e.g.: Mg [19,32,99,100] and Li [12,58,101,102]) have not been extensively explored.

The aim of producing porous networks incorporating lightweight metals could be beneficial with respect to increasing gravimetric storage capacity of adsorbed gases. The lightest metal in the periodic table, lithium, is of particular interest in building networks due to recent experimental[46,47] and theoretical studies [103-107] showing enhanced H_2 uptake in lithium doped metal organic frameworks. The two-fold increase in storage resulting from Li-doping is attributed to the strong electrostatic interaction between uncoordinated lithium centers and hydrogen gas molecules.

With the aim of producing ultra light metal organic frameworks (ULMOFs) having potential for strong interactions with absorbed gases, we synthesized frameworks based on lithium metal centers. Our initial study suggests a rich vein of lithium based frameworks of diverse topology, depending primarily on the reaction condition and organic linker used. In this chapter, the solvothermal synthesis and structural characterization of three lithium based 3-D network Li_2(2,6-NDC) [3.1], [ULMOF-1], Li_2(4, 4'-BPDC) [3.2], [ULMOF-2]**,** and Li_2(4, 4'-SDB) [3.3]**,** [ULMOF-3] are reported.

3.3. Experimental Section

3.3.1 Synthesis

All compounds were synthesized under solvothermal conditions using Teflon –Lined Parr stainless steel autoclaves. Starting materials include lithium nitrate ($LiNO_3$, 99+%, Acros-Organic), 2,6-naphthalenedicarboxylic acid ($C_{12}H_6O_4$, 2,6-NDC, 95%, Sigma-Aldrich), 4,4'-biphenyl dicarboxylic acid ($C_{14}H_{10}O_4$, 4, 4'-BPDC, 97%, Sigma-Aldrich), 4,4'-sulfonyldibenzoic acid ($C_{14}H_{10}O_6S$, 4,4'-SDB, 98%, Sigma-Aldrich), ammonium fluoride (NH_4F, 98%, Sigma-Aldrich), lithium hydroxide ($LiOH{\cdot}H_2O$, 98%, Alfa-Aesar), N,N dimethylformamide (C_3H_7NO, DMF, 99%, Sigma-Aldrich) and ethanol (C_2H_5OH, 99%, Sigma-Aldrich) and were used without any further purification.

Synthesis of compound [3.1], Li_2(2,6-NDC); ULMOF-1

The synthesis was achieved by using a mixture of 0.005 mole of 2,6-NDC (0.565g), 0.01 mole of $LiNO_3$ (0.345g) and 0.002 mole of NH_4F (0.038g). The mixture was dissolved in 15 grams of DMF. The resultant gel was stirred for 4 hrs, transferred to a Teflon lined vessel and heated at 180° C for 5 days. The product was obtained as yellowish, needle shaped crystals

(yield: 60%, 0.347gram, calculated based on lithium salt) which were recovered by filtration and washed with ethanol.

Synthesis of compound [3.2], Li_2(4,4'-BPDC); ULMOF-2

Compound [3.2] was synthesized using a mixture of 0.002 moles of $LiNO_3$ (0.172 g), 0.002 moles of 4, 4'-BPDC (0.625 g) and 0.0008 moles of NH_4F (0.031 g). This mixture was dissolved in 15 grams of DMF and stirred for 4 hours to achieve homogeneity [molar ratio of metal salt: ligand: solvent =1:1:100]. The resultant solution was heated for 5 days at 180°C. The product, obtained as needle shaped crystals (yield: 55% based on lithium), was recovered by filtration and subsequently washed by ethanol.

Synthesis of compound [3.3], $Li_2(C_{14}H_8O_6S)$; ULMOF-3

A typical synthesis of compound [3.3] includes a mixture of 0.002 moles of $LiNO_3$ (0.172 g), 0.002 moles of 4,4'-SDB (0.67 g) and 0.001 moles of LiOH (0.042 g). The mixture was dissolved in 6.5 grams of DMF and stirred for 4 hours [molar ratio of metal salt: ligand: solvent =1:1:45]. The resultant solution was heated at 180°C for 5 days. The product obtained as colorless needle shaped crystals (yield: 45% based on lithium) and was recovered by filtration and subsequent washing by DMF and ethanol.

3.3.2. X-ray Crystallography

Suitable crystals of compounds [3.1] - [3.3] were selected from the bulk samples and were mounted on a glass fiber using epoxy. Reflections for compound [3.2] were collected at ChemMatCars (Sector 15) at the Advanced Photon Source using a three-circle Bruker D8 diffractometer equipped with an APEXII detector at 100 K using synchrotron X-ray radiation (λ= 0.41328Å) and 0.5° φ scans. The raw intensity data were analyzed using the APEXII suite of software,[69] when it was determined that the crystal contained more than one component. Cell_Now [108] was used to determine the nonmerhedral twin law [1 0 0 0 -1 0 -0.381 0 -1] relating the two major components by a 180.0° rotation about the 'a' axis. The data were then integrated using two components and were corrected for absorption using TWINABS.[108] The major component contained 38% of the sample intensity.

Reflections for compound [3.1] and [3.3] were collected using a Bruker four circle P4 single crystal diffractometer equipped with a SMART 1K CCD detector at room temperature (298K) using Mo Kα radiation (λ = 0.71073 Å) and φ and ω scans. The raw intensity data for compound [3.1] and [3.3] were collected and integrated with software packages, SMART[65] and SAINT.[66] An empirical absorption correction was applied using SADABS.[108] The crystal structures were solved using direct methods (SHELXS).[108] All non hydrogen atoms were refined anisotropically and the hydrogen atoms were added to the aromatic rings using geometrical constraints (HFIX command). The crystallographic details for both structures can be found in Table 3.1.

Table 3.1: Crystallographic data and structural refinement details of compounds [3.1] - [3.3]

	[3.1]	[3.2]	[3.3]
Empirical formula	$C_6H_3O_2Li$	$C_7H_4LiO_2$	$C_{14}H_8O_6SLi_2$
Formula weight	114.02	127.04	318.14
Collection Temperature (K)	298(2)	100(2)	298(2)
Wavelength (Å)	0.71073	0.41328	0.71073
Space Group	$\boldsymbol{P}2_1/c$	$\boldsymbol{P}2_1/c$	$\boldsymbol{P}2_1/n$
a (Å)	10.302(5)	12.753(6)	5.5480(11)
b (Å)	5.345(2)	5.138(2)	23.450(5)
c (Å)	8.662(4)	8.420(4)	10.320(2)
α (º)	90	90	90
β (º)	98.659(9)	97.218(13)	96.47(3)
γ (º)	90	90	90
Volume	471.6(4)	547.4(4)	1334.1(5)
Z	4	4	4
Calculated Density (g/cm3)	1.606	1.541	1.584
Absorption coefficient (mm-1)	0.117	0.027	0.269
F(000)	232	260	648
Crystal size (mm)	0.22 × 0.12 × 0.07	0.08×0.03×0.01	0.16×0.08×0.03
Θ range of data collection	2.00 - 26.73	1.87 – 17.21	1.74.25.02
Index range	$13 \leq h \leq 11$ $-6 \leq k \leq 6$ $-10 \leq l \leq 10$	$-18 \leq h \leq 18$ $0 \leq k \leq 7$ $0 \leq l \leq 12$	$-6 \leq h \leq 6$ $-27 \leq k \leq 27$ $-11 \leq l \leq 12$
Total reflection	2931	1544	7670
Independent reflection	997[R (int) = 0.0725]	1544 [R(int) = 0.0000]	2364 [R(int) = 0.0997]
Goodness of fit	1.062	0.836	0.986
Refinement method	Full matrix least squares on F^2	Full matrix least squares on F^2	Full matrix least squares on F^2
Data/ Restraints/parameter	997 / 0 / 82	1544 / 0 / 93	2364 / 0 / 209
R1(*on* F_o^2, $I>2\sigma(I)$)	R1 = 0.0405	0.0788	0.0607
wR2 (*on* F_o^2, $I>2\sigma(I)$)	0.1060	0.1770	0.1257

3.3.3. Powder X-ray diffraction and thermal analysis

Bulk sample identification and phase purity were determined using powder X-ray diffraction. The data were collected using a Scintag Pad-X diffractometer equipped with Cu Kα (λ = 1.5405 Å) radiation within a range of $5° \leq 2\theta \leq 40°$ (step size: 0.02°, counting time: 1s/step). Comparison of the observed and calculated powder X-ray diffraction patterns for compounds [3.1] - [3.3] confirmed phase purity (Figs. 3.1 -3.3).

Combined TGA-DSC experiments for compounds [3.1] - [3.3] were performed using a Netzsch 449C Jupiter instrument. The samples were heated from room temperature to 750°C under N_2 atmosphere with a heating rate of 10°C/minute (Figs. 3.5 - 3.8).

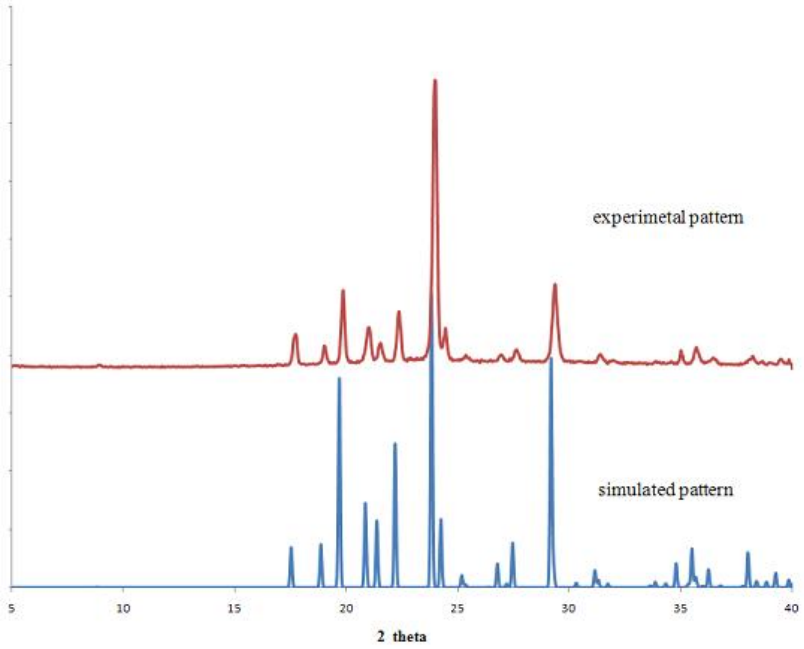

Figure 3.1.simulated vs. experimental PXRD pattern of compound [3.1] (ULMOF-1)

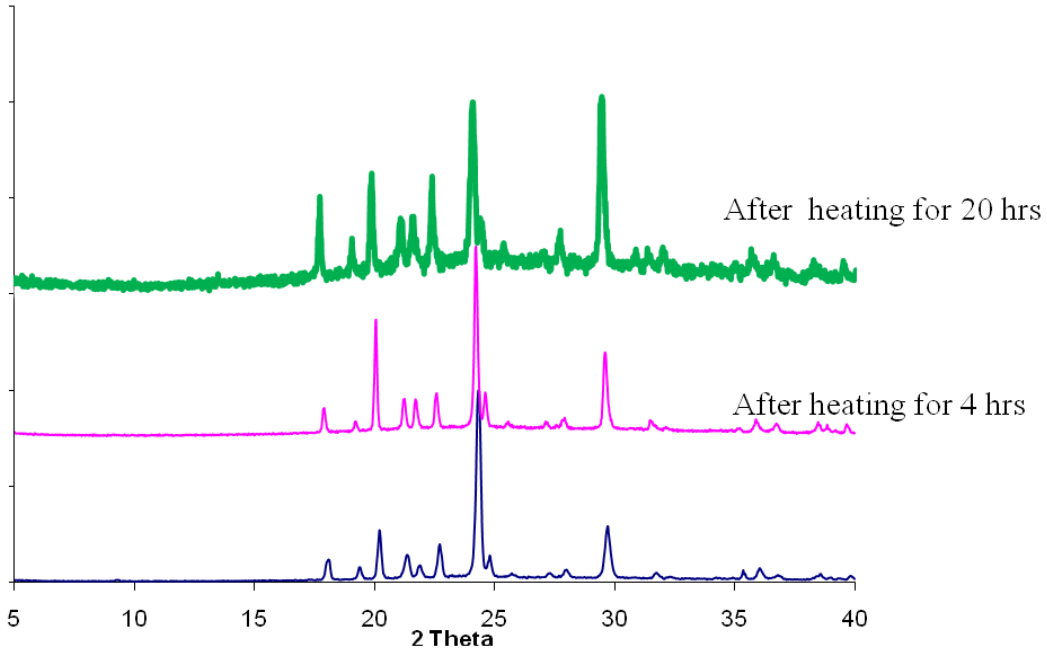

Figure 3.2. Time dependent heating effect on compound [3.1] (ULMOF-1)

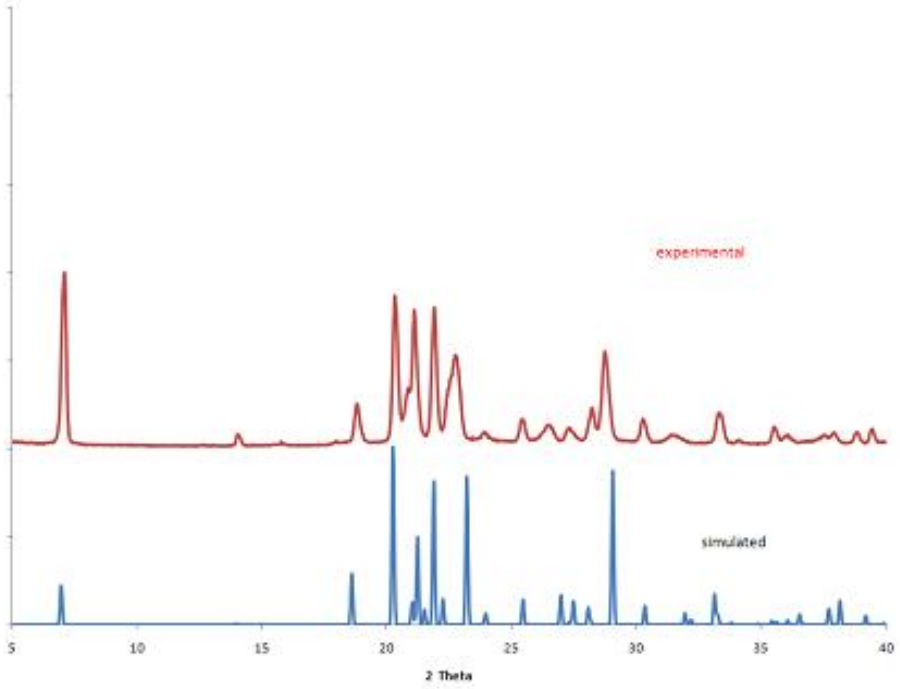

Figure 3.3. Simulated vs. experimental PXRD pattern of compound [3.2] (ULMOF-2)

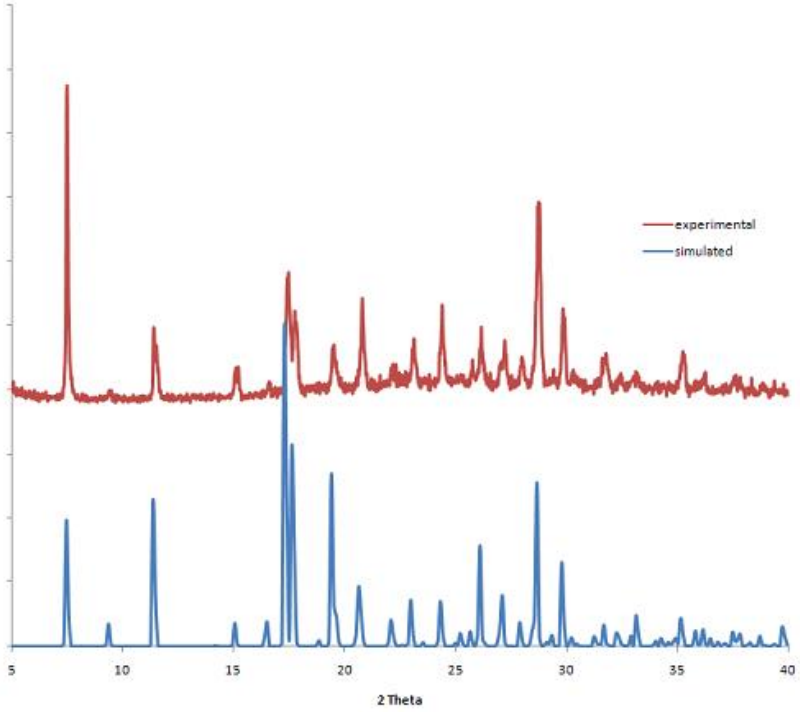

Figure 3.4. Simulated vs. experimental PXRD pattern of compound [3.3] (ULMOF-3)

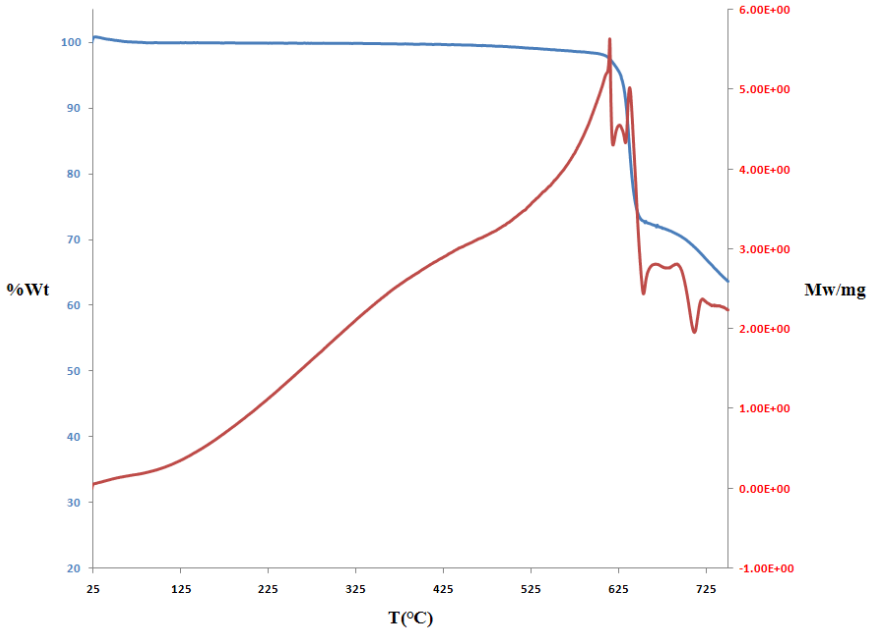

Figure 3.5. Combined TGA-DSC plot of compound [3.1]. The blue line represents TGA plot, while the red line shows the DSC signal associated with it.

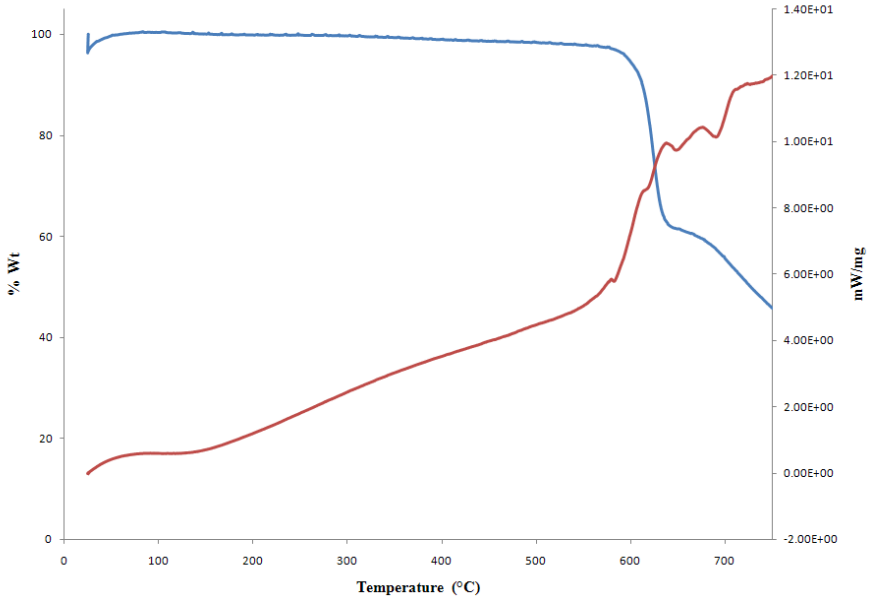

Figure 3.6. TGA-DSC plot of compound [3.2]. The blue line represents TGA plot of ULMOF-2 while the red line shows the DSC signal associated with it.

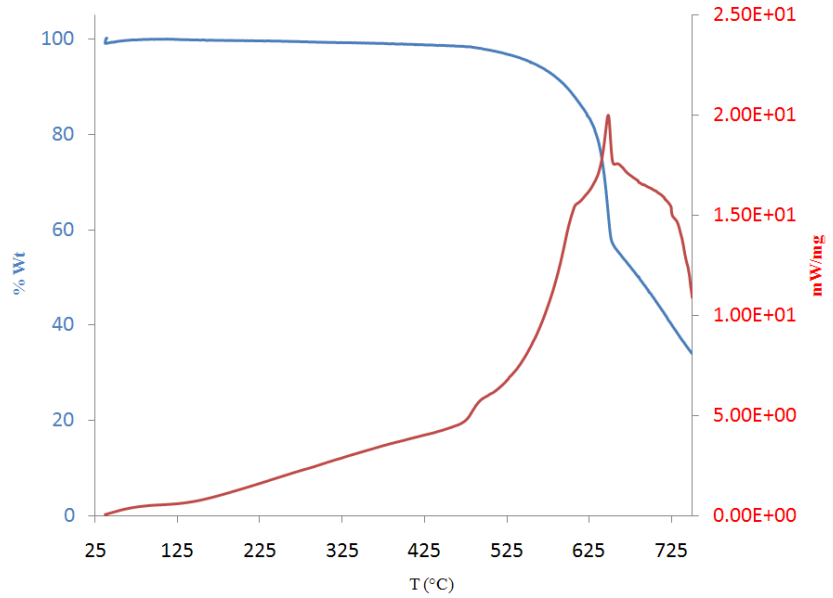

Figure 3.7. TGA-DSC plot of compound [3.2] under ambient condition. The blue line represents TGA plot of ULMOF-2 while the red line shows the DSC signal associated with it.

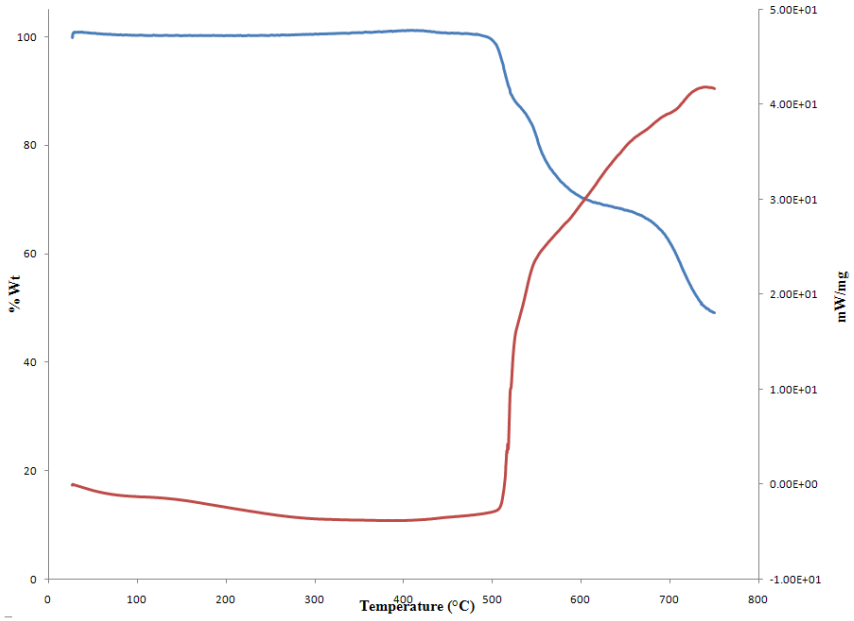

Figure 3.8. Combined TGA-DSC plot of compound [3.3]. The blue line represents TGA plot of ULMOF-3 while the red line shows the DSC signal associated with it.

3.4. Result and Discussion

3.4.1. Structural Description of [3.1], Li_2(2,6-NDC), ULMOF-1

The structure of compound [3.1] consists of a combination of alternating layers of LiO and the aromatic bridging unit (Fig. 3.9). Lithium atom is present in distorted tetrahedral coordination with carboxylate oxygen in the framework (Table 3.2), which has been observed before in recently reported lithium based networks. Each lithium atom is bonded to four carboxylate moieties associated with four different naphthalene rings (Fig. 3.10). The bond length of Li1 with carboxylate oxygen ranges from 1.96(3) Å to 2.02(3) Å, matching well with the expected value of +1 (calculated: 0.97).[109]

The tetrahedrally coordinated lithium forms layered Li-O-Li connectivity. Basic unit of the layer is made with a pair of edge-shared lithium tetrahedra, connected to each other in a corner-shared arrangement. Distances between the lithium atoms in each edge-shared tetrahedron are at average 2.77(6) Ǻ, while the distance between the lithium atoms of the corner-shared tetrahedra is 3.26(4) Ǻ. The oxygen atoms, connecting the lithium metal centers of the two edge shared tetrahedra are joined with the neighboring oxygen atoms of the corner shared tetrahedra through the carboxylate carbon atom. In total, each carboxylate group is coordinated with four lithium centers. The orientation of the carboxylate group in the layer is very well organized, i.e. two-carboxylate groups connect the basic unit of the layer, with one of the carboxylate groups connecting to the lower LiO layer and the other one connecting to the upper layer, forming an antifluorite type structural motif, which is common in LiO based inorganic compounds. The basic difference between the antifluorite motif and the observed LiO layer in [3.1] is in the presence of tetrahedral vacancies within the layer. The antifluorite motif consists of edge-shared tetrahedra, but in the case of [3.1], 1/2 of the lithium tetrahedra are missing. Carboxylate groups

use this free space for connecting adjacent edge shared tetrahedra. Each of these LiO layers is on average 10.3 Å apart from each other with the carboxylate oxygen atoms forming an ABAB type packing. The naphthalene rings are stacked in layers along the [010] direction with an average distance of 3.7Å. The close contacts between the naphthalene rings along [010] direction indicates possible π- π^* interaction between the adjacent rings.

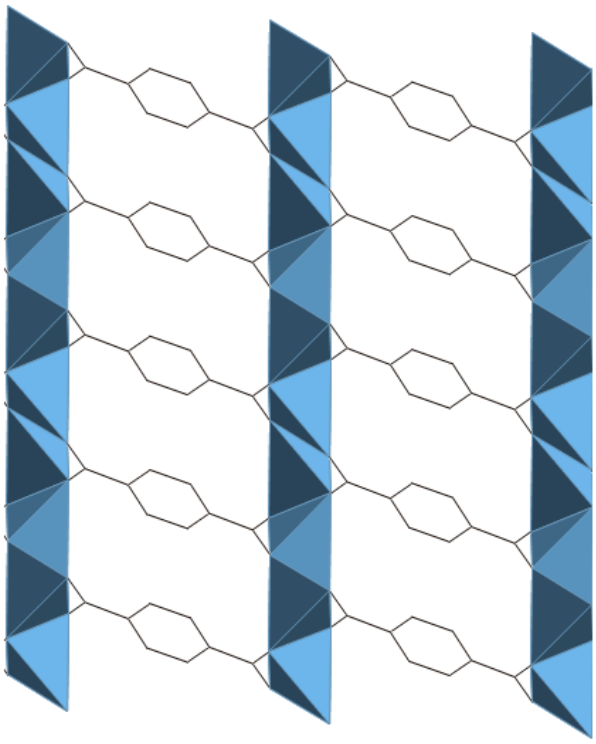

Figure 3.9. View of compound [3.1] from [010] direction showing the connectivity of the organic linkers with the alternating anti-fluorite type LiO layers.

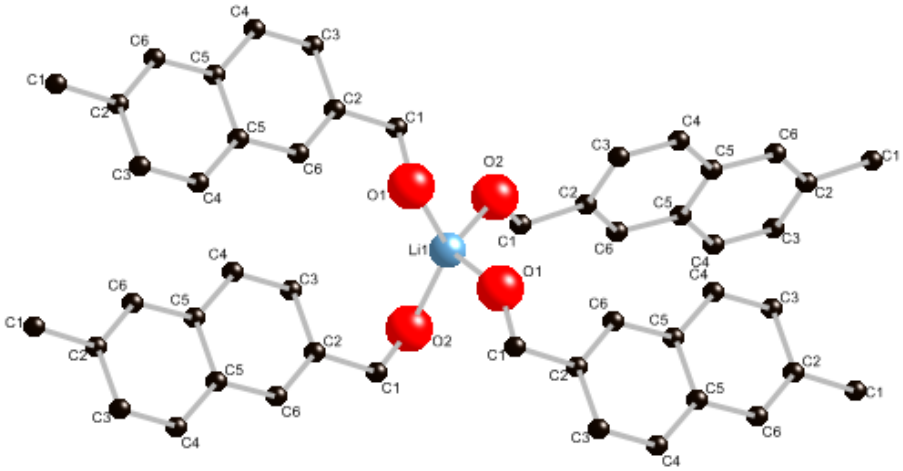

Figure 3.10. The local coordination environment of the lithium (Li1) metal center in compound [3.1].

Table 3.2. Selected Bond distance (Å) and Angle (°) for compound [3.1] [ULMOF-1]

Li(1)-O(1)	2.016(3)	O(2) #4-Li(1)-O(1) #1	103.40(15)
Li(1) #2-O(2)	1.965(3)	O(1) #1-Li(1)-O(1)	91.71(14)
Li(1) #3-O(2)	2.029(3)	O(2) #4-Li(1)-O(2) #3	114.33(15)
Li(1) #1-O(1)	1.968(3)	O(1) #1-Li(1)-O(2) #3	129.53(17)
C1-C2	1.508(2)	O(1)-Li(1)-O(2) #3	99.33(14)

Symmetry code: #1 -x+2, -y, -z+2, #2 x, -y+1/2, z-1/2, #3 x+2, -y+1, -z+2, #4 x, -y+1/2, z+1/2

3.4.2. Structural Description of [3.2], Li_2(4, 4'-BPDC), ULMOF-2

Compound [3.2] consists of a combination of alternating antifluorite type LiO layers connected by aromatic biphenyl bridging units (Fig. 3.11), that form a three-dimensional network, and is isoreticular with compound [3.1]. The asymmetric unit (Fig. 3.12) of compound [3.2] consists of a crystallographically unique lithium center (Li1) connected to four carboxylate oxygen atoms from four independent 4, 4'-BPDC groups. The average Li – O distance is found to be 1.966 Å, which is consistent with reported values (Table 3.3).[58] Each carboxylate group of the 4,4'-BPDC linker is connected to a total of four lithium centers, connecting the layers into an overall 3D structure. The bond valence sum of 1.14 v. u. matches with the expected value of +1.[109]

The tetrahedrally coordinated lithium centers construct a LiO layer, formed by dimers of edge sharing lithium tetrahedra, connected in corner sharing manner. The distance between the lithium atoms in each dimer is 2.73(1) Å. The LiO layer forms an antifluorite type structural motif, which is common in lithium oxide based compounds. The basic difference between the Li_2O antifluorite motif and the observed motif in [3.2] is the presence of square planar vacancies in the LiO layer (Fig. 3.13). The antifluorite type layers, 11.03 Å apart, stack along the [100] direction. The layers are separated by the biphenyl dicarboxylate groups with the biphenyl rings layered along the [100] direction. The distance between two consecutive biphenyl rings is an average of 5 Å in the [010] direction.

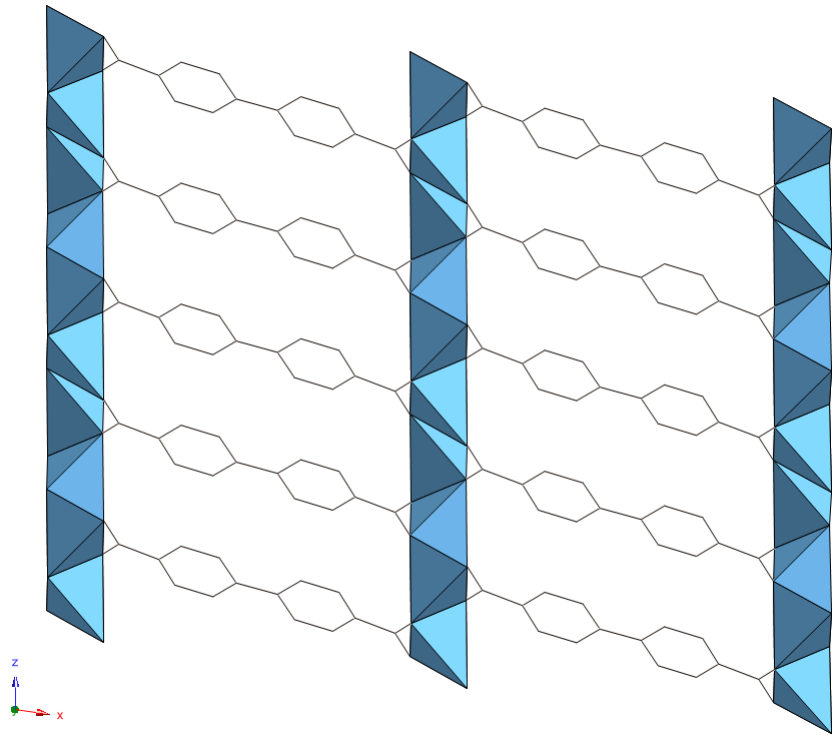

Figure 3.11. View of compound [3.2] from [010] direction showing the connectivity of the organic linkers with the alternating anti-fluorite type LiO layers

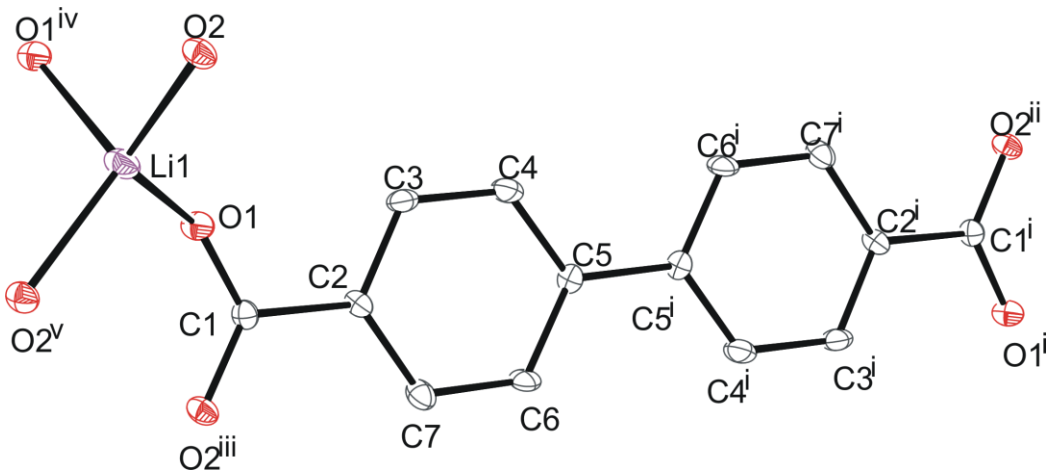

Figure 3.12. ORTEP plot of [3.2] illustrating the numbering scheme. Ellipsoids are shown at the 50% probably level. Hydrogen atoms have been omitted for clarity. Symmetry related atoms are shown to complete the coordination sphere of the lithium center. Symmetry operators: i (-x, -y, -z+1); ii (-x, -y+1, -z+1); iii (x, y-1, z); iv (-x+1, -y+1, -z+1); v (-x+1, y-1/2, -z+1/2)

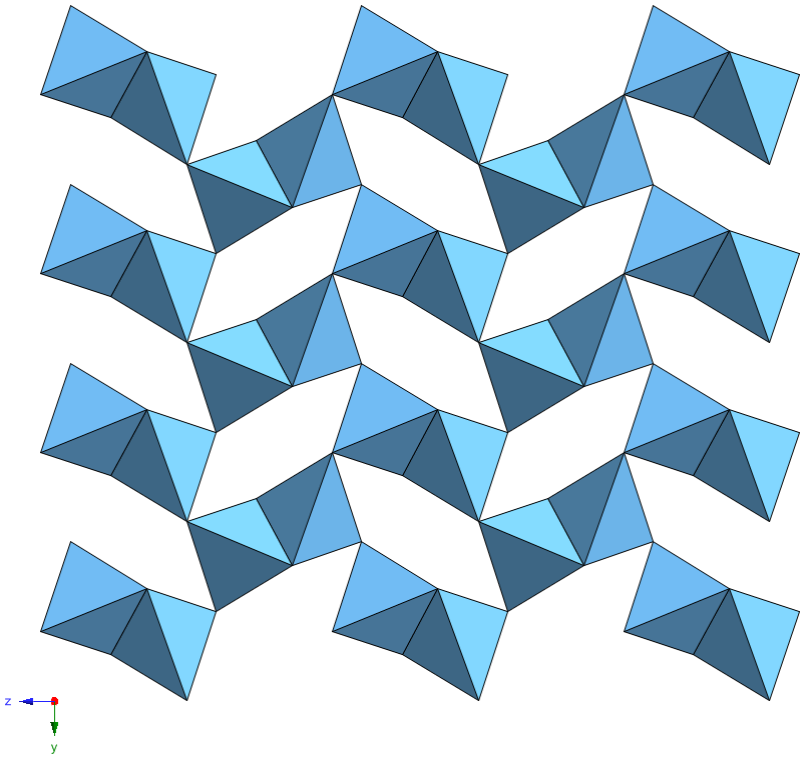

Figure 3.13. Polyhedral view of 2D-antifluorite type LiO layer with square planar vacancies for compounds [3.1] and [3.2]

Table 3.3. Selected bond length (Å) and angle (°) for compound [3.2] [ULMOF-2]

Li(1)-O(1)	1.923(8)	O(2)#2-Li(1)-O(1)#1	112.1(3)
Li(1)-O(2)	1.971(8)	O(1)-Li(1)-O(2)#2	103.0(4)
Li(1)-O(2)#2	1.983(7)	O(1)-Li(1)-O(1)#1	91.7(3)
Li(1)-O(1)#1	1.987(8)	O(2)-Li(1)-O(1)#1	101.5(4)
Li(1)-Li(1)#1	2.725(14)		

Symmetry code: #1 -x+1,-y+1,-z+1, #2 -x+1, y-1/2,-z+1/2

3.4.3. Structural Description of [3.3], Li_2(4, 4'-SDB), ULMOF-3

Compound [3.3] consists of tetrameric clusters of tetrahedral lithium centers connected by 4, 4'-SDB to form a three-dimensional framework (Fig. 3.14). The asymmetric unit (Fig. 3.15) of [3.3] consists of the organic ligand (4,4'-SDB) along with two crystallographically independent lithium centers (Li1, Li2). Each lithium center is present in distorted tetrahedral coordination with oxygen atoms also observed in compounds [3.1] and [3.2]. The bond length of Li1 center tetrahedrally connected with three carboxylate oxygen (O1, O2, O3) and one sulfonyl oxygen (O4), varies between 1.923(9) Å to 2.08(9) Å. In case of Li2, it is coordinated tetrahedrally with four carboxylate oxygen atoms (O1, O2, O3, O5), and the bond length varies between 1.873(9) Å to 2.04(9) Å (Table 3.4). The bond valance sums of the two lithium centers (Li1 and Li2) are 1.02 v. u. and 1.04 v. u., respectively, matching the expected value of +1.[109]

One of the main structural characteristics of [3.3] is the formation of isolated tetrameric clusters, consisting of corner shared pairs of edge sharing lithium polyhedra. The isolated cluster so formed is isostructural with the basic building unit of antifluorite type extended LiO layer in [3.1] and [3.2] with a square planar vacancy. Each of the isolated clusters of lithium polyhedra is connected to others by the organic linker forming an overall 3-D network (Fig. 3.14).

The 4,4'-SDB molecule is not planar as compared to 4,4'-BPDC, but rather V-shaped in nature due to the presence of the sulfur atom in between the two phenyl group, which allows for a torsion angle of 104.1(2)°. Each organic linker is associated with three tetrameric lithium polyhedral clusters using both the carboxylate oxygen atoms and sulfonyl oxygen. The 4,4'-SDB ligand is connected to a total of eight lithium centers. Among the carboxylate oxygen atoms, only one oxygen center (O5) is associated with only one lithium center, whereas the other carboxylate oxygen atoms are associated with two lithium metal centers each. In case of sulfonyl

oxygen, O4 is associated in bonding interaction with lithium center (Li1), while O6 remains uncoordinated. The preference in coordination between the sulfonyl oxygen atoms is mainly due to the geometrical constraint imposed by the V-shaped ligand. The lengths of the sulfur-oxygen bonds are consistent with reported values.[110,111] The phenyl rings of 4,4'-SDB are stacked on each other along [100] and [001] direction. The average distances between the phenyl rings of each successive layer are 5.5 Å and 10.32 Å along [100] and [001] directions, respectively.

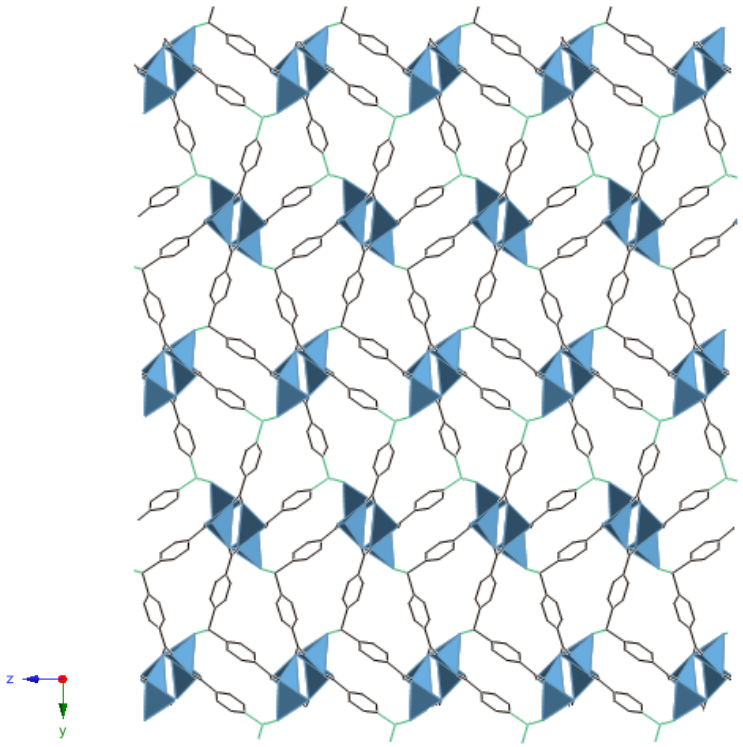

Figure 3.14. 3-D network of compound [3.3] (ULMOF-3) along [100] direction showing the connectivity of organic linkers with the tetrameric lithium cluster

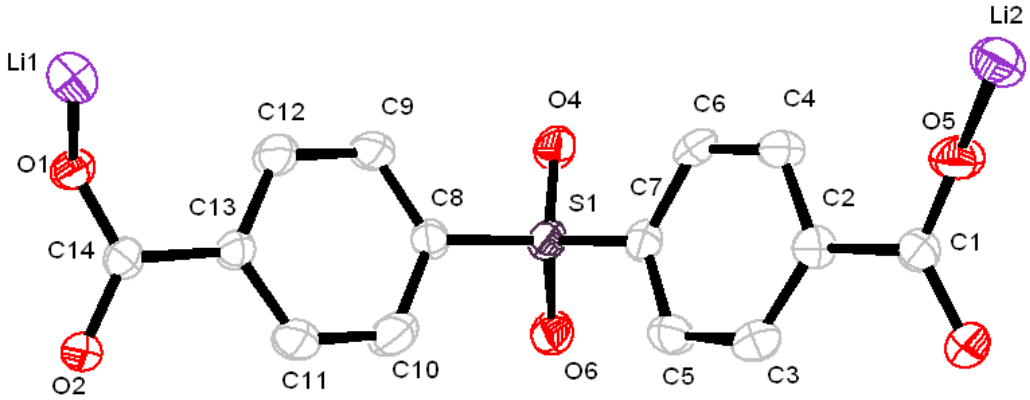

Figure 3.15. ORTEP plot of [3.3] illustrating the numbering scheme. Hydrogen atoms have been omitted for clarity.

Table 3.4. Selected bond length (Å) and angle (°) for compound [3.3] (ULMOF-3)

Li(1)–O(3)#2	1.923(9)	S(1)–O(6)	1.432(3)
Li(1)–O(2)#4	1.961(8)	S(1)–O(4	1.447(3)
Li(1)–O(4)#5	2.080(9)	C(8)–S(1)–C(7)	104.1(2)
Li(1)–Li(2)#6	2.759(12)	O(3)#2–Li(1)–O(1)	117.9(4)
Li(1)–Li(2)#1	3.074(12)	O(3)#2–Li(1)–O(2)#4	91.5(4)
Li(2)–O(3)#4	1.956(9)	O(5)–Li(2)–O(2)#3	113.8(4)
Li(2)–O(2)#3	1.999(9)	O(3)#4–Li(2)–O(1)#5	99.4(4)
Li(2)–O(1)#5	2.040(9)		

Symmetry code: #1 x-1/2,-y+1/2,z-1/2, #2 -x+3/2,y+1/2,-z+5/2, #3 -x+3/2,y-1/2,-z+5/2, #4 x+1,y,z, #5 x+1/2,-y+1/2,z+1/2, #6 -x+5/2,y+1/2,-z+5/2

3.4.4. Discussion

All three organic linkers have similar types of ligand backbones with two phenyl rings. The only difference is the presence of a sulfonyl group between the two phenyl groups in 4,4'-SDB with respect to 2,6-NDC and 4,4'-BPDC. The presence of sulfur forces the two phenyl groups to be out of plane with each other, at an angle of approximately 104°. This angular deviation from planarity affects the orientation of the linker carboxylate groups, at both ends of the phenyl rings, resulting in the formation of completely different network topologies. Compounds [3.1] and [3.2] form layers of antifluorite type lithium polyhedra, with the carboxylate groups present at an angle of 180° to each other.

Compound [3.3] contains isolated tetrameric clusters consisting of corner shared pairs of edge sharing lithium polyhedra, connected by organic linkers forming the overall network. The tetrameric cluster of lithium polyhedra present in [3.3] is also the basic building unit of the LiO layers in [3.1] and [3.2]. The presence of the same basic building unit in all three networks emphasizes the thermodynamic favorability of its formation. The presence of extended inorganic LiO layer in [3.1] and [3.2] imposes unprecedented thermal stability. Due to the nature of packing of the aromatic rings, as well as the lithium-oxygen tetrahedra, compounds [3.1] - [3.3] have no solvent accessible void space.

Although both compounds [3.1] and [3.2] contain stacked aromatic phenyl rings in their structures, the distance between the successive phenyl rings is considerably larger (> 5 Å) than the idealized π-π interaction between aromatic rings. Compounds [3.1] - [3.3] are not soluble in any common organic solvent (e.g. acetone, methanol, ethanol, ethyl acetate, DMF).

Compound [3.1] showed extremely high thermal stability under N_2 atmosphere. Two samples of [3.1] were heated at 500°C for 4 and 20 hours, respectively, to check the thermal

stability of the compound. The diffraction pattern is similar to compound [3.1], with the retention of the original structural stability. Heating the sample for 20 hrs resulted in a slightly different diffraction pattern, with an increase in intensity for the peaks corresponding to the [002] and [112] plane. The change in diffraction maxima, due to prolonged heating, could be attributed to the change in the stacking pattern of the naphthalene rings (Fig. 3.2). The TGA-DSC data show that there is no change of phase until 610°C, which indicates that the network maintains stability up to this temperature (Fig. 3.5). The structure subsequently collapses to a poorly crystalline black powder.

Compounds [3.2] and [3.3] showed very high thermal stability under N_2 atmosphere (Figs. 3.6 - 3.8). TGA data for [3.2] under N_2 atmosphere shows no weight loss until 575°C, confirming the retention of the network up to that temperature. This is supported by the subsequent DSC measurement. Compound [3.2] shows a steady weight-loss after that temperature due to the decomposition of the network. The end product is recovered as black poorly crystalline powder. No further characterization was pursued on this material.

Compound [3.3] shows a nearly identical thermal behavior under N_2 atmosphere except it has a lower stability than [3.2]. Compound [3.3] shows no weight /phase change until 500°C, after which it shows a gradual decomposition indicating destruction of the framework. The lower thermal stability of ULMOF-3 in comparison to ULMOF-2, can be explained by the absence of extended LiO type antifluorite layer in ULMOF-3. The presence of sulfonyl unit in the organic linker may also be the reason of lower stability of ULMOF-3, due to possible formation of SO_2 upon decomposition of the organic linker molecule. The thermal behavior of compound [3.2] was recorded under air (Fig. 3.7). It shows a lower thermal stability under air than N_2 atmosphere

(decomposition temperature: 520°C), indicating lower thermal stability in air compared to inert atmosphere.

3.5. Conclusion

Three lithium based networks were synthesized using 2-6-NDC ([3.1], ULMOF-1) 4, 4'-BPDC ([3.2], ULMOF-2) and 4,4'-SDB ([3.3], ULMOF-3) as organic linkers. Compounds [3.1] and [3.2] are isostructural and consist of layered antifluorite type LiO layers, connected by organic linkers Compound [3.3] is constructed by V-shaped 4,4'-SDB linker, connecting tetrameric clusters of lithium polyhedra. Compound [3.1] shows the highest thermal stability reported till date among inorganic-organic hybrid materials. The detailed structural characterization through single crystal X-ray diffraction enables us to understand the underlying chemistry of this potentially interesting new class of networks, containing ultra-light metal centers.

Chapter 4

Solvothermal Synthesis and Structural Characterization of Ultralight Metal Coordination Networks Using Pyridinedicarboxylates

The content of this chapter is published in

(a) Solvothermal Synthesis and Structural Characterization of Ultralight Metal Coordination Networks. Banerjee, D.; Kim, S. J.; Borkowski, L. A.; Xu, W. Q.; Parise, J. B., *Cryst. Growth Des.* **2010,** 10 (2), 709-715 & (b) Synthesis and Structural Characterization of a 3-D Lithium Based Metal-Organic Framework Showing Dynamic Structural Behavior. Banerjee, D.; Kim, S. J.; Li, W.; Wu, H. H.; Li, J.; Borkowski, L. A.; Phillips, B. L.; Parise, J. B., *Cryst. Growth Des.* **2010,** 10 (6), 2801-2805.

4.1. Abstract

Two lithium based coordination polymers and two frameworks $Li_3(C_7H_3O_4N)_2 \cdot 0.21(H_2O)(C_2H_8N)$ [Li_3(2,6-PDC)$_2 \cdot 0.21(H_2O)$(DMA), [4.1], ULCP-1, ULCP=Ultra-Light Coordination Polymer]; $Li_3(C_7H_3O_4N) \cdot (C_6H_3O_2N)$ [Li_3(2, 6 PDC)·(2-PC), [4.2], ULCP-1A]; $Li_2(C_7H_3O_4N)$ [Li_2(3,5-PDC), [4.3], ULMOF-4, ULMOF = Ultra Light Metal Organic Framework]; $Li_2(C_7H_3NO_4) \cdot (C_3H_7NO)$ [Li_2(2,5-PDC)·(DMF), [4.4], ULMOF-5]; were synthesized using solvothermal techniques and characterized using single-crystal X-ray diffraction. Compounds [4.1] and [4.2] form layered structure, consists of trimeric corner- and edge-sharing lithium tetrahedral chains, connected by organic linkers. Compounds [4.3] and [4.4] are 3-D networks, formed by corner and edge sharing chains of lithium tetrahedra, connected by the organic linkers. The desolvated compound [4.4] reverts to the original form upon exposure to DMF showing dynamic structural behavior. All compounds are stable above 250°C under N_2 atmosphere, with [4.3] stable to 550°C.

4.2. Introduction

A wide range of metal-centers forms coordination networks (CNs) and frameworks (MOFs) through linkages with multifunctional organic ligands.[7,73] First row transition metals[76,78,82,98] are popular choices as coordination centers for the design and discovery of these materials, due to their well known coordination behavior with polycarboxylates and their tendency to form secondary building units (*e.g.* the paddle wheel unit for copper (II) center).[98,112] These properties are used to design 3-D networks potentially useful in gas storage,[10,17,75-82] ion exchange,[85-87] catalysis,[88-90] and separation.[92,93] Recently dense frameworks have been explored for possible functionality in fields such as magnetism and metallic conductance. Further, the gravimetric advantages of using lightweight coordinating centers (Li, [58,101] B, [75,113,114] Mg [17,19,32,99]) for the design of MOFs have also recently been recognized. Frameworks constructed with lithium are of particular interest, since studies indicate strong electrostatic interactions between adsorbed H_2 and the lithium centers. [46,47,98,103,104,106,107]

The nature of the organic linkers also controls the topology and properties of the networks. Different structural isomers of pyridine dicarboxylic acids (2,6-; 2,5-; 3,5-; and 2,4-PDC) are of contemporary interest as linkers, due to the presence of both nitrogen and oxygen based functional group along with a rigid aromatic backbone. These linkers have been used to form first row transition metal and lanthanide based networks of varying topologies.[115-118]

We were motivated to explore networks that form by combining the potential of lithium metal centers to strongly interact with adsorbed gases, with the structural diversity present in the pyridine dicarboxylate system. In this chapter, we describe solvothermal synthesis and structural characterization of four compounds, forming either as layered coordination polymers Li_3(2,6-

PDC)$_2$·0.21(H_2O)(DMA) [4.1], Li_3(2,6-PDC)·(2-PC) [4.2] or 3-D networks [Li_2(3,5-PDC) [4.3] and Li_2(2,5-PDC)·DMF [4.4] as part of our study on ultra-light metal (Li) based metal organic coordination polymers and frameworks.

4.3. Experimental Section

4.3.1 Synthesis

All compounds were synthesized under solvothermal condition using Teflon lined stainless steel Parr autoclaves. Starting materials include lithium nitrate ($LiNO_3$, 99+%, Acros-Organic), lithium hydroxide ($LiOH·H_2O$, 98%, Alfa-Aesar), 2,6-Pyridine dicarboxylic acid (2,6-PDC, 99%, Acros-Organic), 3,5-pyridinedicarboxylic acid (3,5-PDC, 98%, Sigma-Aldrich), 2,5-pyridinedicarboxylic acid (2,5-PDC, Sigma-Aldrich, 98%) N,N-dimethylformamide (DMF, 99%, Sigma-Aldrich) and ethanol (99%, Sigma-Aldrich) and were used without any further purification.

Synthesis of Compound [4.1]: $Li_3(C_7H_3NO_4)_2·0.21(H_2O)(C_2H_8N)$, ULCP-1

A mixture of 0.005 mole of 2,6-PDC (0.85 gram), 0.0025 mole of $LiNO_3$ (0.175g) and 0.0005 mole of $LiOH·H_2O$ (0.0214 g) was dissolved in 15 grams of DMF and stirred for 4 hours to achieve homogeneity [molar ratio of metal nitrate: ligand: solvent= 1:2:82]. The resultant solution was heated at 100°C for 5 days. Colorless plate shaped crystals were recovered as products and washed with DMF and ethanol (Yield: 55% based on Li).

Synthesis of Compound [4.2]:$Li_3(C_7H_3O_4N)·(C_6H_3O_2N)$, ULCP-1A

A mixture of 0.005 mole of 2,6-PDC (0.85 gram), 0.0025 mole of $LiNO_3$ (0.175 gram) and 0.0005 mole of $LiOH·H_2O$ (0.021gram) were dissolved in 14 grams of DMF. The resultant solution was stirred for 3 hours to achieve homogeneity and subsequently heated at 180°C for 5

days [molar ratio of metal nitrate: ligand: solvent= 1:2:76]. The product was obtained as needle shaped crystals and washed with DMF and ethanol (Yield: 45% based on lithium).

Synthesis of Compound [4.3]: $Li_2(C_7H_3O_4N)$, ULMOF-4

A mixture of 0.0025 mole of 3,5-PDC (0.425 g), 0.0025 mole of $LiNO_3$ (0.174 g) and 0.001 mole of LiOH (0.042 g) were dissolved in 8 grams of DMF. The resulting solution was stirred for 1 hour [molar ratio of metal nitrate: ligand: solvent= 1:1:43] to ensure the homogeneity of the solution and then was heated for 5 days at 180°C. Colorless needle shaped crystals were recovered by filtration and subsequently washed by DMF (Yield: 50% based on Li).

Synthesis of compound [4.4]: $Li_2(C_7H_3NO_4)\cdot(C_3H_7NO)$, ULMOF-5

A mixture of 0.005 mole of 2,5-PDC (0.85 gram), 0.005 mole of $LiNO_3$ (0.345 gram) and 0.0005 mole of $LiOH.H_2O$ (0.021 gram) were dissolved in 15 gram of DMF [molar ratio of metal salt: ligand: solvent = 1:1:41]. The resultant solution was stirred for 4 hours and heated at 180°C for 5 days. The product was obtained as needle shaped colorless crystals (Yield: 50% based on Li) from a filtrate rinsed with DMF.

4.3.2. X-ray crystallography

Suitable single crystals of compounds [4.1] - [4.4] were selected from the bulk sample and were mounted on a glass fibers using epoxy. Reflections for the compounds were collected using a Bruker four circle P4 single crystal diffractometer equipped with a SMART 1K CCD detector at room temperature (298K) using Mo Kα radiation (λ = 0.71073 Å) and φ and ω scans. The raw intensity data were collected and integrated with software packages, SMART[65] and SAINT.[66] An empirical absorption correction was applied using SADABS[67] and the crystal structures were solved using direct methods (SHELXS).[67] Oxygen atoms were located first, followed by the determination of other atoms positions (C, N, Li) from the Fourier difference map, with all of the non-hydrogen atoms being refined anisotropically. Hydrogen atoms were added to the pyridine rings using geometrical constraints. The crystallographic details can be found in Table 4.1.

Contained within the structure of [4.1] is a site partially occupied solvent water molecule. After the positions of atoms comprising the layer and dimethylamine (DMA) solvent had been assigned, a large residual electron density peak remained. This peak was assigned as a site for a solvent water molecule and its occupation factor was refined to a value of 20.5 (6) %.

Table 4.1.Crystallographic data and structural refinement details of compounds [4.1] - [4.4]

	[4.1]	[4.2]	[4.3]	[4.4]
Empirical formula	$C_{16}H_{14.40}N_3O_{8.21}Li_3$	$C_{13}H_7N_2O_6Li_3$	$C_7H_3NO_4Li_2$	$C_{10}H_{10}N_2O_5Li_2$
Formula weight	400.82	308.03	178.98	252.08
Collection Temperature(K)	298(2)	298(2)	298(2)	298(2)
Wavelength(Å)	0.71073	0.71073	0.71073	0.71073
Space Group	***P*** $2_1/c$	***P*** $2_1/c$	***C*** 2/c	***P****bcn*
a (Å)	11.51(2)	10.190(2)	12.692(3)	15.8(3)
b (Å)	15.33(3)	13.390(3)	10.977(2)	8.59(2)
c (Å)	10.93(2)	10.450(2)	11.2(2)	18.46(4)
α (°)	90	90	90	90
β (°)	99.98(3)	106.02(3)	105.83(3)	90
λ (°)	90	90	90	90
Volume	1899.4(7)	1370.5(5)	1501.2(5)	2507.1(9)
Z	4	4	8	8
Calculated Density(g/cm^3)	1.401	1.493	1.584	1.336
Absorption coefficient(mm^{-1})	0.111	0.115	0.126	0.105
F(000)	824	624	720	1040
Crystal size (mm)	0.25×0.21×0.04	0.18×0.06×0.02	0.18 x 0.08 x 0.03	0.15×0.08×0.03
Θ range of data collection	1.80-26.73	2.08-26.37	2.50-26.01	2.21-26.73
Index range	-13<=h<=14	-11<=h<=12	-15<=h<=15	-19<=h<=20
	-19<=k<=18	-16<=k<=16	-12<=k<=13	-10<=k<=10
	- 13<=l<=13	-13<=l<=12	-13<=l<=13	-23<=l<=20
Total reflection	12605	8778	4770	15743
Independent reflection	4022 [R(int) = 0.0556]	2803 [R(int) = 0.0378]	1487 [R(int) = 0.0877]	2664 [R(int) = 0.0229]
Goodness of fit	0.973	1.055	0.992	1.041
Data/restraints/parameter	4022 / 4 / 294	2803 / 0 / 217	1487 / 0 / 127	2664 / 6 / 215
R1(*on* F_o^2, $I>2\sigma(I)$)	R1 = 0.0436	R1 = 0.0391	R1 = 0.0546	0.0405
wR2 (*on* F_o^2, $I> 2\sigma(I)$)	0.0949	0.0905	0.1152	0.1169

4.3.3. Powder XRD and Thermal Analysis

Bulk sample identification and phase purity were determined using powder X-ray diffraction. The data were collected using a Scintag Pad-X diffractometer equipped with Cu Kα radiation within a range of $5° \leq 2\theta \leq 40°$ (step size: 0.02° , counting time: 1s/step). The powder patterns collected were consistent with the simulated patterns based on the single crystal data (Figs. 4.1-4.4). *In situ* high temperature X-ray powder diffraction of compound [4.1] was conducted on a Bruker AXS diffractometer equipped with an electronic multiwire area detector system, in order to observe the changes in the X-ray diffraction pattern during the thermal decomposition of the sample. A powder sample was obtained by grinding and this was loaded in a Kapton® capillary for heating by an air blower heater. The temperature was maintained at 330°C during the data collection (Figs. 4.1 - 4.4).

Combined TGA-DSC data analysis was performed using a Netzsch 449C Jupiter instrument. The samples were heated from room temperature to 750°C (compounds [4.1] - [4.3]) and 700°C (compound [4.4]) under a flowing N_2 atmosphere with a heating rate of 10°C/minute (Figs. 4.5-4.8).

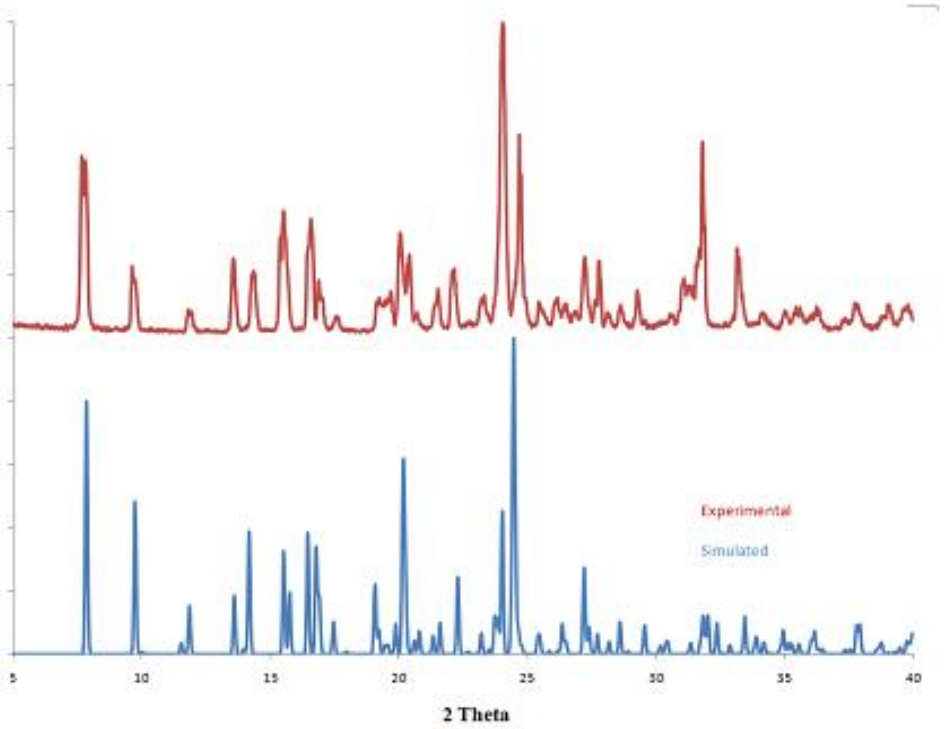

Figure 4.1. Simulated vs. experimental powder pattern of compound [4.1].

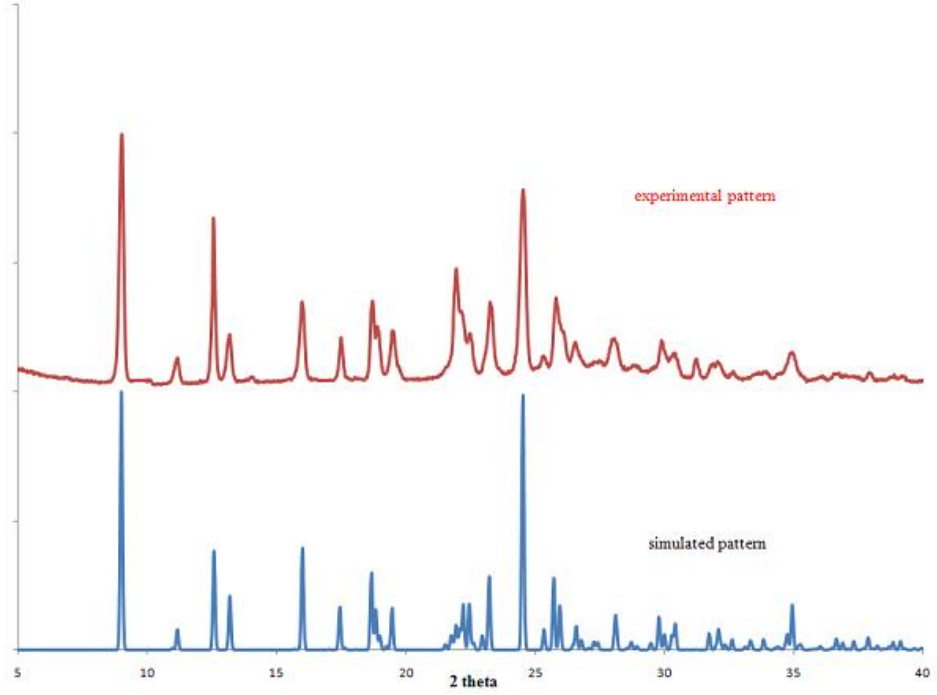

Figure 4.2. Simulated vs. experimental powder pattern of compound [4.2].

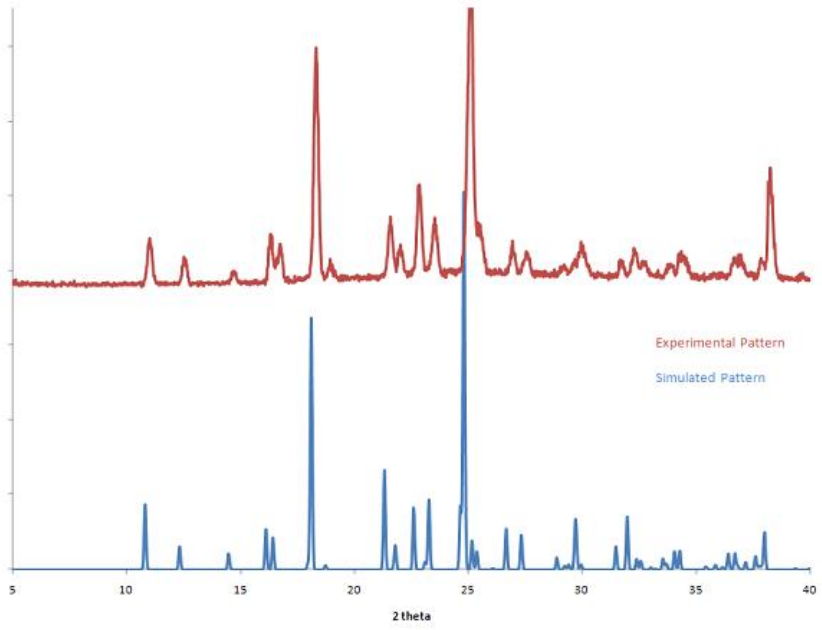

Figure 4.3. Simulated vs. experimental powder pattern of compound [4.3].

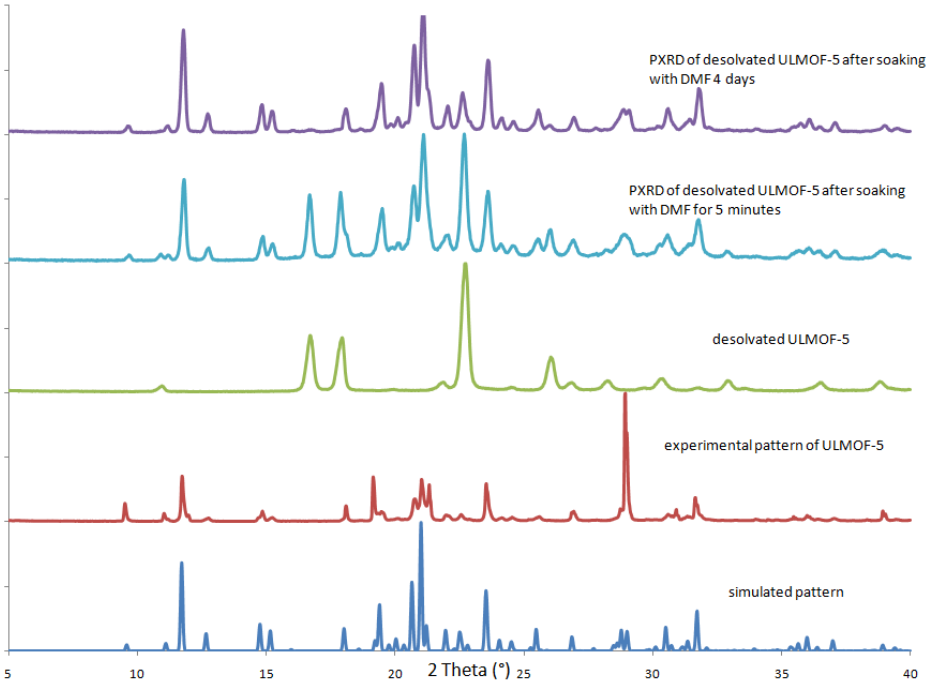

Figure 4.4. PXRD pattern of compound [4.4] after desolvation and soaking with DMF.

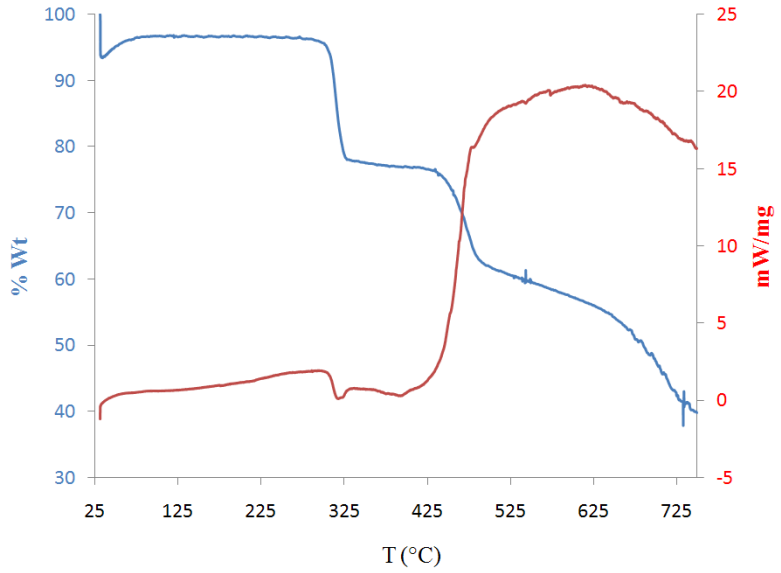

Figure. 4.5. Combined TGA-DSC of compound [4.1] (ULCP-1). The blue line represents the TGA curve while the red line show the associated DSC signal.

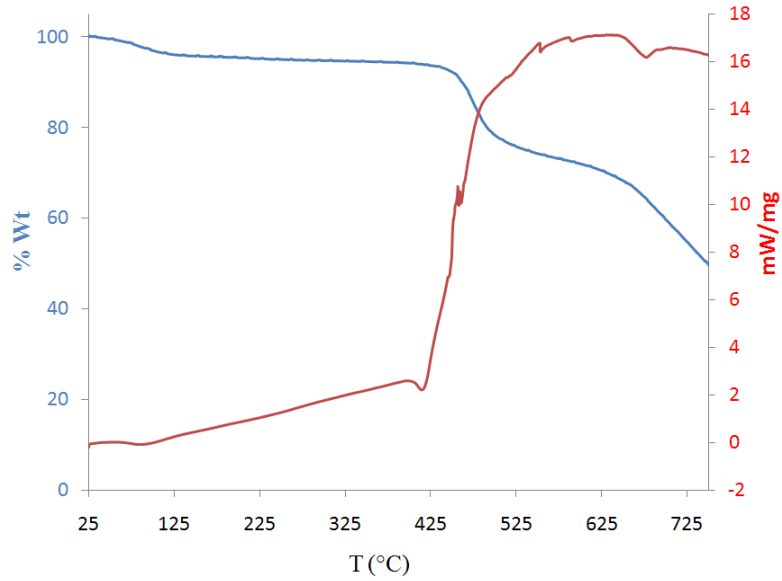

Figure. 4.6. Combined TGA-DSC of compound [4.2] (ULCP-1A). The blue line represents the TGA curve while the red line show the associated DSC signal.

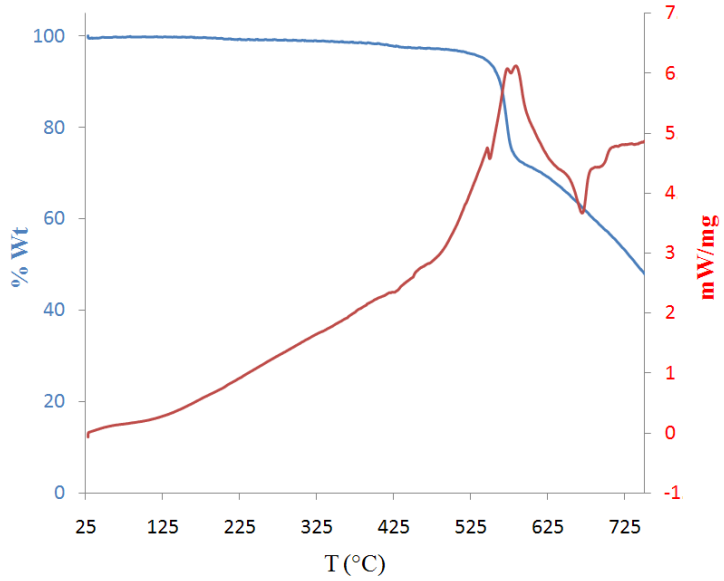

Figure 4.7. Combined TGA-DSC of compound [4.3] (ULMOF-4). The blue line represents the TGA curve while the red line show the associated DSC signal.

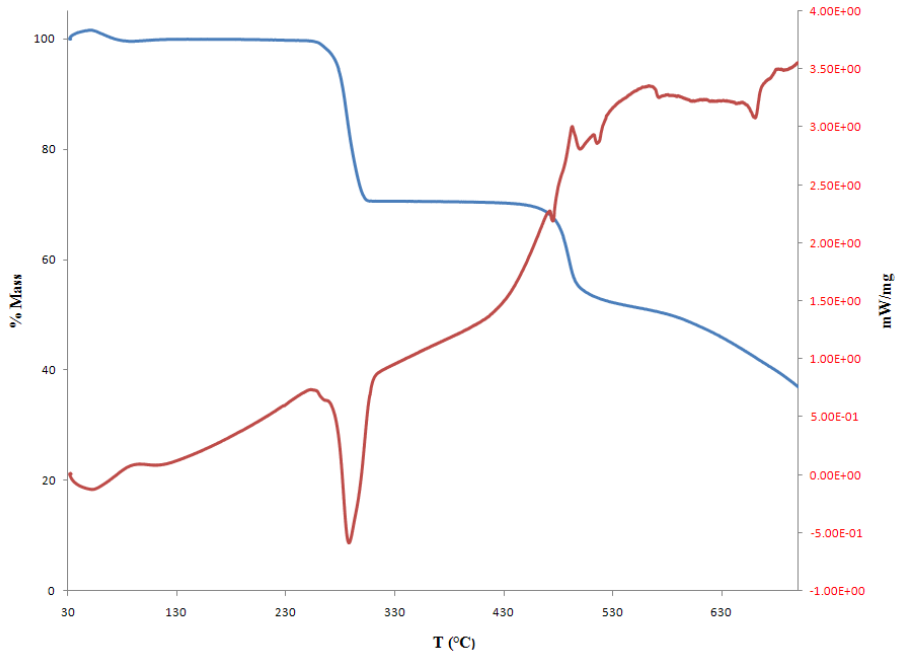

Figure 4.8. Combined TGA-DSC plot of compound [4.4] (ULMOF-5). The blue line represents TGA plot of ULMOF-2 while the red line shows the DSC signal associated.

4.3.4. BET analysis

The surface area measurement of compound [4.4] was carried out using a Quantachrome Nova 2200e surface area analyzer. To avoid structural collapse of the material due to rapid degassing, the sample was first evacuated at room temperature for one hour and then the temperature was increased at the rate of 3˚C/min to 295˚C. After a 12-hour degassing period, the sample was weighed to confirm the complete removal of both free and coordinated DMF molecules (33% of the starting weight) and analyzed. The surface area was calculated from a linear 5-point BET plot acquired from analysis at liquid N_2 temperature (77 K) using N_2 adsorbate gas.

4.3.5. ^{6}Li solid state NMR

Solid-state ^{6}Li single-pulse MAS NMR spectra were collected on a 400 MHz Varian Inova spectrometer (9.4 T), with Larmor frequencies of 58.9 MHz. Spectra were collected using a Varian/Chemagnetics T3-type probe samples contained in 3.2mm (o. d.) normal wall ZrO_2 rotors with a spinning speed of 15KHz. 3 μs rf pulse length was chosen based on a calibrated 8.5μs 90° pulse by using the LiCl solution standard. The pulse delay was optimized as 200 s and ca. 300 scans ware collected for each spectrum to obtain a decent signal-to-noise ratio. The ^{6}Li chemical shifts ($\delta_{iso,Li}$) are reported relative to external 1M LiCl solution set to $\delta_{iso,Li}$ = 0 ppm.

4.4. Result and Discussion

4.4.1 Structural description of [4.1], $Li_3(2,6\text{-}PDC)_2 \cdot 0.21(H_2O)(DMA)$,ULCP-1

Compound [4.1] forms a negatively charged layered structure with charge compensating protonated dimethyl amine (DMA) and solvent water molecules occupying sites between the layers (Fig. 4.9). The asymmetric unit of [4.1] contains two 2,6-PDC linkers, connected to three crystallographically unique lithium centers (Fig. 4.10). Each lithium center is present in distorted tetrahedral coordination. Li1 is connected to four carboxylate oxygen atoms from four different organic linkers. Li2 and Li3 are each connected to three carboxylate oxygen atoms and one pyridyl nitrogen from three different organic linkers. One organic linker acts as a bidentate chelating ligand (O6 – Li2 – N2) among the contributing ligands. The Li-O bond lengths of Li2 and Li3 vary between 1.917(4) and 2.189(6) Å. For Li1, the Li-O bond lengths vary between 1.880(4) and 1.993(4) Å (Table 4.3). The bond valance sum of the lithium centers, 1.08 (Li1), 0.94 (Li2) and 0.95 (Li3) v. u. (v. u. = valance unit), are close to the expected value of +1 (v. u. = valance unit**).**[109]

The strength of the bonding interactions between the carboxylate oxygen atoms and the metal centers appear to depend on the position of the oxygen with respect to the pyridyl nitrogen in the aromatic ring. The carboxylate oxygen atoms (O3, O4, O5 and O6) geometrically positioned towards the pyridyl nitrogen show a very weak interaction with the metal centers. One oxygen center is not coordinated with any metal centers; rather it interacts with the amine present within the layers. The average Li-N bond distance is found to be 2.08 Å in compound [4.1].

The lithium tetrahedra form trimers by edge- and corner-sharing manner. The trimers are further connected by 2,6-PDC to form layers, which pack in such a way that channels large enough to accommodate the DMA and water molecules are formed. These molecules (DMA and

water) are involved in strong H-bonding with the carboxylate oxygen of the organic linkers. The position of the DMA molecules can be seen as a result of the H-bonding with the protonated nitrogen, interacting with the carboxylate oxygen atoms from the layer. The water molecules are present between two DMA molecules along [001] direction with an average distance of 3.5 Å from each DMA molecule. The small size of the channel, the zigzag type layer and strong H-bonding makes it unlikely for DMA and water molecules to move freely along the [001] direction in the channel.

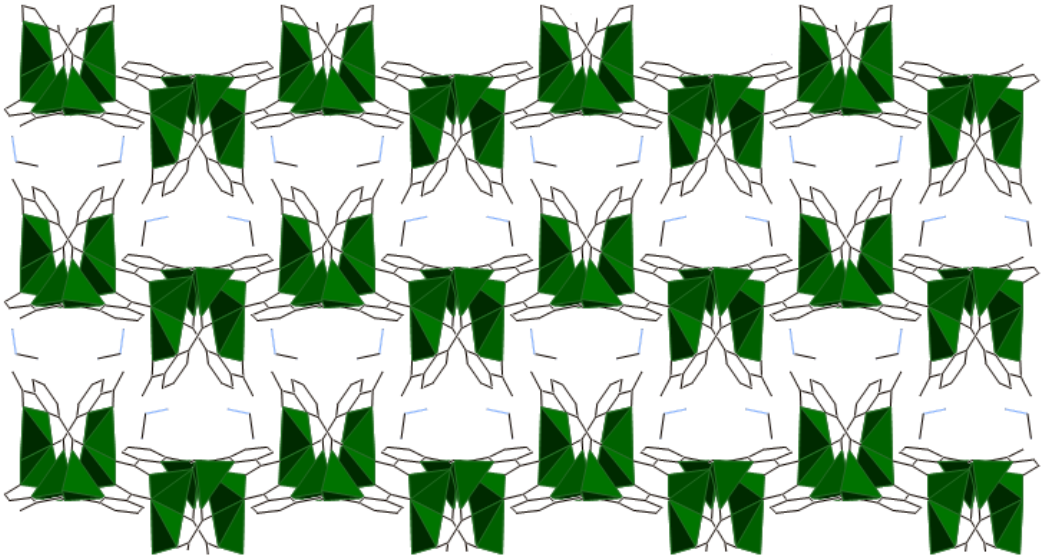

Figure 4.9. Packing of compound [4.1] (ULCP-1) along [001] direction showing the positively charged DMA molecules within the layers. The solvent water molecules and hydrogen atoms have been omitted for clarity.

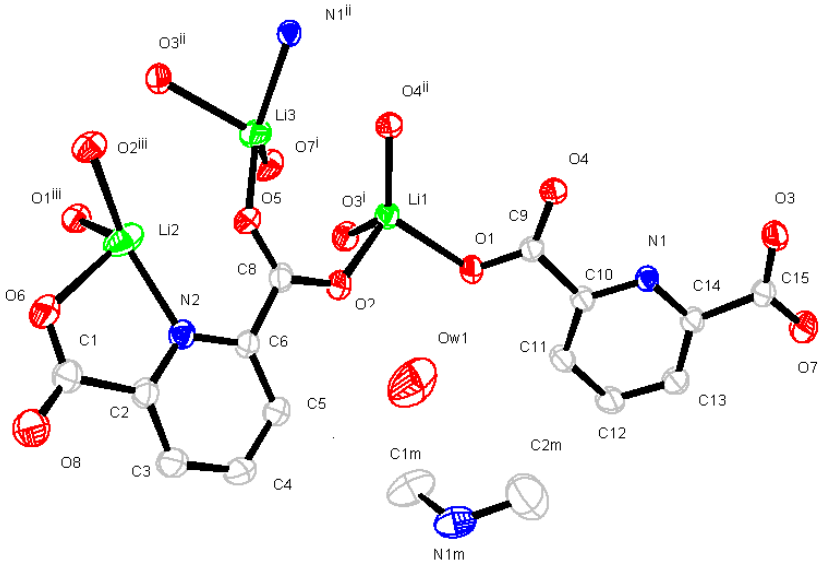

Figure 4.10. ORTEP plot of compound [4.1] (ULCP-1) illustrating the numbering scheme. Ellipsoids are shown at the 50% probability level. Hydrogen atoms have been omitted for clarity. Symmetry related atoms are shown to complete the coordination sphere of the lithium center. Symmetry operators: i (-x, y, z), ii (-x, y+1/2, -z+1/2), iii (-x, -y, -z).

Table 4.2. Hydrogen bonding distances in compound [4.1]

D-H…A	d(D-H) (Å)	d(H…A) (Å)	d(D…A) (Å)	<DHA (°)
N1M-HM1…O8[a]	0.907	1.852	2.745	167.93
N1M-HM2…O6	0.890	1.818	2.688	164.86
OW1-HW1…O7	0.855	1.993	2.690	137.96
OW1-HW2…O7	0.851	2.133	2.690	122.73

Symmetry code: a -x+2, y-1/2, -z+1/2.

Table 4.3. Selected bond lengths (Å) and angles (°) for structure [4.1]

Li(1)-O(1)	1.971(4)	Li3-O(4)#1	2.597(4)
Li(1)-O(2)	1.993(4)	O(4)#1-Li(1)-O(3)#2	123.0(2)
Li(1)-O(4)#1	1.880(4)	O(4)#1-Li(1)-O(1)	118.7(2)
Li(1)-O(3)#2	1.963(4)	O(3)#2-Li(1)-O(1)	118.7(2)
Li(2)-O(6)	2.189(6)	O(3)#2-Li(1)-O(2)	99.08(18)
Li(2)-O(1)#3	1.963(5)	O(1)#3-Li(2)-O(2)#3	92.72(19)
Li(2)-N(2)	2.075(4)	O(1)#3-Li(2)-N(2)	123.4(2)
Li(2)-O(2)#3	1.970(4)	O(1)#3-Li(2)-O(6)	104.3(2)
Li(2)-O5	2.454(5)	O(2)#3-Li(2)-O(6)	95.59(19)
Li(3)-O(5)	2.008(5)	O(7)#2-Li(3)-O(5)	106.53(18)
Li(3)-O(7)#2	1.917(4)	O(5)-Li(3)-O(3)#1	104.38(19)
Li(3)-O(3)#1	2.148(4)	N(1)#1-Li(3)-O(3)#1	77.42(13)
Li(3)-N(1)#1	2.097(4)	O(7)#2-Li(3)-O(3)#1	113.3(2)

Symmetry codes: #1 -x+1, -y, -z, #2 -x+1, y+1/2, -z+1/2, #3 x, -y+1/2, z-1

4.4.2. Structural description of [4.2], Li_3(2, 6 PDC)·(2-PC), ULCP-1A

Compound [4.2] consists of trimeric clusters of tetrahedral lithium metal centers connected by 2,6-PDC and 2-PC to form a layered structure (Fig. 4.11). The asymmetric unit of ULCP-1A includes two organic linker molecules (2,6-PDC, 2-PC) and three crystallographically unique lithium centers (Fig. 4.12). Although each Li atom is found in distorted tetrahedral coordination, there are differences between the coordination environments of the three Li centers, arising from the type of ligand functionalities and bonding involved. Li1 is connected to four separate organic linkers (three 2,6-PDC and one 2-PC) through four carboxylate oxygen atoms. Li2 and Li3 are each connected to three organic linkers by coordination with three carboxylate oxygen atoms and pyridyl nitrogen. 2,6-PDC and 2-PC act as bidentate chelating agents in the case of Li2 and Li3, respectively. The average Li-O bond length is found to be 1.971 Å, while the pyridyl nitrogen atoms (N1, N2) are found to reside at an average distance of 2.09 Å from their respective lithium metal centers (Table 4.4). The bond valance calculation showed, that the bond valance sum of the lithium centers are 1.07 v. u. (Li1) and 1.02 (Li2, Li3) which are close to the expected value of +1.[109]

The major structural feature of ULCP-1A is the *in-situ* formation of 2-pyridinedicarboxylic acid (2-PC) by the partial decarboxylation of 2,6-PDC molecule. The formation of 2-PC gives rises to significant structural difference between ULCP-1 and ULCP-1A. ULCP-1A forms a neutral layered structure, due to the presence of 2-PC as the constituent of the layer. The basic building unit of each layer is the trimeric corner- and edge-shared lithium tetrahedral clusters. Li1 and Li3 form edge-shared dimers that are connected by Li2 tetrahedra by corner-sharing to form the trimeric basic building unit. The distance between two Li centers in the dimer is 2.579(4) Å. The average distance between the corner-shared lithium centers is found

to be 3.35 Å. The building units are connected to each other by both organic linkers forming the layer. The direction of connectivity depends on the type of linker *e.g.* 2,6-PDC connects the building unit in both [010] and [001] directions, while 2-PC connects along the [001] direction only. The layers are arranged in an ordered fashion such that the hydrophobic aromatic rings from successive layers point towards each other. The average distance between each layer is 1.8 Å indicating strong van der Waals interaction between each layers.

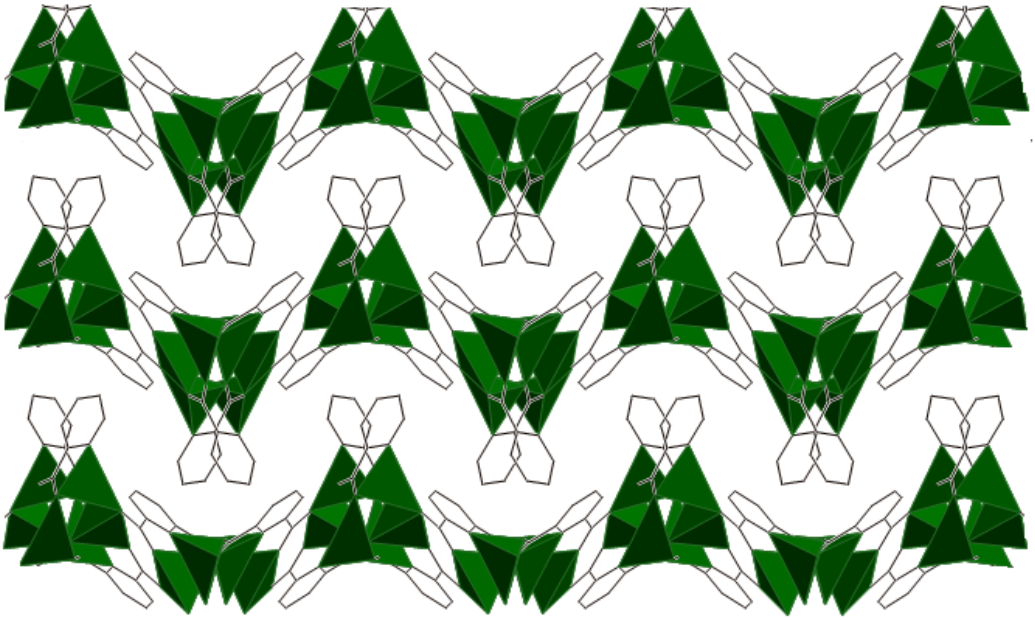

Figure 4.11. Packing of compound [4.2] (ULCP-1A) viewed along the [001] direction.

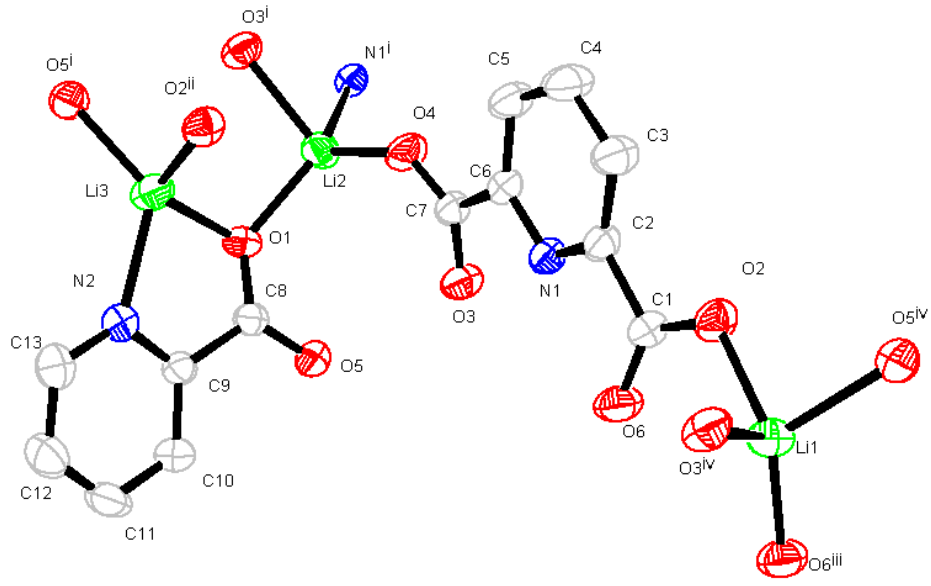

Figure 4.12. ORTEP plot of compound [4.2] (ULCP-1A) illustrating the numbering scheme. Ellipsoids are shown at the 50% probability level. Hydrogen atoms have been omitted for clarity. Symmetry related atoms are shown to complete the coordination sphere of the lithium center. Symmetry operators: i (x, y, z), ii (-x, y+1/2, -z+1/2), iii (-x, -y, -z), iv (x, -y+1/2, z+1/2)

Table 4.4. Selected bond lengths (Å) and angles (°) for compound [4.2]

Li(1)-O(2)	1.982(3)	O(6)#2-Li(1)-O(3)#3	117.98(16)
Li(1)-O(6)#2	1.853(3)	O(3)#3-Li(1)-O(2)	99.77(14)
Li(1)-O(3)#3	1.953(3)	O(6)#2-Li(1)-O(5)#3	119.04(17)
Li(1)-O(5)#4	2.042(3)	O(3)#2-Li(1)-O(5)#3	96.81(14)
Li(2)-N(1)#4	2.067(3)	O(4)-Li(2)-O(1)	107.95(15)
Li(2)-O(3)#4	2.072(3)	O(4)-Li(2)-N(1)#4	111.93(16)
Li(2)-O(1)	1.990(3)	O(4)-Li(2)-O(3)#4	110.85(17)
Li(2)-O(4)	1.910(3)	O(1)-Li(2)-O(3)#4	99.36(15)
Li(3)-O(1)	1.992(4)	O(2)#1-Li(3)-O(1)	109.62(17)
Li(3)-N(2)-	2.119(4)	O(2)#1-Li(3)-O(5)#4	92.27(14)
Li(3)-O(2)#1	1.926(4)	O(1)-Li(3)-O(5)#4	131.62(19)
Li(3)-O(5)#4	1.994(3)	O(2)#1-Li(3)-N(2)	119.64(18)

Symmetry codes : #1 -x, -y+1, -z, #2 -x, -y+1, -z-1, #3 -x, y+1/2 ,-z-1/2, #6 x, -y+1/2, z+1/2

4.4.3. Structural description of [4.3], Li_2(3,5-PDC), ULMOF-4

Compound [4.3] consists of a chain of edge- and corner-shared lithium polyhedra, connected by organic linkers to form a three-dimensional network (Fig. 4.13). The asymmetric unit of [4.3] comprises of the organic linker (3,5-PDC) and two crystallographically unique lithium metal centers (Fig. 4.14). Each lithium metal center is present in distorted tetrahedral coordination, as observed before in case of ULCP-1/1A. The average bond length of Li1, tetrahedrally connected to four carboxylate oxygen atoms (O2, O3 and O4) is found to be 1.977 Å. In the case of Li2, it is coordinated to three carboxylate oxygen atoms and one pyridyl nitrogen with an average Li-O distance of 1.93 Å (Table 4.5). Each of the lithium metal centers is coordinated to four different organic linkers through their respective coordinating atoms (carboxylate oxygen atoms or pyridyl nitrogen atoms). One of the major differences between [4.3] and the two preceding structures ([4.1] and [4.2]) is the absence of chelating mode of the organic linkers in [4.3]. All the carboxylate oxygen atoms are connected to two lithium centers except O2, which is connected only to Li1. The bond valance sums of two lithium centers (Li1 and Li2) are 1.01 and 1.10 v. u., respectively, matching well with the expected value of +1. [109]

The main structural feature of [4.3] is the presence of infinite edge- and corner- shared lithium polyhedra chain. It is distinct from the isolated trimeric lithium polyhedra clusters observed in [4.1] and [4.2]. Each type of lithium center (Li1 and Li2, respectively) forms a dimer by edge-sharing. These edge-shared dimers are then connected to each other by corner-sharing manner, to form an infinite chain with the average distance between the lithium centers in the dimer being 2.72 Å. The chains are then connected to each other by the organic linkers forming the overall 3-D network. Each 3,5-PDC molecule connects with three 1-D chains. The distance between each chain is on average 4.97 Å along the [100] direction.

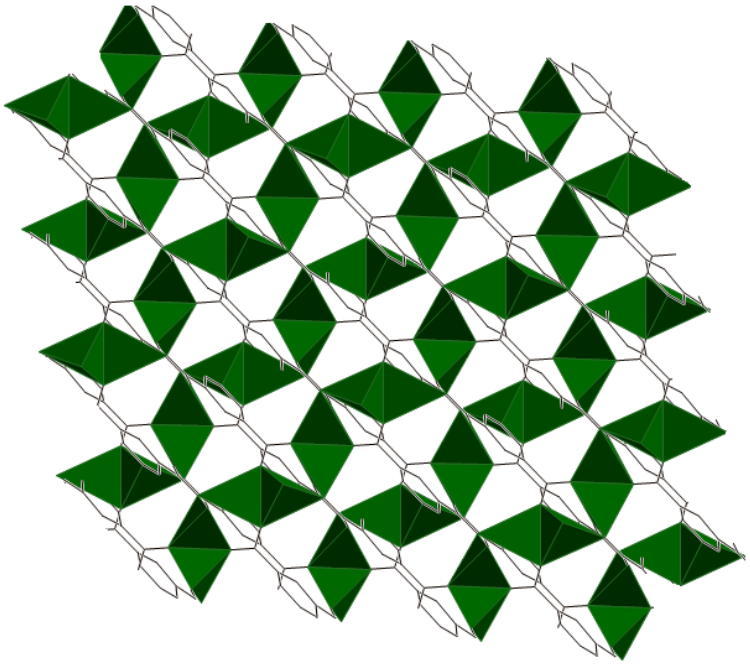

Figure 4.13. View of compound [4.3] (ULMOF-4) looking down the [010] direction.

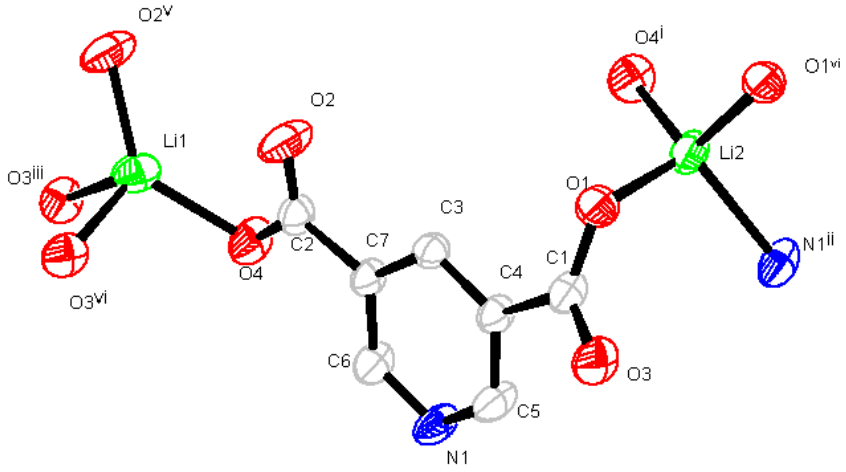

Figure 4.14. ORTEP plot of compound [4.3] (ULMOF-4), illustrating the numbering scheme. Ellipsoids are shown at the 50% probability level. Hydrogen atoms have been omitted for clarity. Symmetry related atoms are shown to complete the coordination sphere of the lithium center. Symmetry operators: i (x, y, z), ii (-x, y, -z+1/2), iii (x+1/2, y+1/2, z), v (-x, -y, -z), vi (x, -y, z+1/2)

Table 4.5. Selected bond lengths (Å) and angles (°) for structure [4.3].

Li(1)-O(2)#1	1.878(6)	O(2)#2-Li(1)-O(3)#3	114.3(3)
Li(1)-O(3)#3	1.992(7)	O(3)#3-Li(1)-O(3)#5	91.4(3)
Li(1)-O(3)#5	1.996(7)	O(3)#3-Li(1)-O(4)	100.9(3)
Li(1)- O(4)	2.044(6)	O(3)#5-Li(1)-O(4)	108.6(3)
Li(2)-O(4)#4	1.865(7)	O(4)#4-Li(2)-O(1)	112.2(3)
Li(2)-O(1)	1.985(7)	O(4)#4-Li(2)-O(1)#1	114.9(3)
Li(2)-N(1)#6	2.120(6)	O(4)#4-Li(2)-N(1)#6	123.5(3)
Li(2)-O(1)#1	1.955(6)	O(1)#1-Li(2)-N(1)#6	103.0(3)

Symmetry codes: #1 -x+1/2, -y+1/2, -z. #2 -x, -y+1, -z+1. #3 -x+1/2, -y+1/2, -z+1. #4 -x, y, -z+1/2. #5 x-1/2, -y+1/2, z+1/2. #6 x, -y, z-1/2.

4.4.4. Structural Description of [4.4], Li_2(2,5-PDC)·(DMF), ULMOF-5

Compound [4.4] consists of tetrameric corner and edge sharing lithium tetrahedral clusters, connected by the organic linkers to form a 3-D network (Fig. 4.15). The organic linker (2,5-PDC), one coordinated DMF molecule and two crystallographically independent lithium metal centers (Li1 and Li2) are present in the asymmetric unit of the compound (Fig. 4.16). Each lithium center is in distorted tetrahedral coordination, with Li1 coordinated to three carboxylate oxygen atoms (O1, O2, O3) and one DMF oxygen (O1M) at distances between 1.892(2) Å to 1.976(3) Å, and Li2 coordinated to three carboxylate oxygen atoms (O1, O4) and one pyridyl nitrogen atom (N1) at distances between 1.901(2) Å to 2.082(3) Å. These Li-coordination geometries are consistent with recently reported lithium based frameworks.[119,120] Further details of coordination geometries are summarized in Table 4.6. The bond valance sum of Li1 and Li2 are calculated as 1.07 and 1.16 v. u. (v. u. = valance unit) close to the expected value of 1.[109]

The tetrameric lithium polyhedral cluster serves as the backbone of compound [4.4]. The edge sharing dimer of Li2 tetrahedra, connected by corner sharing Li1 tetrahedra on both sides composes the tetramer. The average distance between each Li2 center within the dimer is 2.66 Å, while the distance between each corner sharing lithium centers (Li1 and Li2) is on average 3.07 Å. Each of this tetrameric chains are joined by the carboxylate groups of the organic linkers along [001] direction to form a quasi chain of lithium tetrahedra (Fig. 4.17). The DMF molecules are connected with the Li1 center at one the vertex of the tetrahedra.

Each organic linker (2,5-PDC) is associated with a total of six lithium metal centers. Among the four carboxylate oxygen atoms, only O4 and O1 are connected with two lithium centers, while the other two are connected with one lithium center each. Compound [4.4] forms 1-D channel along [001] direction. The coordinated DMF molecules are directed towards each

other within the channel. Four quasi 1-D lithium tetrahedral chains surround each channel. The channels along the [001] direction have dimensions 4.1 Å × 11.4 Å, estimated using van der Waals radii.

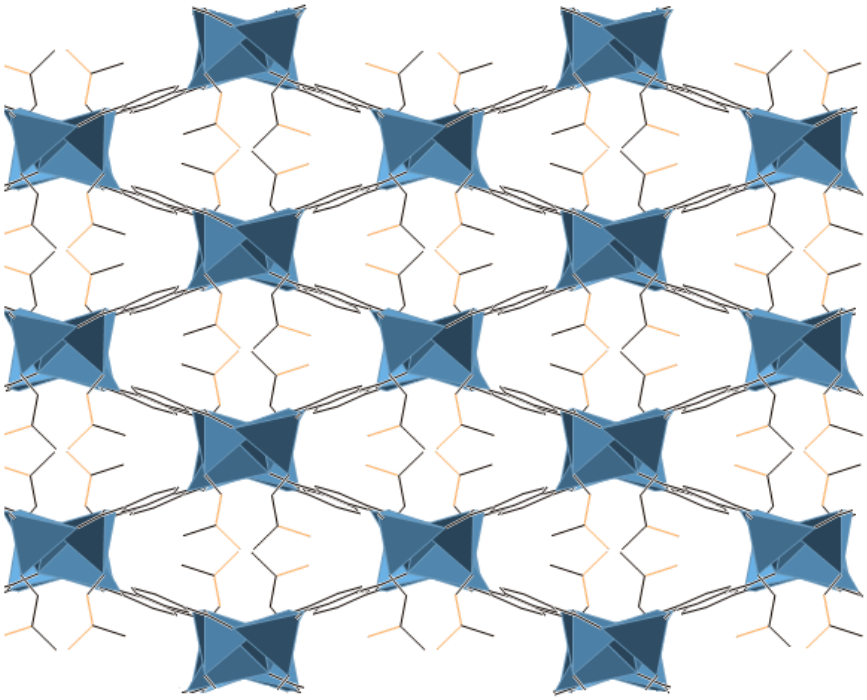

Figure 4.15. View of 3-D network of compound [4.4] (ULMOF-5) from [001] direction.

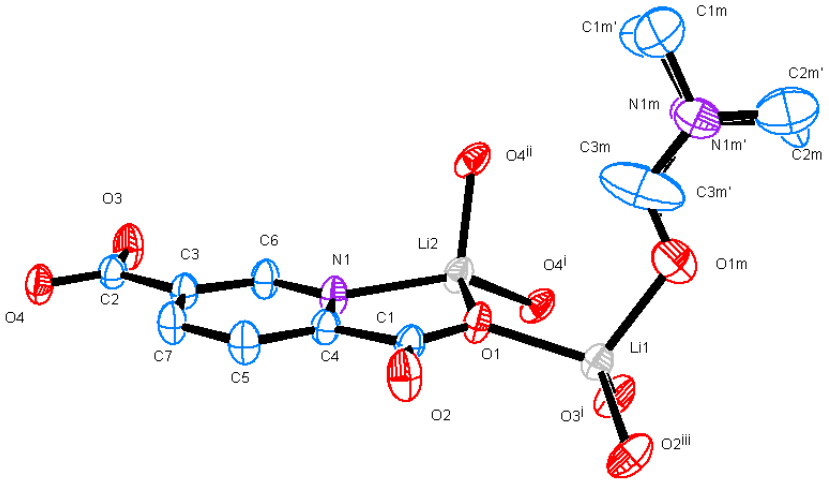

Figure 4.16. Ellipsoidal plot of the asymmetric unit of compound [4.4] (ULMOF-5). Ellipsoids are shown at the 50% probability level. Hydrogen atoms have been omitted for clarity. Symmetry related atoms are shown to complete the coordination sphere of the lithium center. Symmetry operators: i (x, y, z), ii (-x+1/2, -y+1/2, z+1/2), iii (-x, y, -z+1/2).

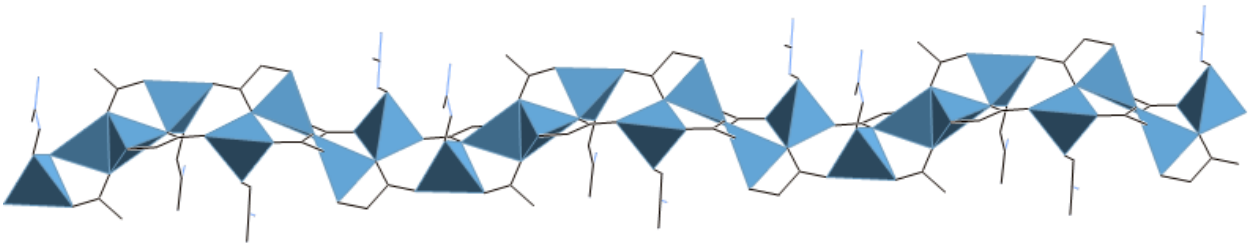

Figure 4.17. The arrangement of lithium tetrahedra from [100] direction (DMF molecules are shown to be connected with the Li1 center).

Table 4.6. Selected bond length (Å) and angle (°) for compound [4.4].

O(1)-Li(1)	1.962(3)	O(2)#1-Li(1)-O(1)	115.36(13)
O(3)-Li(1)	1.975(3)	O(1)-Li(1)-O(3)	107.18(11)
Li(1)-O(2)#1	1.892(2)	O(2)#1-Li(1)-O(1M)	109.49(13)
Li(1)-O(1M)	1.976(3)	O(1)-Li(1)-O(1M)	108.41(13)
O(1)-Li(2)	1.914(3)	O(1)-Li(2)-N(1)	84.15(9)
O(4)-Li(2)	1.901(2)	O(4)#2-Li(2)-N(1)	108.65(11)
N(1)-Li(2)	2.082(3)	O(4)-Li(2)-O(1)	112.54(12)
Li(2)-O(4)#2	1.942(3)	O(1)-Li(2)-O(4)#2	123.74(14)

Symmetry codes: #1 -x, y, -z+1/2, #2 -x, -y+1, -z+1

4.4.5. Discussion

The approach to design multi-dimensional coordination networks is influenced by the coordination geometry of the metal centers and functionality of organic linkers. As an example, in the presence of carboxylate groups, lithium centers commonly form distorted tetrahedra, [58] which cause the position of the functional groups on the organic linker to play a pivotal role in determining the overall topology. Three structural isomers of pyridinedicarboxylic acid were used in the current study with different carboxylate positions with respect to the pyridyl nitrogen. Lithium, a hard acid center is expected to interact with the carboxylate oxygen rather than softer pyridyl nitrogen. However, the position of pyridyl nitrogen appears to be the driving force behind the formation of the structures. Two different types of lithium centers are present in the structures, based on the nature of the coordinating atoms of the ligands. One type of lithium center is coordinated with four oxygen atoms, while the other type is coordinated with three carboxylate oxygen atoms and a pyridyl nitrogen. Lithium metal centers are present in distorted tetrahedral coordination in both cases. The bonding contributions of Li-N bonds are similar to that of Li-O bonds based on calculation of bond-valence. The presence of pyridyl nitrogen between two carboxylate groups, enhances the chelating ability of the ligand (2,6-PDC) to the metal center, constraining the possible coordination modes of the ligand. The effort to increase the dimensionality by (a) increasing the OH^- content of the solution (i.e. the addition of more LiOH) or (b) increasing the reaction temperature to 180°C under similar solvothermal condition, failed to give a higher dimensional structure. The higher temperature reaction under similar molar ratios of the reactants yields a 2-D polymeric layered structure (ULCP-1A). The chelating ability of 2,6-PDC thus proved to be the decisive factor in the formation of both the layered structures (ULCP-1 and ULCP-1A).

The interaction between lithium metal centers and 3,5-PDC and 2,5-PDC on the other hand, generates 3D networks with under similar solvothermal conditions at 180°C. The position of the two carboxylate groups with respect to the pyridyl nitrogen group in 3,5-PDC and 2,5-PDC prevents it from acting as a chelating agent, unlike 2,6-PDC. The higher degree of freedom for possible coordination mode results in 3-D networks: [4.3] and [4.4]. Further, the orientation of carboxylate groups between 3,-5- and 2,5-analogue of PDC, influence the topologies of compounds [4.3] and [4.4] as well.

All four networks are thermally stable over 300°C under N_2 atmosphere. Compound [4.1] follows a two-step decomposition pathway (Fig 4.5). The first weight loss is attributed to the loss of the solvent water and DMA molecules and decarboxylation of one of the carboxylate groups (calculated: 23.35%, observed 23.1%), followed by collapse of the structure at 450°C. Compound [4.2] shows similar thermal stability and decomposes at 425°C in a single step, due to absence of any solvent molecules within the layer (Fig.4.6). The stability of [4.3] is much higher (550^{o}C) than [4.1] and [4.2], as expected due to the 3D nature of the framework (Fig. 4.7). Compound [4.4] shows lower thermal stability than [4.3], with the removal of the coordinated DMF molecule (calculated: 28.9%, observed 29.4%) at 280°C under N_2 atmosphere (Fig. 4.8). The requirement of high temperature to remove the coordinated solvent molecule indicates strong bonding interaction.

The decarboxylation and solvent removal upon heating of compound [4.1] under nitrogen atmosphere motivates us to investigate the mechanism using *in-situ* PXRD technique at 330°C (Fig 4.19). The time dependent *in-situ* PXRD study showed that a new phase is generated upon heating over time. This new phase is formed through an intermediate transitional amorphous phase and is an irreversible transition. Due to its poor crystallinity, we were unable to

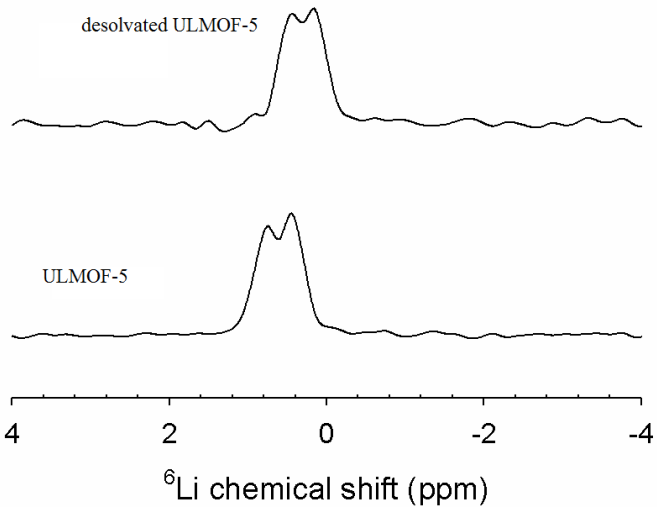

Figure 4.18. ^{6}Li single pulse NMR spectra for compound [4.1] and [4.1a], collected with a spinning rate of 15KHz, pulse delay of 200 s and ca. 300 scans each.

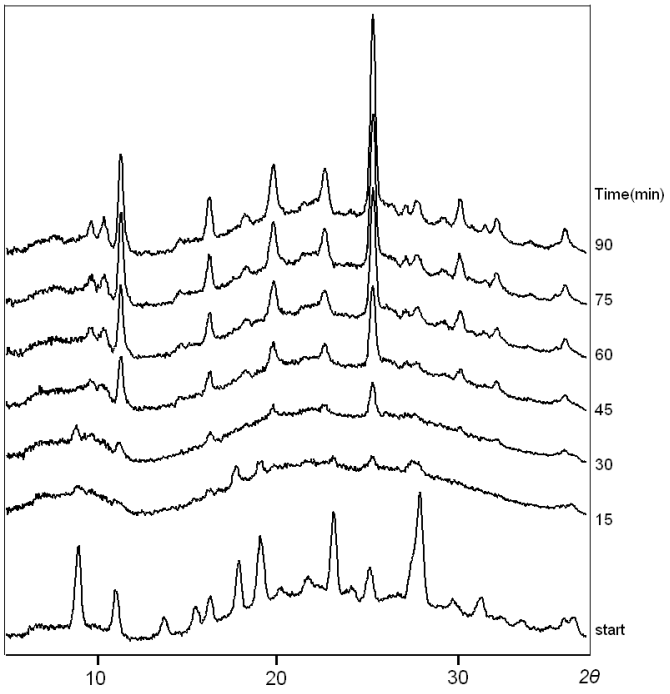

Figure 4.19. *In-situ* diffraction study on compound [4.1] at 330°C demonstrating change in diffraction pattern with time

characterize the final phase using single crystal XRD. The addition of DMF or DMA did not regenerate the initial compound [4.1]. The irreversibility of this process is expected, as the removal of the solvent molecules and the partial decarboxylation of the ligand would destroy the interaction between the layers**.**

Compound [4.4] possesses a theoretical 37% (400 $Å^3$) void space after removal of coordinated DMF molecules from the Li1 center. The removal of coordinated DMF molecules from the channel thus could generate unsaturated lithium sites, the accessibility of which depends on the retention of the pore volume. The desolvated compound [4.4] shows a BET surface area of 25.06m^2/g. The successive H_2 and CO_2 adsorption shows very limited uptake (0.1 wt %) at 77K and 1atm pressure. The low surface area and limited H_2 uptake indicates the destruction of channel after removal of coordinated DMF molecules. Compound [4.4] forms an unidentified polycrystalline phase (compound [4.4a]) upon desolvation as evident from the PXRD pattern (Fig.4.4).

The local structure of lithium centers in compound [4.4] and [4.4a] were investigated by ^{6}Li solid state NMR. Two distinct peaks were observed for compound [4.4] at chemical shift of 0.79 and 1.47 ppm, respectively (Fig. 4.18). These chemical shifts indicate two four-coordination Li environments, consistent with the structure obtained from single crystal X-diffraction data. Compound [4.4a] also showed two different peaks in ^{6}Li NMR, but with two different chemical shifts at 0.81 and 0.17 ppm respectively. The deference in chemical shifts confirms the changes in structure as observed in powder XRD data. The small values of chemical shits do not support the three-coordination Li environment. The absence of 3 coordinated Li center after removal of DMF suggest rearrangement of bonding around lithium site (Li1).

The nature of lithium coordination in both compound [4.4] and [4.4a] were further investigated by solvent exchange studies. Both compound [4.4] and [4.4a] are soluble in water and methanol. Compound [4.4] and [4.4a] do not show any structural change under common organic solvent like ethanol, acetonitrile, acetone, ethyl acetate and dichloromethane, while interestingly compound [4.4a] reverts to the original structure upon soaking with DMF as evident by PXRD. Parent structure can be regenerated by soaking the desolvated form in the coordination solvent in rare occasions depending on the dynamic nature of the framework structure. The observation of the similar phenomenon in this case confirms the presence of ‘dynamic structural behavior’ in lithium-based framework emphasizing the flexibility of the coordination environment around Li1 center and the favorable interaction of lithium center and DMF molecules.

4.5. Conclusion

Two new coordination polymers and two 3-D networks have been synthesized using lithium as the metal center and three structural isomers of pyridinedicarboxylic acid. The networks contain both edge- and corner-sharing lithium tetrahedra, connected by organic linkers. The resulting topologies differ from each other, based on the position of the functional carboxylate groups with reference to the pyridine group in the ring. The detailed structural characterization and thermal study enables us to understand the chemistry of this underexplored and potentially interesting class of materials.

Chapter 5

Synthesis and Structural Characterization of Magnesium Based Coordination Networks in Different Solvents

The content of this chapter is published in

Synthesis and Structural Characterization of Magnesium Based Coordination Networks in Different Solvents. Banerjee D., Finkelstein, J., Smirnov, A., Forster, P. M., Borkowski, L. A., Teat, S. J., Parise, J. B., *Cryst. Growth. Des.* **2011**, 11 (6), 2572-2579

5.1 Abstract

Three magnesium based 3-D coordination networks, $Mg_3(3,5\text{-PDC})_3(DMF)_3 \cdot DMF$ [5.1], $Mg(3,5\text{-PDC})(H_2O)\cdot(H_2O)$ [5.3], $Mg_4(3,5\text{-PDC})_4(DMF)_2(H_2O)_2 \cdot 2DMF \cdot 4.5H_2O$ [5.4], and a layered network, $[Mg(3,5\text{-PDC})(H_2O)_2]$ [5.2] were synthesized using a combination of DMF, methanol, ethanol and water. Compound [5.1] consists of a combination of isolated and corner-sharing magnesium octahedra connected by the organic linkers to form a 3-D network, with 12.2 Å × 4.6 Å channel. The channel contains coordinated and free DMF molecules. In compound [5.2], PDC connects isolated seven coordinated magnesium metal center into a layered structure. Compound [5.3] contains isolated magnesium octahedra connected by the organic linker, forming a 3D network. Compound [5.4] also exhibits a 3D network based on isolated magnesium octahedra with square cavities containing both disordered DMF and water molecules. The structural topologies originate due to the variable coordination ability of solvent molecules with the metal center. Water molecules coordinate with the magnesium metal centers preferably over other polar solvents (DMF, methanol, and ethanol), used to synthesize the coordination networks.

5.2. Introduction

Because of their potential application in gas storage,[17,44,75,76,78,81,121,122] separation,[92,93] catalysis[52,88,123] and conductivity,[124,125] the discovery of new metal organic frameworks (MOFs) or coordination networks (CNs)[1,7,56,74] is of great topical interest. The structural chemistry of MOFs covers a range of organic ligands[96,126] and metal ions.[83,98,116,127] First row transition metals[76,78,82,112] are the most common metal ions, used to construct coordination networks mostly because of their well-known bonding interactions with carboxylates. Recently, networks built with lightweight metal ions (Li, [29,31] Mg, [17,19,83,128] B [113,114]) have been explored due to their potential gravimetric advantage for gas storage applications.

The choice of organic linkers and solvents is critical for varying the coordination behavior of metal ions and determining the overall characteristics of the networks. The isomers of pyridine dicarboxylic acids form a variety of network topologies with first row transition and lanthanide metal ions, because of their diverse coordination modes utilizing carboxylate oxygen atoms and pyridyl nitrogen.[116,117] Solvent often influences the coordination behavior of the metal ions,[129-131] and this behavior may determine the connectivity and dimensionality of the overall framework.[130,132-134] The extent of deprotonation of organic carboxylate linkers, that largely decide its coordination mode, can be controlled by adjusting the basicity of the solvent medium.[18,34] Extra-framework solvent molecules can also influence the thermal and desolvation properties via intermolecular interaction with the parent network.[135,136] In this chapter, we report the solvent-dependent formation of coordination networks based on magnesium ions and 3,5-pyrdinedicarboxylate (PDC), including a layered network, Mg(3,5-PDC)$(H_2O)_2$ [5.2] formed in ethanol or water or 3-D networks [Mg_3(3,5-PDC)$_3$$(DMF)_3$·DMF [5.1], Mg(PDC)$(H_2O)$·$(H_2O)$

[5.3] $Mg_4(3,5\text{-PDC})_4(DMF)_2(H_2O)_2 \cdot 2DMF \cdot 4.5H_2O$ [5.4] formed in DMF, DMF/ethanol and DMF/methanol, respectively.

5.3. Experimental Section

5.3.1. Synthesis

Compounds [5.1] - [5.4] were synthesized under solvothermal conditions using Teflon® – lined 23-mL Parr stainless steel autoclaves. Starting materials include magnesium nitrate hexahydrate ($Mg(NO_3)_2 \cdot 6H_2O$, 99%, Sigma-Aldrich), 3,5-pyridinedicarboxylic acid ($C_7H_3O_4N$, 3,5-PDC, 99%, Sigma-Aldrich), N,N-dimethylformamide (C_3H_7NO, DMF, 99%, Sigma-Aldrich), ethanol (C_2H_5OH, 95%, Fisher) and methanol (CH_3OH, 99.8%, Sigma-Aldrich). Ethanol and methanol were dried overnight over calcium oxide (CaO) before use as reaction solvent.

Synthesis of compound [5.1], $Mg_3(3,5\text{-PDC})_3(DMF)_3 \cdot DMF$

A typical synthesis includes a mixture of $Mg(NO_3)_2 \cdot 6H_2O$ (0.258 g,) and 3,5-PDC (0.17 g) dissolved in 9.5 g of DMF and stirred for 3 hours to achieve homogeneity [molar ratio of metal salt: ligand: solvent = 1:1:130]. The resultant solution was heated for 5 days at 100°C and the product (yield: 60% based on Mg, 0.172 g), was collected as needle shaped crystals by filtration and washed by DMF.

Synthesis of compound [5.2], $Mg(3,5\text{-PDC})(H_2O)_2$

Compound [5.2] was synthesized from a mixture of $Mg(NO_3)_2 \cdot 6H_2O$ (0.255 g) and 3,5-PDC (0.167 g) dissolved in 6 g of ethanol, which was stirred for 2 hours [molar ratio of metal salt: ligand: solvent=1:1:130]. The resultant solution was heated for 5 days at 100°C. The

product was collected as needle shaped crystals (yield: 50% based on Mg, 0.112 g) by filtration and rinsed with ethanol.

Synthesis of compound [5.3], $Mg(3,5\text{-}PDC)(H_2O)\cdot(H_2O)$

Compound [5.3] was synthesized by dissolving $Mg(NO_3)_2\cdot 6H_2O$ (0.257 g) and 3,5-PDC (0.168 g) in a mixture of DMF (4.7 g) and ethanol (2.99 g) and stirred for 1 hour [molar ratio of metal salt: ligand: DMF : Ethanol=1:1: 65 :65]. The resulted solution was heated for 5 days at 100 °C. The product was obtained as crystalline material (Yield 60% based on Mg, 0.135g) by filtration and washed with ethanol.

Synthesis of compound [5.4], $Mg_4(3,5\text{-}PDC)_4(DMF)_2(H_2O)_2\cdot 2DMF\cdot 4.5H_2O$

Compound [5.4] was synthesized by dissolving $Mg(NO_3)_2\cdot 6H_2O$ (0.261 g) and 3,5-PDC (0.171 g) in a mixture of DMF(4.7 g) and ethanol (2.08 g) and stirred for 2 hour to achieve homogeneity [molar ratio of metal salt: ligand: DMF : methanol=1:1:65 :65]. The resulted solution was heated for 5 days at 100°C. A yellow colored phase was collected by filtration as a side product along with needle shaped crystals of compound [5.4]. Efforts to obtain a pure phase of compound [5.4] by (a) increasing reaction temperature or (b) increasing solvent ratio were not successful.

5.3.2. X-ray crystallography

Suitable crystals of compounds [5.1] - [5.4] were selected from bulk samples and were mounted on glass fibers using epoxy adhesive. The microcrystalline nature of the compounds [5.1] and [5.2], formed under the reaction conditions described above, prevented full structure elucidation from data collected on in-house X-ray sources. Synchrotron X-ray sources at the Advanced Photon Source ChemMatCars beamline, and at the Advanced Light Source 11.3.1 microcrystal diffraction beam line, were used to collect low temperature (100K) single crystal diffraction data for compounds [5.1] and [5.2], respectively. Reflection data for compound [5.1] were collected using a three-circle Bruker D8 diffractometer equipped with an APEXII detector (λ = 0.41328 Å) with 0.5° φ scans. The raw intensity data were analyzed using the APEXII suite of programs,[69] and were corrected for absorption effects using SADABS.[67] Reflection data for compound [5.2] were collected using 180° ω scans, at 0.3° steps, with setting of φ = 90°, 180° and 270° on a similar instrument to that described for [5.1], using X-rays with λ = 0.7749 Å. For compound [5.2], program Cell_Now[137] identified a 2-component twin with domains related by a 180° rotation about reciprocal axis [0 1 1]. The data were integrated using APEXII software, [69] applying the orientation matrices for both twin components and were corrected for absorption effects using TWINABS.[108] The intensity data were output in both SHELXTL HKLF4 and HKLF5 file formats.

Reflections for compounds [5.3] - [5.4] were collected using a Bruker four circle P4 single crystal diffractometer equipped with a SMART 1K CCD detector at room temperature (298K) with Mo Kα radiation (λ= 0.71073 Å) and φ and ω scans. The raw intensity data were collected and integrated with software packages, SMART[65] and SAINT[66] respectively. An empirical absorption correction was applied using SADABS.[67]

The structures were solved using direct methods and were refined using SHELXL.[67] All non-hydrogen atoms were refined anisotropically with the hydrogen atoms placed in idealized positions using geometrical constraints. Four DMF molecules are present in the asymmetric unit of compound [5.1]. Three of them are coordinated to metal ions and one is present in an uncoordinated state within the channel. The uncoordinated and two of the coordinated DMF molecules are found disordered and were modeled using the PART command in SHELXL.[67] The coordinated DMF molecules were found disordered over the C, N positions with site occupancies of 68.1(1)% and 54.7(1)% for the major component. The uncoordinated DMF molecule is disordered over all the atom positions and site occupancy was refined to 61.8(1)% for the major component. Table 5.1 lists the crystallographic parameters from the refinements of [5.1] - [5.4]. The unit cell of compounds [5.3] and [5.4] contains highly disordered solvent molecules. We were not able to assign the residual electron density peaks in case of compound [5.3]. TGA-DSC data was used to determine the possible nature of the solvent species within the channel. For compound [5.4], the residual electron density peaks in the channel were assigned as heavily disordered water and DMF molecules.

Table 5.1: Crystallographic data and structural refinement details of compound [5.1] - [5.4]

	[5.1]	[5.2]	[5.3][a]	[5.4][a]
Empirical formula	$C_{33}H_{37}N_7O_{16}Mg_3$	$C_7H_7NO_6Mg$	$C_7H_5NO_5Mg$	$C_{17}H_{15}N_3O_{10}Mg_2$
Formula weight	860.63	225.45	207.43	469.94
Collection Temperature(K)	100(2)	100(2)	298(2)	298(2)
Wavelength (Å)	0.41328	0.77490	0.71073	0.71073
Space Group	$P\ 2_1/n$	$C\ 2/c$	$P\ 6_122$	$P\ 2_1/c$
a (Å)	12.3475(5)	9.9364(5)	11.479(1)	13.7442(14)
b (Å)	11.1929(5)	12.0694(6)	11.479(1)	14.2887(15)
c (Å)	28.673(1)	7.2763(4)	14.735(3)	16.9809(13)
β (°)	98.816(1)	106.49(1)°	90	126.545(5)
Volume ($Å^3$)	3916.0(3)	836.70(7)	1681.7(4)	2679.2(4)
Z	4	4	6	4
Calculated Density(g/cm^3)	1.460	1.790	1.229	1.165
Absorption coefficient (mm^{-1})	0.037	0.270	0.154	0.137
F(000)	1792	464	636	968
Crystal size (mm)	0.06 x 0.03 x 0.01	0.1 x 0.04 x 0.04	0.3 x 0.2 x 0.06	0.3 x 0.17 x 0.08
Θ range of data collection	1.11-16.00	2.97 -33.68	2.05 -26.72	1.84 - 26.73
Index range	$-13 \le h \le 16$	$-14 \le h \le 13$	$-13 \le h \le 14$	$-17 \le h \le 16$
	$-14 \le k \le 14$	$0 \le k \le 17$	$-13 \le k \le 14$	$-17 \le k \le 18$
	$-38 \le l \le 36$	$0 \le l \le 10$	$-16 \le l \le 18$	$-21 \le l \le 19$
Total reflection	74698	8262	11624	17953
Independent reflection	9731 [R(int) = 0.0681]	1258 [R(int) = 0.0630]	1205 [R(int) = 0.0366]	5648 [R(int) = 0.0422]
Goodness of fit	1.037	1.071	1.102	1.067
Refinement method	Full matrix least squares on F^2	Full matrix least squares on F^2	Full matrix least squares on F^2	Full matrix least squares on F^2
Data/ Restraints/parameter	9731 / 21 / 674	1258 / 2 / 76	1205 / 0 / 67	5648 / 0 / 291
R1($on\ F_o^2,\ I>2\sigma(I)$)	0.0530	0.0521	0.0239	0.0473
wR2 ($on\ F_o^2,\ I> 2\sigma(I)$)	0.1382	0.1611	0.0662	0.1318

[a] data based on the PLATON/SQUEEZE model[138]

5.3.3. Powder XRD and thermal analysis

Bulk sample identification and phase purity were determined using powder X-ray diffraction. The data were collected using a Scintag Pad-X diffractometer equipped with Cu Kα (λ= 1.5405 Å) radiation within a range of $5° \leq 2\theta \leq 40°$ (step size: 0.02°, counting time: 1s/step. Comparison of the observed and calculated powder XRD patterns for [5.1] - [5.3] confirmed phase purity (Figs. 5.1-5.3)

Combined TGA-DSC experiments for compounds [5.1] - [5.3] were performed using a Netzsch 449C Jupiter instrument. The samples were heated from room temperature to 750°C under a N_2 atmosphere with a heating rate of 10°C/minute (Figs. 5.4-5.6).

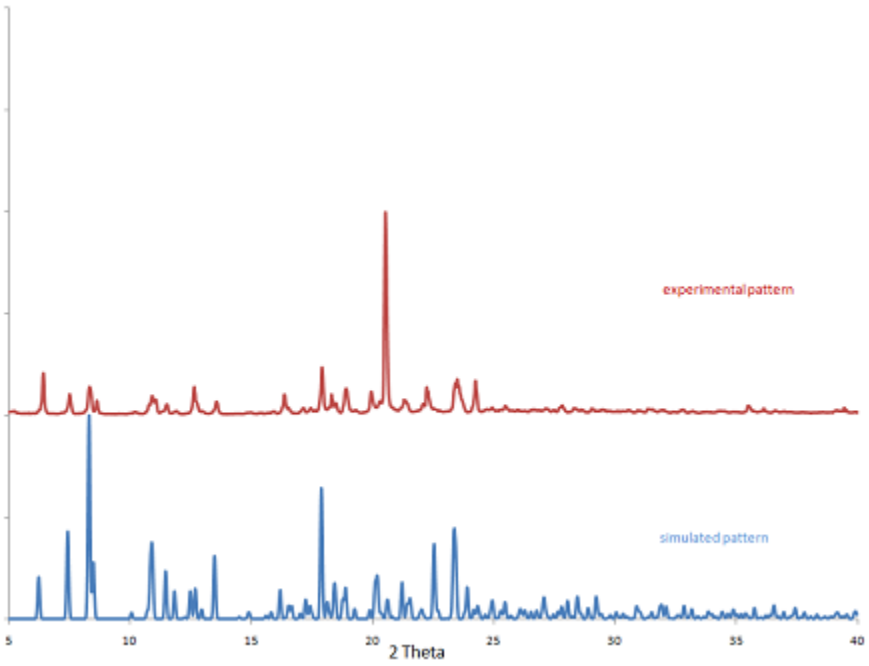

Figure. 5.1. Simulated and experimental PXRD of compound [5.1]

.

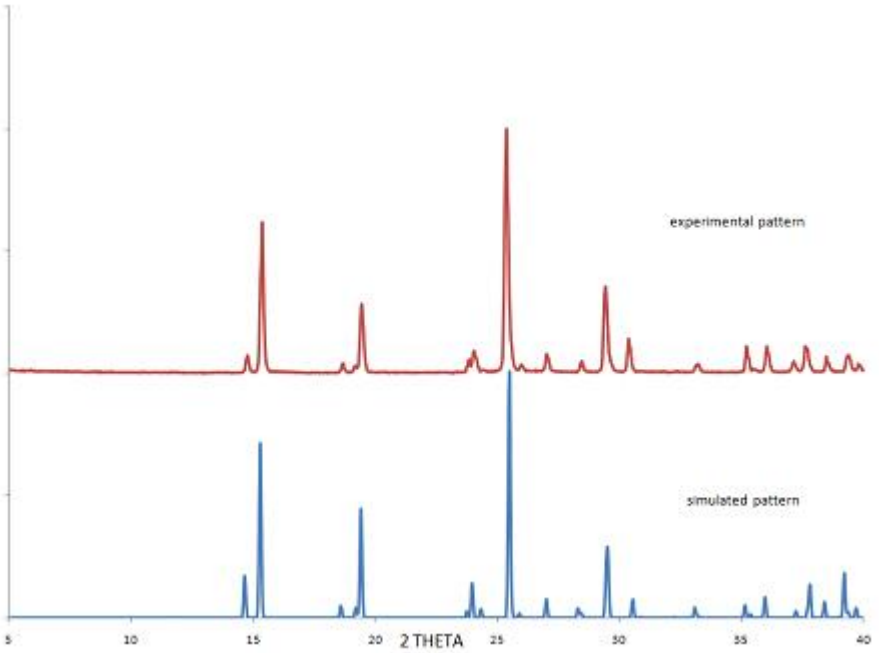

Figure. 5.2. Simulated and experimental PXRD of compound [5.2]

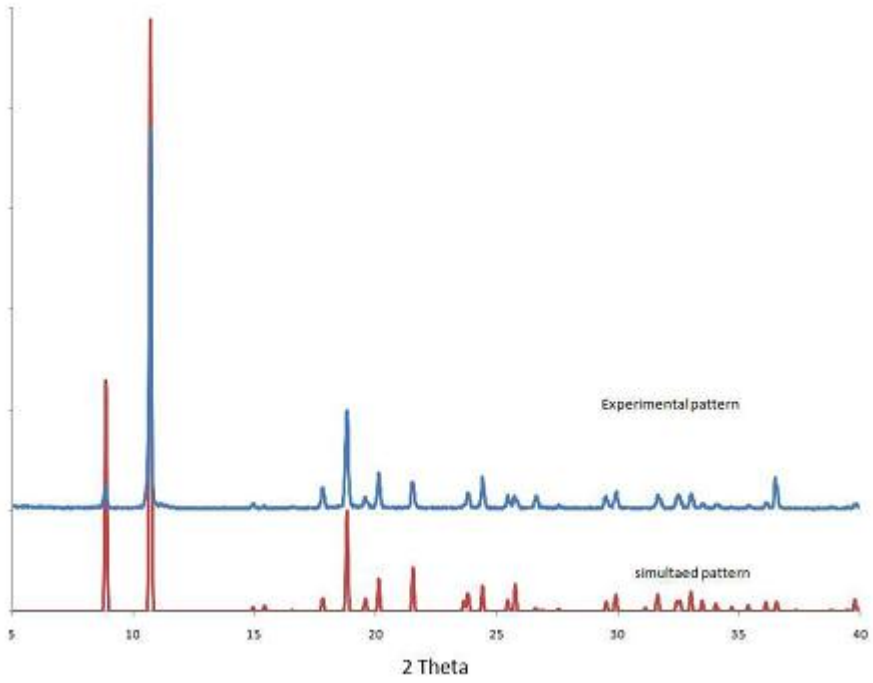

Figure. 5.3. Simulated and experimental PXRD of compound [5.3]

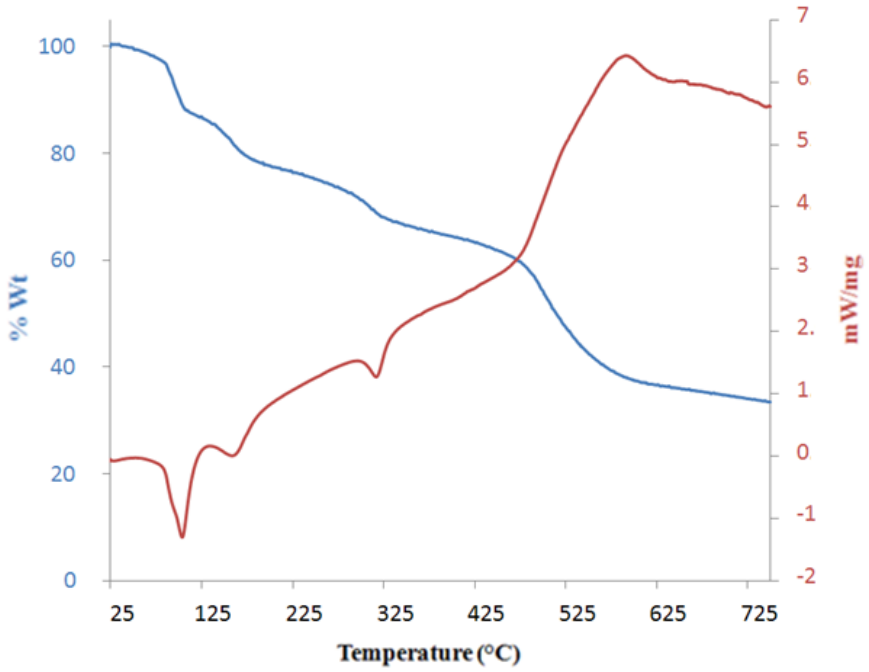

Figure. 5.4. Combined TGA-DSC plot of compound [5.1]. The blue line represents the TGA plot while the red line shows the associated DSC signal.

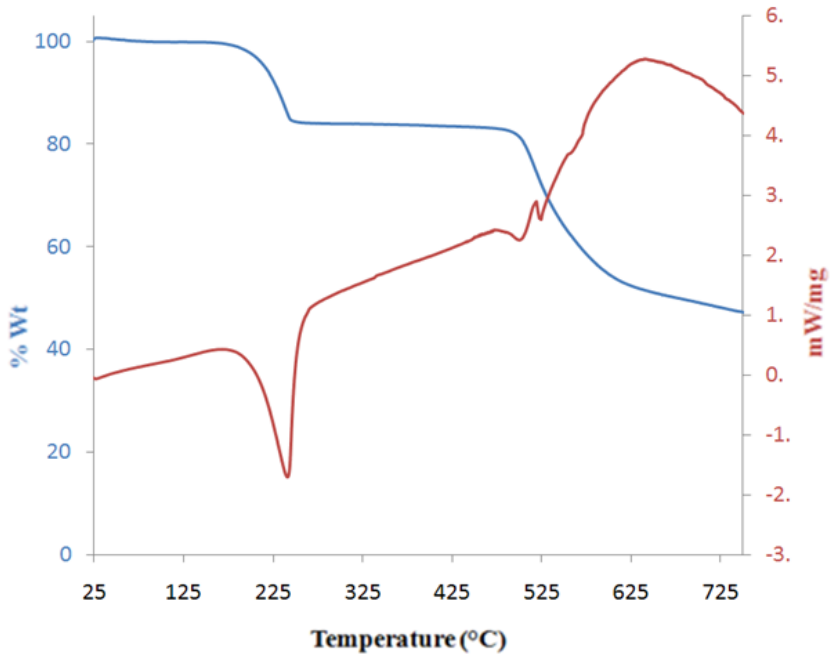

Figure 5.5. Combined TGA-DSC plot of compound [5.2]. The blue line represents the TGA plot while the red line shows the associated DSC signal.

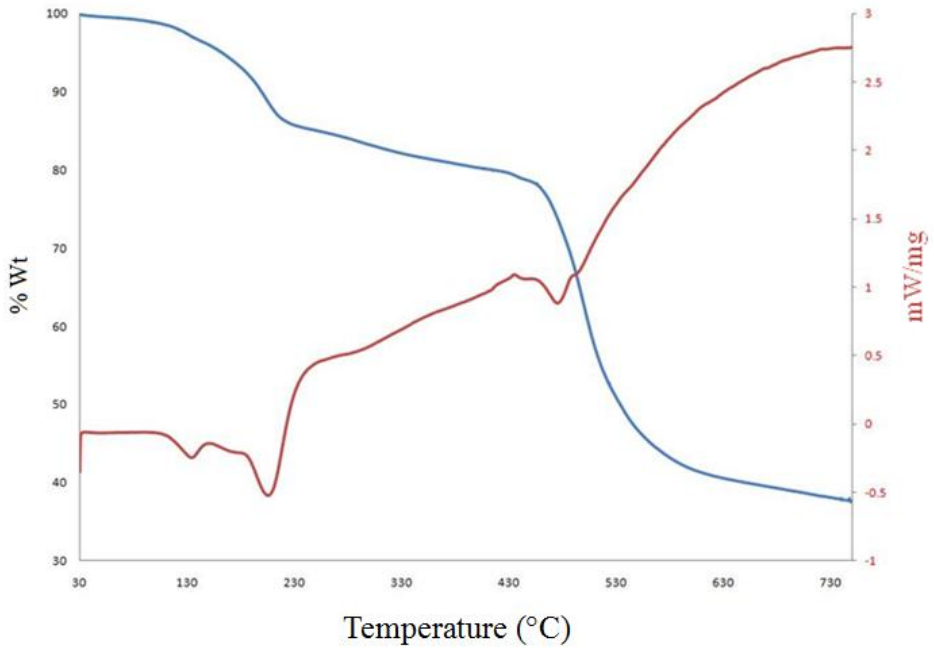

Figure 5.6. Combined TGA-DSC plot of compound [5.3]. The blue line represents the TGA plot while the red line shows the associated DSC signal.

5.4. Results and Discussion

5.4.1. Structural description of [5.1], $Mg_3(3,5\text{-}PDC)_3(DMF)_3 \cdot DMF$

There are three unique magnesium environments in compound [5.1]; the Mg1-octahedron is isolated while Mg2 and Mg3 octahedra form a corner-sharing dimer. Three crystallographically independent PDC linkers bridge these magnesium atoms forming a 3-D network decorated by four unique DMF molecules (Fig. 5.7). All Mg-sites exhibit distorted octahedral coordination by carboxylate oxygen and pyridyl nitrogen atoms, from the ligand as well as solvent DMF molecules, with bond distances between 2.006(2) Å [Mg1-O6] to 2.237(2) Å [Mg3-N2]. Selected bond distances are summarized in Table 5.2. The bond valence sums of the magnesium ions are 2.163 v. u., 2.174 v. u. and 2.12 v. u. for sites Mg1, Mg2 and Mg3, respectively, matching the expected value of +2 v. u. (valence unit).[109]

The isolated magnesium octahedra are connected with the dimeric corner sharing magnesium octahedra through carboxylate oxygen atoms along [010] direction. The magnesium polyhedra are further connected in [100] and [001] direction, through pyridyl nitrogen and carboxylate oxygen atoms of PDC linker, forming channels filled with both coordinated and free DMF molecules. The solvent molecules exhibit various degrees of disorder. The dimensionalities of the channels are on average 12.2 Å × 4.6 Å along the [010] direction, when calculated based on van dar Waals radii, in absence of both coordinated and free DMF molecules in the channel. Calculations using PLATON indicate a 51.5% (2018.2 $Å^3$) void space after removal of coordinated and free DMF molecules from the channel.[138]

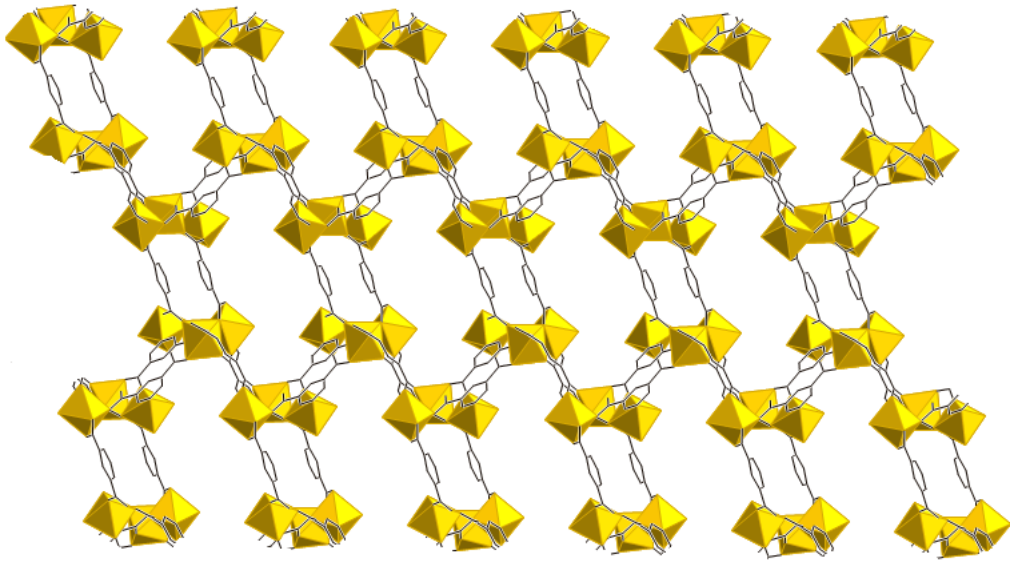

Figure 5.7. View of compound [5.1] from the [010] direction, showing the connectivity of the organic linkers with the magnesium octahedra.

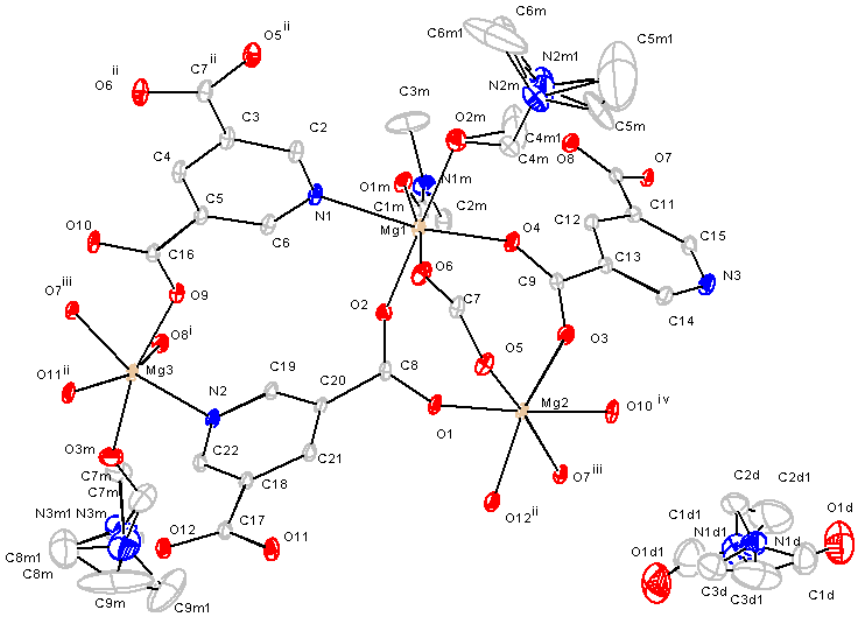

Figure 5.8. ORTEP view of compound [5.1] illustrating the numbering scheme. Ellipsoids are shown at 50% probability level. Hydrogen atoms are omitted for clarity. Symmetry related atoms are shown to complete the organic ligand and coordination sphere of the magnesium centers. Symmetry operators: i (x, y, z), ii (-x+1/2, y+1/2, -z+1/2), iii (-x, -y, -z), iv (x+1/2, -y+1/2, z+1/2).

Table 5.2. Selected interatomic distances (Å) and angles (°) for compound [5.1].

Mg(1)-O(6)	2.006(2)	Mg(3)-O(8)#5	2.139(2)
Mg(1)-O(4)	2.048(2)	Mg(3)-O(7)#5	2.185(2)
Mg(1)-O(2)	2.089(2)	Mg(3)-N(2)	2.237(2)
Mg(1)-O(2M)	2.120(2)	O(6)-Mg(1)-O(4)	102.36(7)
Mg(1)-N(1)	2.254(2)	O(4)-Mg(1)-O(1M)	85.85(7)
Mg(1)-O(1M)	2.070(2)	O(4)-Mg(1)-O(2)	93.92(7)
Mg(2)-O(1)	2.028(2)	O(1M)-Mg(1)-O(2M)	93.11(8)
Mg(2)-O(3)	2.038(2)	O(1)-Mg(2)-O(3)	95.86(7)
Mg(2)-O(5)	2.045(2)	O(1)-Mg(2)-O(5)	93.09(7)
Mg(2)-O(7)#3	2.206(2)	O(3)-Mg(2)-O(5)	101.58(7)
Mg(2)-O(10)#2	2.074(2)	O(12)#1-Mg(2)-O(5)	86.81(7)
Mg(2)-O(12)#1	2.042(2)	O(9)-Mg(3)-N(2)	80.31(7)
Mg(3)-O(11)#4	2.004(2)	O(3M)-Mg(3)-N(2)	89.67(8)
Mg(3)-O(9)	2.039(2)	O(9)-Mg(3)-O(7)#5	86.96(7)
Mg(3)-O(3M)	2.050(2)	O(3M)-Mg(3)-O(7)#5	101.63(8)

Symmetry codes: #1 -x+1/2, y-1/2, -z+1/2, #2 x, y-1, z, #3 -x+1, -y+1, -z, #4 -x+1/2, y+1/2, z+1/2, #5 -x+1, -y+2, -z

5.4.2. Structural description of [5.2], Mg(3,5-PDC)(H_2O)$_2$

Compound [5.2] consists of isolated Mg-monomers connected by the organic linkers to form a layered structure (Fig. 5.9). The asymmetric unit of compound [5.2] consists of a crystallographically unique magnesium ion, a portion of the organic linker (3,5-PDC) and one water molecule bound to magnesium metal center (Fig. 5.10). The magnesium ion, pyridyl nitrogen and one carbon atom (C4) of the aromatic ring lie on a special position (Wyckoff position *e*, site symmetry 2) with site occupancy factor of 1/2. The coordination environment for the magnesium is assigned to rare pentagonal bipyramidal geometry, consistent with bond valence calculations (expected: 2.00, calculated: 1.94).[109] Each magnesium ion connects with three organic ligands through bidentate chelating carboxylate oxygen atoms (O2, O3) and pyridyl nitrogen (N8). Two water molecules are coordinated with the magnesium metal center with 2.04 Å average bond lengths.

Each organic ligand is connected with three magnesium ions along the [110] and [-110] directions to form the basis of the layered network; Mg coordination sites that might lead to connectivity in the third dimension are occupied by terminal water molecules. The distance between successive layers are on average 3.64 Å along the [001] direction. No significant π-π packing occurs; instead, interlayer interactions are primarily through hydrogen bonds between the bound water molecule (O1w) and the carboxylate oxygen atoms (O2, O3) in the adjacent layer (O-O distances 2.751 Å and 2.761Å).

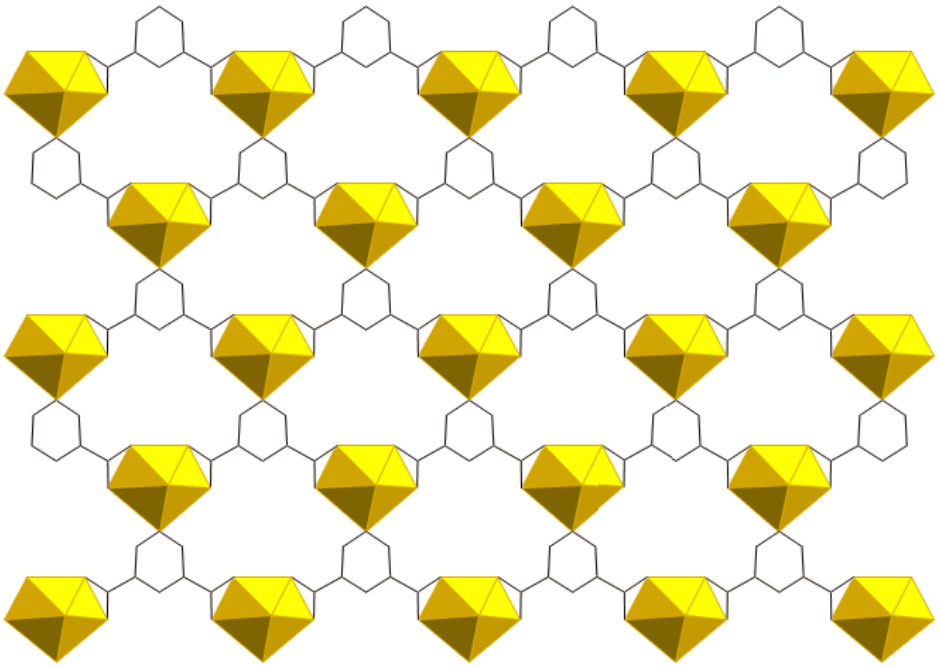

Figure. 5.9. View of compound [5.2] from the [001] direction showing the connectivity of the organic linker with the magnesium metal ions

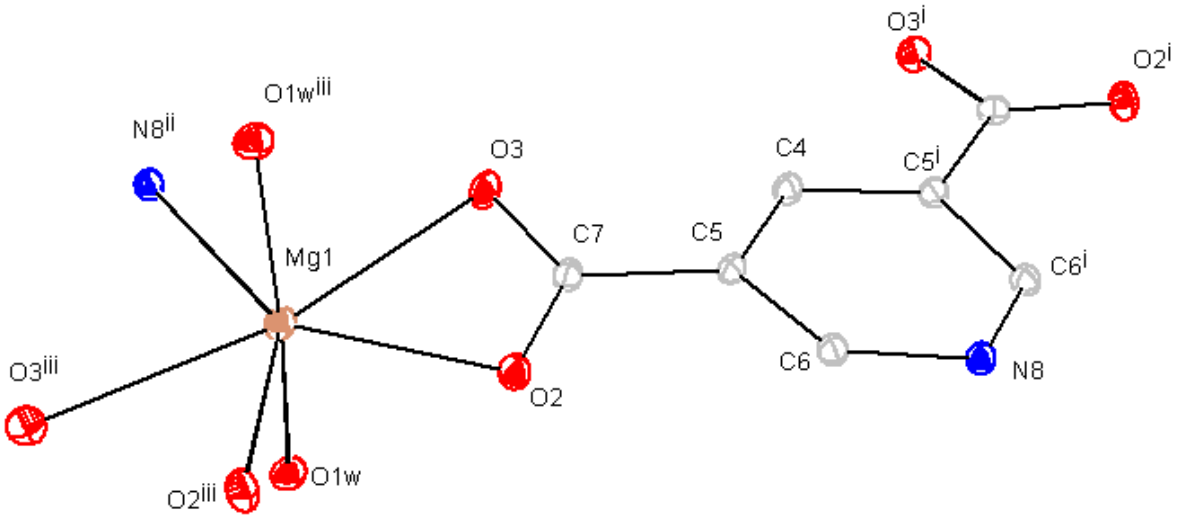

Figure. 5.10. ORTEP view of compound [5.2] illustrating the numbering scheme. Ellipsoids are shown at 50% probability level. Hydrogen atoms are omitted for clarity. Symmetry related atoms are shown to complete the organic ligand and coordination sphere of the magnesium metal ions. i Symmetry operator : (x, y, z), ii (-x, y, -z+1/2), iii (x+1/2, y+1/2, z)

Table 5.3. Selected interatomic distances (Å) and angles (°) for compound [5-2].

Mg(1)-O(1W) (×2)	2.032(1)	O(1W)-Mg(1)-O(1W)#1	172.04(7)
Mg(1)-O(2) (×2)	2.148(1)	O(1W)-Mg(1)-O(2)	90.10(4)
Mg(1)-O(3) (×2)	2.423(1)	O(1W)#1-Mg(1)-O(2)	95.98(4)
Mg(1)-N(8)#2	2.290(2)	O(2)#1-Mg(1)-N(8)#2	139.73(3)
N(8)-C(6)	1.348(1)	O(2)#1-Mg(1)-O(2)	80.53(6)

Symmetry codes: #1 -x+1, y, -z+1/2, #2 x+1/2, y+1/2, z.

5.4.3 Structural Description of [5.3], Mg(3,5-PDC)(H_2O)·(H_2O)

Compound [5.3] contains isolated magnesium-centered octahedra connected by the organic linkers to form a 3-D network (Fig. 5.11). The asymmetric unit of compound [5.3] contains one crystallographically unique magnesium metal center, portion of the organic linker (3,5-PDC) and one bound water molecule (Fig. 5.12). The octahedral coordination of the magnesium center has contributions from four carboxylate oxygen atoms (O1, O2), one pyridyl nitrogen (N1) and the oxygen atom from a coordinating water molecule. The bond distance varies between 2.025 Å (Mg1-O1) and 2.252 Å (Mg1-N1) with a bond valence sum for magnesium calculated as 2.17 v. u. matching well with the expected value of +2.[109]

Each magnesium center in compound [5.3] is associated with five organic linkers through bonding with four carboxylate oxygen atoms and one pyridyl nitrogen. The other coordination is occupied by the oxygen atom of the water molecule. This type of connectivity leads to formation of a circular shaped channel of approximately 5.5 Å diameter along the [001] direction, containing coordinated water molecules. Highly disordered solvent molecules are present within the void accounting for approximately 36.7% (617 $Å^3$) of the unit cell's volume.[138]

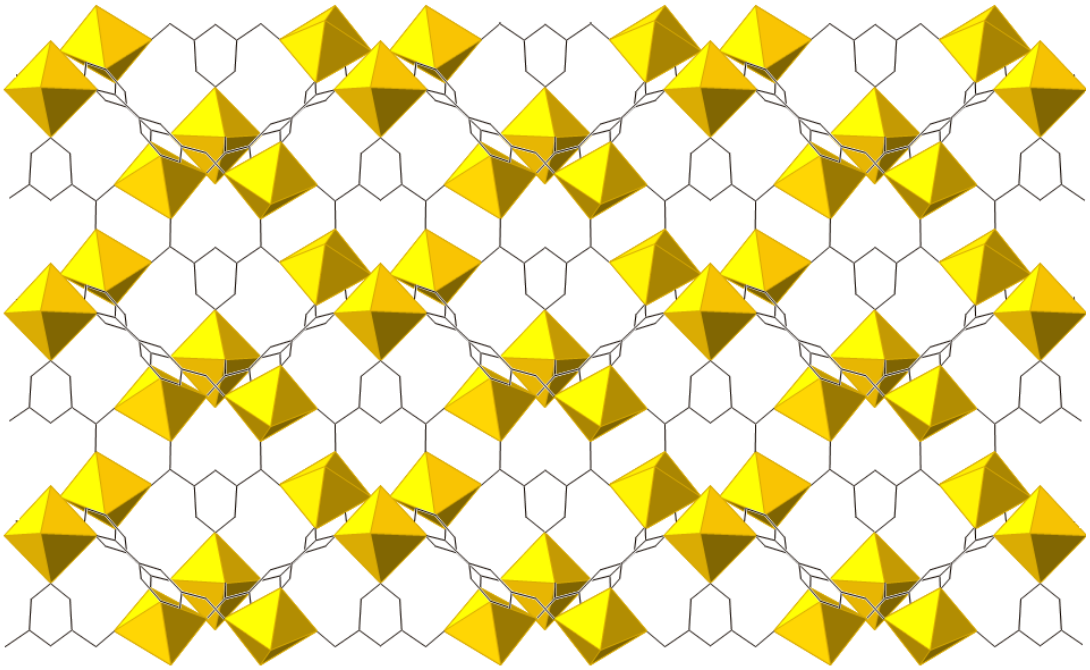

Figure 5.11. View of compound [5.3] from the [010] direction, showing the connectivity of the organic linker with the magnesium metal ions.

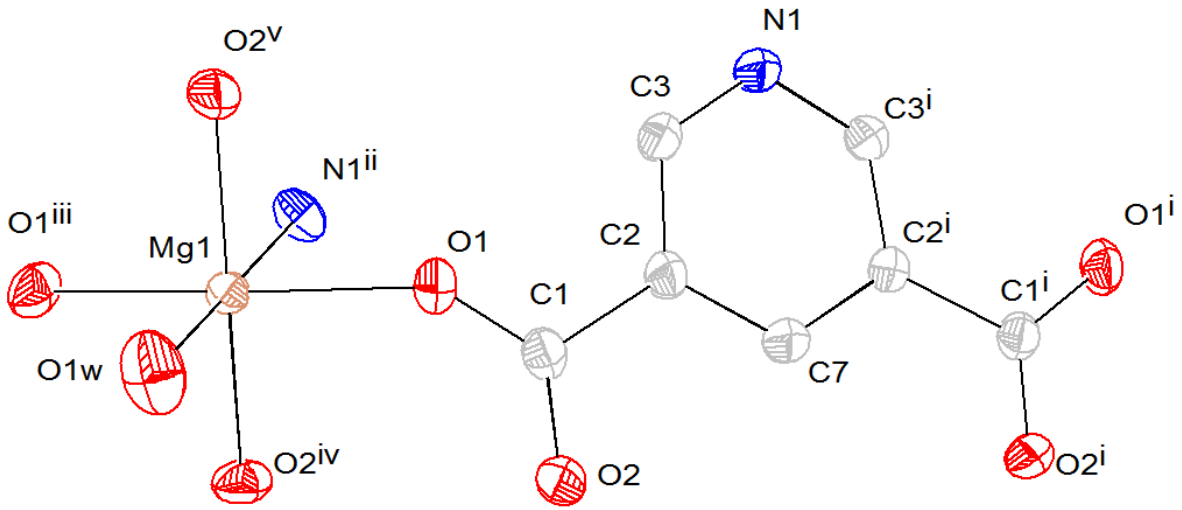

Figure 5.12. ORTEP view of compound [5.3] illustrating the numbering scheme. Ellipsoids are shown at 50% probability level. Hydrogen atoms are omitted for clarity. Symmetry related atoms are shown to complete the organic ligand and coordination sphere of the magnesium metal ions. Symmetry operators: i (x, y, z) ii (x-y, x, z+5/6), iii (-y, x-y, z+2/3), iv (-x, -y, z+1/2) v. (-x+y, -x, z+1/3).

Table 5.4. Selected interatomic distances (Å) and angles (°) for compound [5.3].

Mg(1)-O(1)	2.091(1)	O(2)#1-Mg(1)-O(3)	90.36(4)
Mg(1)-O(2)#1	2.024(1)	O(2)#1-Mg(1)-O(1)#3	93.94(4)
Mg(1)-N(1)#4	2.2533(1)	O(2)#2-Mg(1)-O(1)#3	86.02(4)
Mg(1)-O(3)	2.090 (1)	O(2)#2-Mg(1)-N(1)#4	89.64(4)

Symmetry codes: #1 x-y, x, z+1/6, #2 y, x,-z+1/3, #3 -x+y, y,-z+1/2, #4 -y+1, x-y+1, z+1/3

5.4.4 Structural description of [5.4], $Mg_4(3,5\text{-}PDC)_4(DMF)_2(H_2O)_2 \cdot 2DMF \cdot 4.5H_2O$

Compound [5.4] is formed from a combination of corner sharing dimers of magnesium polyhedra, connected by organic linkers forming a 3-D network (Fig. 5.13). The asymmetric unit of compound [5.4] contains two crystallographically independent metal centers, two organic linkers along with a coordinated DMF and water molecule (Fig. 5.14). Both the magnesium centers are present in distorted octahedral coordination with oxygen and nitrogen atoms of the ligand, and oxygen atoms from the coordinating water and DMF molecules, with bond distance varying between 1.986(2) Å [Mg2-O4] to 2.743(2) Å [Mg2-O7] (Table 5.5). The bond valence sums [53] of the magnesium metal centers (Mg1 and Mg2) are 2.212 v. u. and 2.1 v. u., respectively, matching well with the expected value of +2 v. u.[109]

Each magnesium polyhedra is connected with others in corner sharing fashion through carboxylate oxygen atom (O7) forming a dimer. Each dimer is further connected by functional groups (carboxylate oxygen atoms and pyridyl nitrogen) of the organic linkers in all three crystallographic directions. Such an arrangement leads to the formation of diamond shaped 1-D channels with average size of 8.5 Å × 3.5 Å. Coordinated and uncoordinated solvent molecules including DMF and water are present in the channels. PLATON indicates a 32.1 % (858.7 $Å^3$) void space after removal of free DMF and water molecules from the channel.[138]

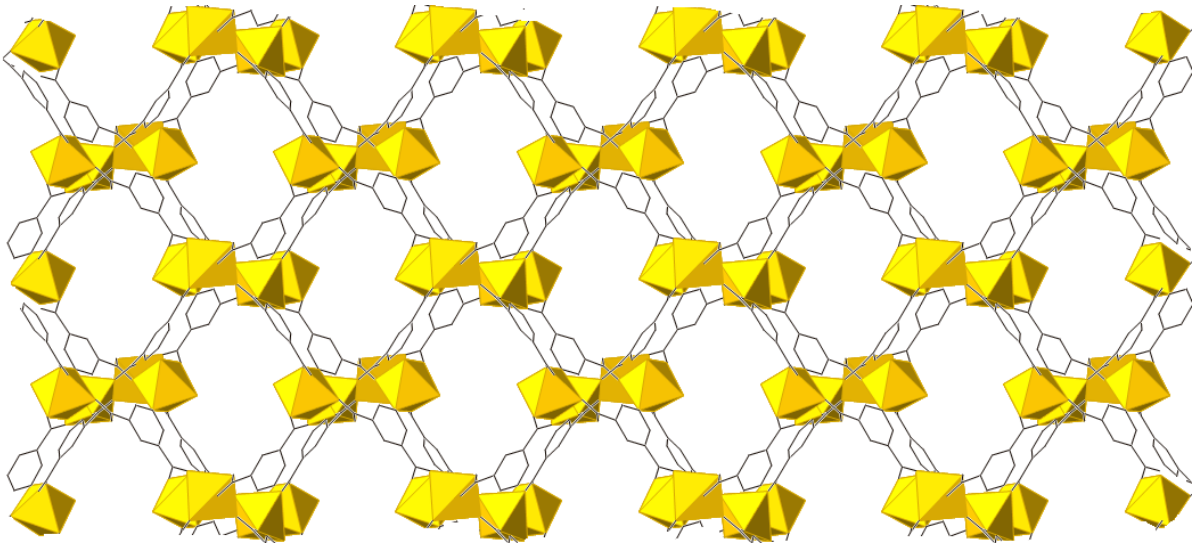

Figure 5.13.View of compound [5.4] from the [100] direction, showing the connectivity of the organic linker with the magnesium metal ions.

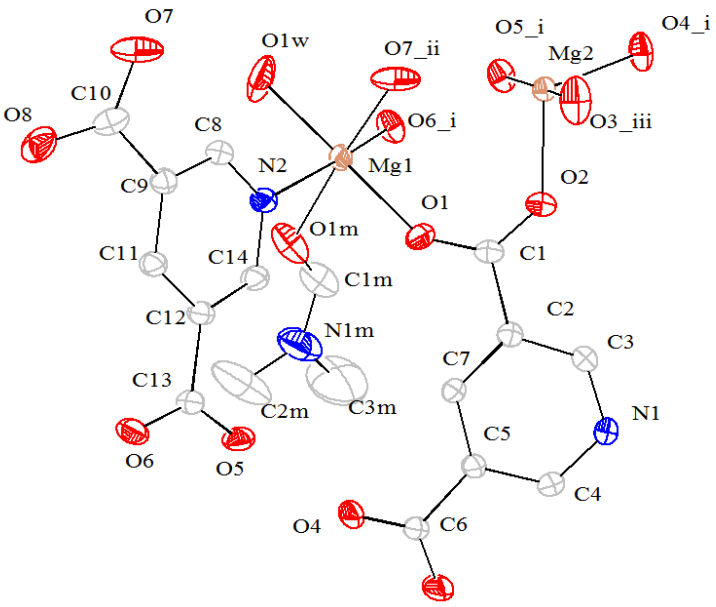

Figure 5.14. ORTEP view of compound [5.4] illustrating the numbering scheme. Ellipsoids are shown at 50% probability level. Hydrogen atoms are omitted for clarity. Symmetry related atoms are shown to complete the organic ligand and coordination sphere of the magnesium metal ions. Symmetry operators: i (x, y, z) ii (-x, y+1/2, -z+1/2), iii (-x, -y, -z).

Table 5.5. Selected interatomic distances (Å) and angles (°) for compound [5.4].

Mg(1)-O(6)	2.028(1)	O(6)-Mg(1)-O(1)	95.64(7)
Mg(1)-O(1)	2.032(1)	O(1)-Mg(1)-O(1W)	178.50(9)
Mg(1)-O(1W)	2.061(1)	O(1)-Mg(1)-O(7)	88.85(8)
Mg(1)-O(7)	2.066(1)	O(1W)-Mg(1)-O(7)	90.50(11)
Mg(1)-O(1M)	2.109(2)	O(6)-Mg(1)-O(1M)	87.90(7)
Mg(1)-N(2)	2.233(1)	O(4)-Mg(2)-O(2)	109.22(8)
Mg(2)-O(4)	1.987(1)	O(5)-Mg(2)-O(2)	93.34(8)
Mg(2)-O(5)	2.024(1)	O(4)-Mg(2)-O(5)	86.66(7)
Mg(2)-O(2)	2.032(1)	O(4)-Mg(2)-O(8)	105.13(8)

5.4.5. Discussion

The dimensionality of the networks produced in this study is determined by the coordination environment of magnesium, which is clearly dictated by the coordinating strength of the solvent molecules. A total of four different coordination networks were synthesized based on the selection of reaction solvents (Table 5.6), while the other synthetic parameters were intentionally held constant. The reaction in pure DMF results in the formation of compound [5.1], while compound [5.2] forms in either pure ethanol or water. Surprisingly, the same reaction employed in pure methanol results in clear solution. Given the intermediate polarity and relative permittivity of methanol compared to water and ethanol, this is not an intuitive result. Since water from the hydrated metal salt used in synthesis is present in sufficient quantities to hydrate, but at a much lower concentration than ethanol, we can conclude that solvation by water is more favorable than by ethanol especially that no reactions resulted in ethanol-containing products. A range of solvent mixtures combining methanol, ethanol, water and DMF in different ratios was further used to determine the role of solvent on the formation of Mg-3,5-PDC networks. Water, even when used in combination with other solvents, always favored the formation of the hydrated compound [5.2]**,** as evident from the PXRD (Table 5.6)

The higher dimensionality of compound [5.3], compared to compound [5.2], primarily arises from the number of solvent water molecules present in the coordination sphere of the metal center. The presence of two terminal water molecules in the crystallographic [001] direction for compound [5.2] preclude extended connectivity in that direction, limiting covalent connectivity to two dimensions. The presence of a fifth available coordination in compound [5.3] for the linker functional groups leads to the formation of a 3-D network as the additional coordination site is available perpendicular to the planar arrangement of PDC coordination sites

as seen in [5.2]. The reason for lower extent of water molecule coordination may relate to the better solubility and higher rate of deprotonation of the organic linker in presence of DMF.

Moving this study further, a 1:1 mixture of DMF/methanol leads to the formation of compound [5.4] as the minor phase. While both DMF and water molecules are present within the network in coordinated and uncoordinated form, methanol is not incorporated in the network structure. Further characterization of [5.4] was not possible as we were unable to synthesize this compound in pure form, despite repeated efforts. The lack of metal coordination by methanol implies that, again coordination is more favorable for water and DMF than for small alcohols. Finally, the mutual coordination ability of methanol, ethanol and DMF was compared using a mixture of three (DMF: ethanol: methanol: 1:1:1) and the mixture of two (methanol: ethanol: 1:1) solvents, respectively, under similar synthetic conditions. Compound [5.3] is the product when DMF, methanol and ethanol are used in 1:1:1 ratio. In only a few cases have we have noticed the formation of both compound [5.2] and compound [5.3] together, possibly due to the presence of excess water in Teflon liners. Compound [5.2] is formed exclusively when 1:1 methanol-ethanol mixtures are employed (Table 5.6).

Thermal stabilities of compounds [5.1] - [5.3] were investigated using the combination of TGA and DSC techniques under N_2 atmosphere. Compound [5.1] shows a ready removal of both coordinated and free DMF molecules up to 325°C (calculated: 32.3%, observed 33.1%), followed by pyrolysis of the ligand over 425°C (Fig. 5.4). Compound [5.2]**,** on the other hand, shows a stepwise decomposition pathway. The first weight loss that occurs at 225°C is due to the removal of water molecules (calculated: 15.9 wt. % observed 16.1 wt. %), and it is followed by a stable plateau to 515°C where pyrolysis of the ligand occurs (Fig. 5.5). Compound [5.3] shows similar two step decomposition pathway. In the first step, coordinated and free water molecules

are removed (calculated: 15.9%, observed: 16%) in a continuous fashion within 225°C. This step is followed by a stable plateau up to 520°C, followed by pyrolysis of the organic linker (Fig. 5.6).

Porous alkali- and alkaline-earth metal carboxylates are scarce. As compound [5.1] possesses a theoretical 51.5% (2018.2 $Å^3$) void space, we attempted to activate a sample under dynamic vacuum at 200°C. The powder diffraction pattern of the desolvated sample shows poor crystallinity. BET study revealed poor surface area of 51.9 m^2/g and Langmuir surface area of 69.7 m^2/g. The small surface area indicates destruction of network which is also supported by the PXRD data. In a few reported cases, magnesium networks show non-porosity towards N_2 due to smaller pore size, but show permanent porosity towards other gases e.g. O_2, CO_2 due to their smaller kinetic diameters. In this case, it is highly unlikely, as compound [5.1] does show adsorption of N_2 as evident in the BET/Langmuir studies. Further the PXRD pattern of desolvated compound [5.1] does not show retention of network.

Compound [5.1] is soluble in water, but insoluble in common organic solvents (e.g. acetone, methanol, ethanol, ethyl acetate, ether and hexane). A solvent exchange study was performed on compound [5.1] to replace the DMF molecule in the channel with more volatile solvents (e.g. methanol, ethanol, acetonitrile, dichloromethane). We were only able to produce X-ray amorphous materials using solvent exchange. Compound [5.2] is also soluble in water but not soluble in organic solvents like methanol, ethanol, and acetone. It forms a poorly crystalline product after removal of the coordinated water solvent. The desolvated compound [5.2] is also soluble in water but insoluble in ethanol. The powder XRD pattern of the desolvated compounds [5.1] - [5.2] soaked in DMF and ethanol, respectively, did not show any change of the structure,

confirming the irreversibility of transformation. Compound [5.3] is soluble in water but insoluble in common organic solvents like ethanol, methanol and ethyl acetate.

The chemistry of magnesium CNs is driven by ionic forces rather than covalent bonding. The preference towards ionic bonding of magnesium leads to the absence of secondary building units (SBUs), with dominance of crystal packing forces. As a consequence, the network topology is strongly dependent on nature of organic linkers and solvents, and less dependent on the nature of magnesium metal center. Because of the dimensionless nature of its bond, magnesium can easily change its coordination environment after desolvation. Though, the ionic nature of Mg-O bond might help in adsorption of certain polar gases like carbon monoxide, hydrogen sulfide and ammonia.

Table 5.6. Solvent dependent formation of magnesium coordination networks.

Solvent System	Composition	Product	Metal Polyhedra
DMF	Pure	[1]	Monomer + Dimer
Ethanol	Pure	[2]	Monomer
Water	Pure	[2]	Monomer
Methanol	Pure	Clear solution	
DMF/water	1:1	[2]	Monomer
DMF/Ethanol	1:1	[3]	Monomer
DMF/Methanol	1:1	[4]	Dimer
Methanol/Ethanol	1:1	[2]	Monomer
DMF/ethanol/water	2:1:1	[2]	Monomer
DMF/methanol/water	2:1:1	[2]	Monomer
DMF/methanol/ethanol	1:1:1	[3]	Monomer
Methanol/Ethanol/Water	1:1:1	[2]	Monomer

5.6. Conclusion

Four magnesium based coordination networks were synthesized using different solvents under solvothermal conditions. Compounds [5.1], [5.3] and [5.4] form 3-D open networks with the infinite channels, while compound [5.2] is a layered structure with isolated magnesium polyhedra. The relative coordination ability of the solvents to coordinate metal centers plays a vital role in determining the topologies of the networks. It was determined that water has the highest affinity to coordinate with the magnesium metal centers followed by DMF, while solvents like methanol and ethanol tend not to coordinate with the metal center in presence of the water and DMF, respectively. The detailed characterization of [5.1] - [5.4] by single crystal XRD and thermal analysis shed light on the chemistry of magnesium - pyridinedicarboxylate systems. The use of different solvents as synthetic variables will further generate different network topologies and properties.

Chapter 6

A Calcium Coordination Framework Having Permanent Porosity and High CO_2/N_2 Selectivity

The content of this chapter is published in

A Calcium Coordination Framework Having Permanent Porosity and High CO_2/N_2 Selectivity. Banerjee, D., Zhang, Z., Plonka, A. M., Li, J., Parise, J. B., *Cryst. Growth Des*. **2012,** 12(5), 2162 - 2165.

6.1. Abstract

A thermally stable, microporous calcium coordination network shows a reversible 5.75 wt% CO_2 uptake at 273K and 1 atm pressure. The activated compound shows an enthalpy of interaction of~-31 kJ/mol with adsorbed CO_2 molecules with a CO_2/N_2 selectivity over 45 under ideal flue gas conditions. The absence of open metal sites in the activated material suggest a different mechanism for selectivity and high interaction energy compare to frameworks with open metal sites.

6.2. Introduction

Selective removal of carbon dioxide (CO_2) from gas streams and the atmosphere is an important process in energy production, and in mitigating the environmental damage resulting from energy consumption.[139,140] The selectivity of zeolite molecular sieves, used commercially for the separation of gases, including CO_2, is attributed to the presence of regularly spaced pores and channels and to the different interaction potentials of gases with extra-framework cations within the pores.[141-144] The extra-framework cations are often from s-block series.[145,146] The structurally diverse porous metal-organic frameworks (MOFs)[147] and coordination networks (CNs)[56] emulate favorable properties for gas storage,[3,139,148,149] separation[4,150] and catalysis[5,151] attributed to zeolites. Frameworks constructed using s-block metals, such as environmentally abundant magnesium and calcium, are particularly promising because these metals are lightweight and have high enthalpies of interaction with adsorbed gas-molecules.[19,56] As partial confirmation of this strategy, several magnesium coordination networks are reported and show permanent porosity and interesting gas-adsorption properties.[17-19,128] For example, the presence of open metal-sites in MOF-74(Mg) framework, akin to extra-framework sites in many zeolites, was implicated in the observed high CO_2 selectivity in absence of water vapor.[22]

On the other hand, the role of calcium in natural CO_2 separation and storage suggests research directed towards synthesis of calcium based porous networks may also be fruitful.[11] Despite several reports of calcium based coordination networks they are found to be non-porous, after activation; removal of coordinated and/or uncoordinated solvents leads to structural collapse, rendering the framework unsuitable for selective sorption.[152-155] In this chapter, we report the synthesis, and selective CO_2/N_2 gas-adsorption properties of a highly robust

microporous calcium based coordination network [Ca(SDB)]·H_2O [6.1] with sustainable and accessible pores upon guest removal.

6.3. Experimental Section

6.3.1. Synthesis

Compound [6.1] was synthesized under solvothermal conditions using Teflon lined stainless steel Parr autoclaves. Starting materials include calcium chloride ($CaCl_2$, 96%, Acros-Organics), 4,4'-sulfonyldibenzoic acid (4,4'-SDB, 98%,Sigma-Aldrich) and ethanol (95%, Fisher-Scientific) and were used without purification.

Synthesis of compound [6.1] Ca(4,4'-SDB)·(H_2O)

A mixture of 0.0006 moles of $CaCl_2$ (0.074g) and 0.0006 moles of 4,4'-SDB (0.198 g) was dissolved in 10.05 gram of ethanol and stirred for 2 hours to achieve homogeneity [molar ratio of metal chloride: ligand: solvent =1:1:380]. The resultant solution was heated at 180°C for 5 days. Colorless needle shaped crystals were recovered as products and washed with and ethanol (Yield: 50% based on calcium in anhydrous $CaCl_2$, 0.112 gram). The water comes from the 95% ethanol solvent and adsorbed moisture in the $CaCl_2$ reactant. The use of pure water as the synthesis solvent under identical synthesis conditions leads to formation of recrystallized organic linker as the main product.

6.3.2. Single Crystal X-ray Crystallography

A suitable crystal of compounds [6.1] and the activated form ([6.1a]) were selected from the bulk sample and was mounted on a glass fiber using epoxy. Reflections for compound [6.1] and [6.1a] were collected using a four-circle Oxford Gemini diffractometer equipped with an Atlas detector (λ = 0.71073 Å) with 1° omega scans. The raw intensity data were collected, integrated and corrected for absorption effects using CrysAlis PRO software.[68] The crystal structure was solved using direct methods (SHELXS).[67] Calcium and sulfur atoms were located first followed by determination of other atom (O, C) positions from the Fourier difference map with all the non-hydrogen atoms being refined anisotropically. Hydrogen atoms were added in the structure using geometrical constraints (HFIX command). The crystallographic details can be found in Table 6.1.

Table 6.1. Crystallographic data and structural refinement details of compound [6.1] and [6.1a]

	[6.1]	[6.1a]
Empirical formula	$C_{14}H_8O_7SCa$	$C_{14}H_8O_6SCa$
Formula weigh	360.34	344.34
Collection Temperature(K)	298(2)	298(2)
Wavelength(Å)	0.71073	0.71073
Space Group	$P\ 2_1/n$	$P\ 2_1/n$
a (Å)	11.8214(3)	11.8783(5)
b (Å)	5.56730(13)	5.5485(2)
c (Å)	22.7603(6)	22.7982(8)
α (°)	90	90
β (°)	100.356(2)	101.535(4)
γ (°)	90	90
Volume($Å^3$)	1473.53(6)	1472.21(10)
Z	4	4
Calculated Density(g/cm^3)	1.624	1.554
Absorption coefficient(mm^{-1})	0.601	0.593
F(000)	736	704
Crystal size (mm)	0.35 × 0.2 × 0.1	0.2 × 0.15 × 0.10
Θ range of data collection	3.50 -28.28	3.78 - 26.37
Index range	$-15 \leq h \leq 15$	$-14 \leq h \leq 14$
	$-7 \leq k \leq 7$	$-6 \leq h \leq 6$
	$-30 \leq l \leq 30$	$-28 \leq h \leq 28$
Total reflection	28011	23972
Independent reflection	3675 [R(int) = 0.0415]	2998 [R(int) =0.0403
Goodness of fit	1.239	1.082
Data/ Restraints/parameter	3675 / 0 / 208	2998/ 0 / 200
R1(*on* F_o^2, $I>2\sigma(I)$)	0.0321	0.0441
wR2 (*on* F_o^2, $I> 2\sigma(I)$)	0.0960	0.1132

6.3.3 Powder XRD and thermal analysis

Bulk sample identification and phase purity were determined using powder X-ray diffraction. The data were collected using a Scintag Pad-X diffractometer equipped with Cu Kα (λ = 1.5405 Å) radiation within a range of $5° \leq 2\theta \leq 40°$ (step size: 0.02°, counting time: 1s/step). Comparison of the observed and calculated powder X-ray diffraction patterns for compound [6.1] confirmed phase purity (Fig. 6.1). To check the water stability of the as-synthesized compound [6.1] and activated [6.1a] in water, 10 ml of deionized water were added to ~100 mg of compounds [6.1] and [6.1a], kept in two separate vials. The materials were recovered after 5 days by filtration and the PXRD of the materials were collected (Fig. 6.2 - 6.3).

The Thermogravimetric (TG) data for compounds [6.1] and [6.1] were collected using a TGA Q500 instrument. The sample was heated from room temperature to 750 °C under a N_2 atmosphere with a heating rate of 10°C/minute (Fig. 6.4 - 6.5).

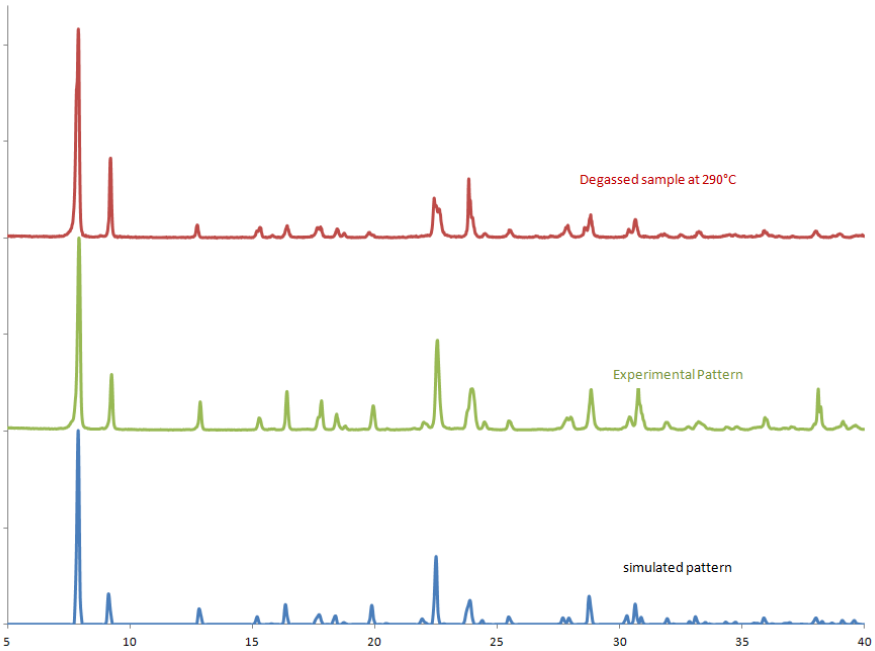

Figure.6.1. The simulated (bottom), experimental (middle) and activated (top) PXRD patterns of compound [6.1].

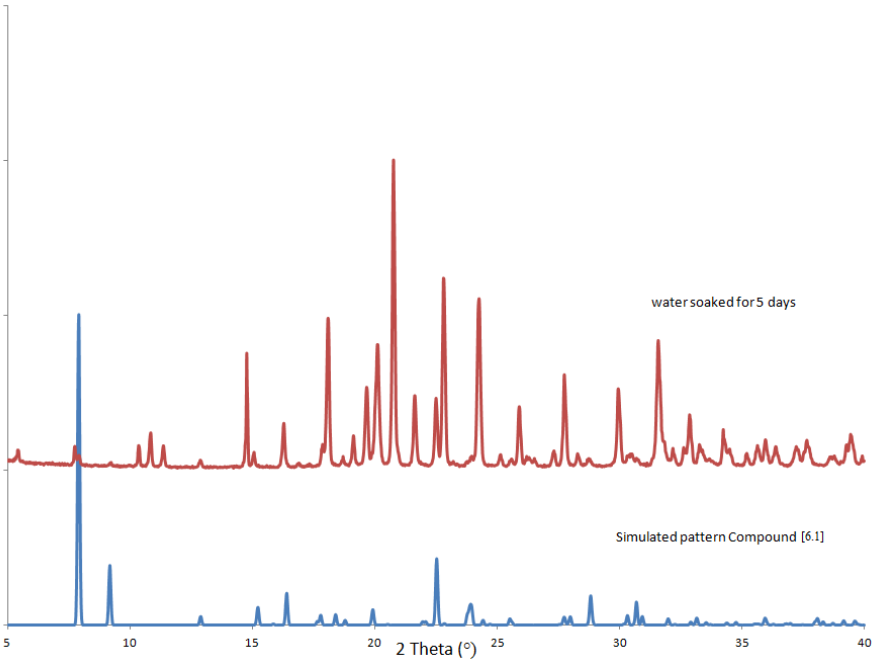

Figure 6.2. The PXRD pattern of water soaked (for 5 days) compound [6.1]

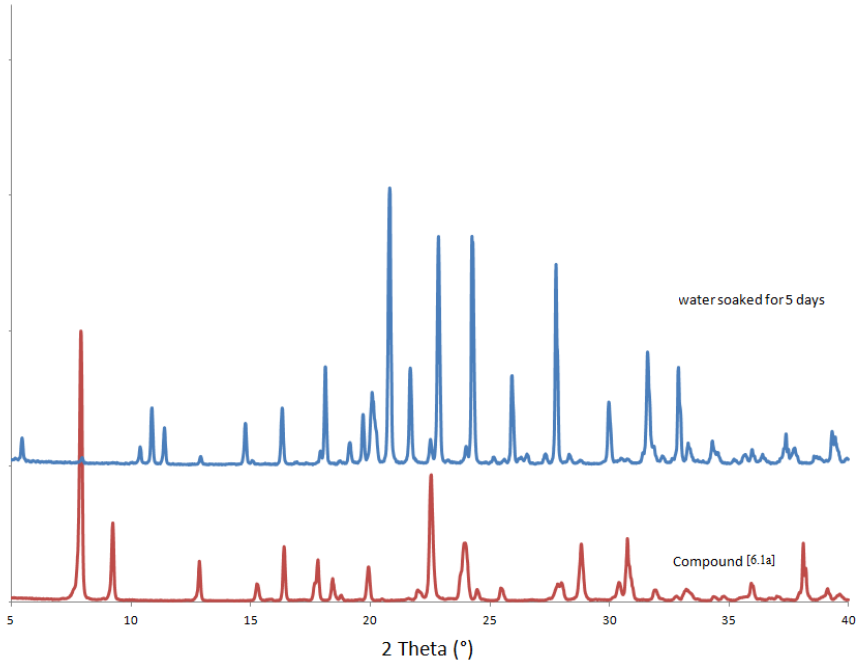

Figure 6.3. The PXRD pattern of water soaked (for 5 days) compound [6.1a]

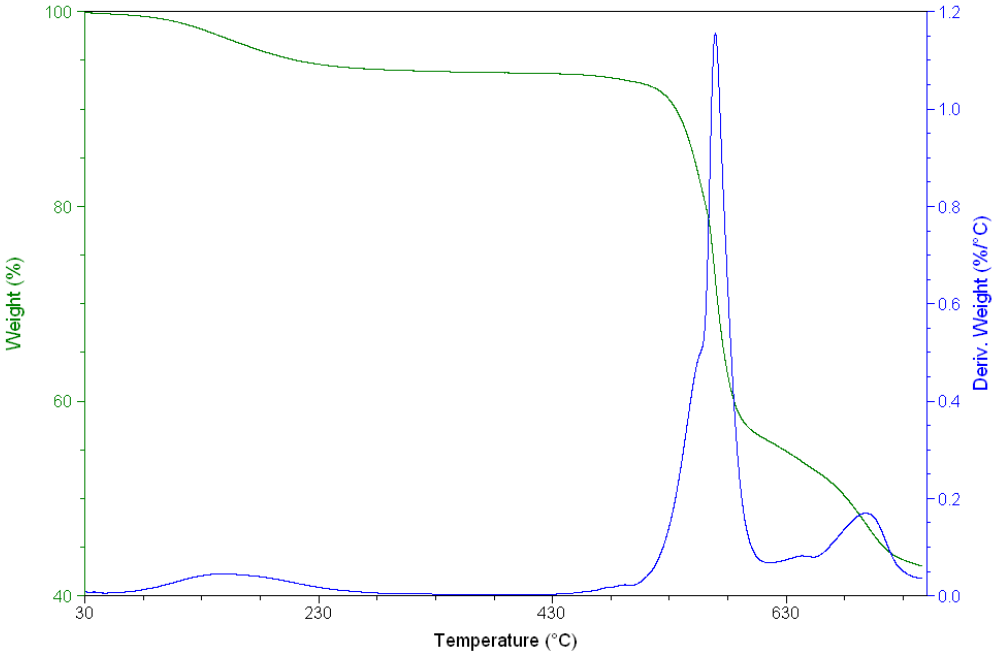

Figure 6.4. The TG plot of compound [6.1]. The green line represents the weight loss profile and the blue line shows the associated derivatives of weight loss.

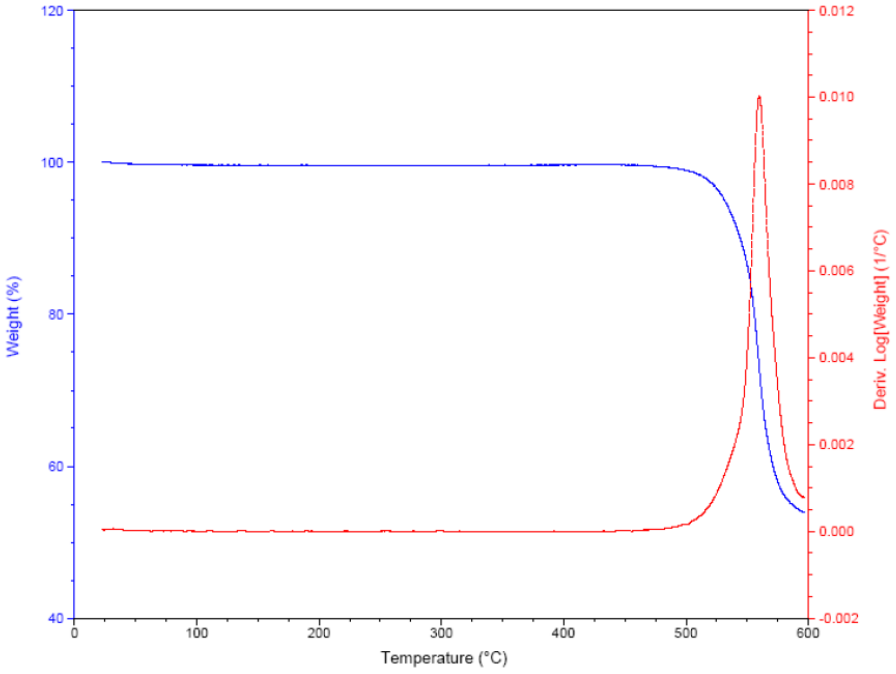

Figure 6.5. TG-profile of compound [6.1a] after exposure to air for 2 days

6.3.4. Gas Adsorption Experiments

All gas sorption experiments were performed on a volumetric gas sorption analyzer (Autosorb-1-MP, Quantachrome Instruments). Liquid nitrogen and liquid argon were used as coolant to achieve cryogenic temperatures (77 and 87 K). Ultra high purity H_2, N_2 and CO_2 (99.999%) were used. The initial outgassing process for [6.1] was carried out at 563 K under vacuum overnight. Outgassing samples in the amount of around 100-110 mg were used for gas sorption measurements and the weight of [6.1a] was recorded before and after outgassing to confirm the removal of guest molecules and to ensure the framework integrity. The outgassing procedure was repeated on the same sample between experiments for about 2-3 hours. The hydrogen adsorption-desorption isotherms were collected in the pressure range from 10^{-4} to 1 atm at 87 and 77 K, respectively. Results for [6.1a] are plotted in Figs 6.6 - 6.13. Temperature-dependent adsorption-desorption isotherms of CO_2 and N_2 (273, 288 and 298 K) on [6.1a] were collected from 10^{-3} to 1 atm.

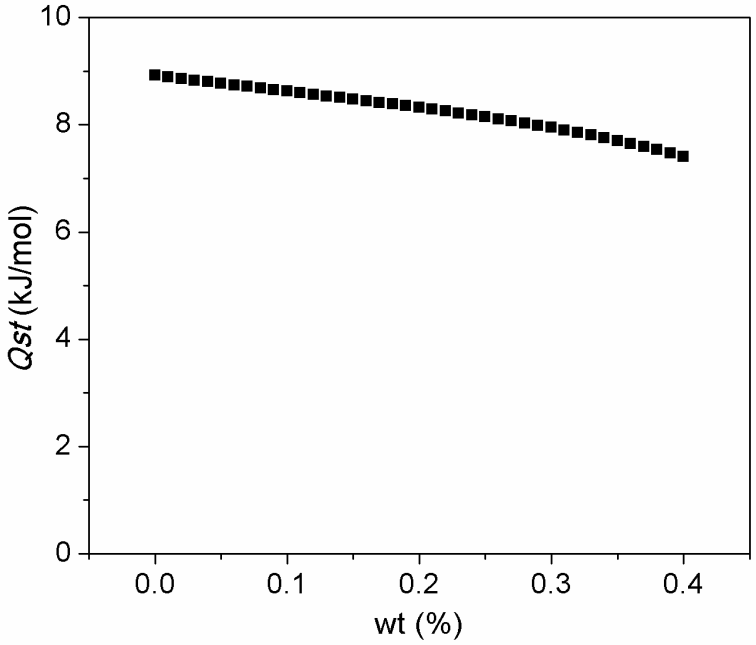

Figure 6.6. Isosteric heats of H_2 adsorption of [6.1] calculated based on adsorption isotherms at 77 K and 87 K using Virial method.

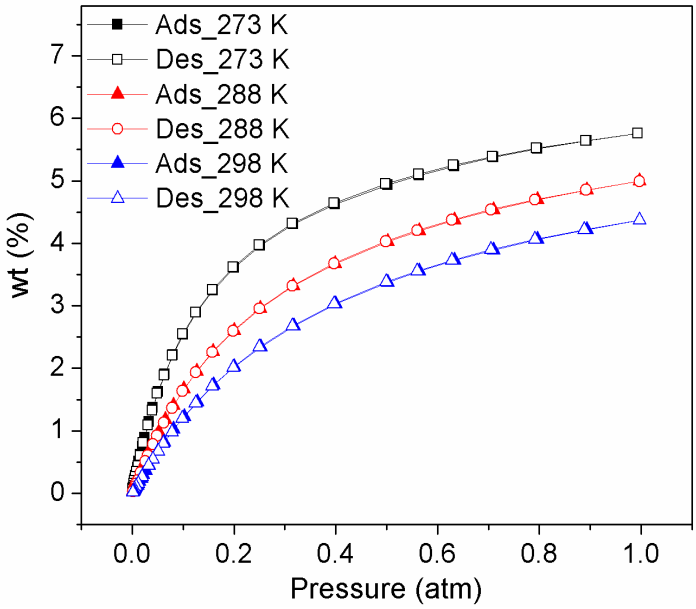

Figure 6.7. CO_2 adsorption-desorption isotherms of compound [6.1] at 273 K (black), 288 K (red) and 298 K (blue).

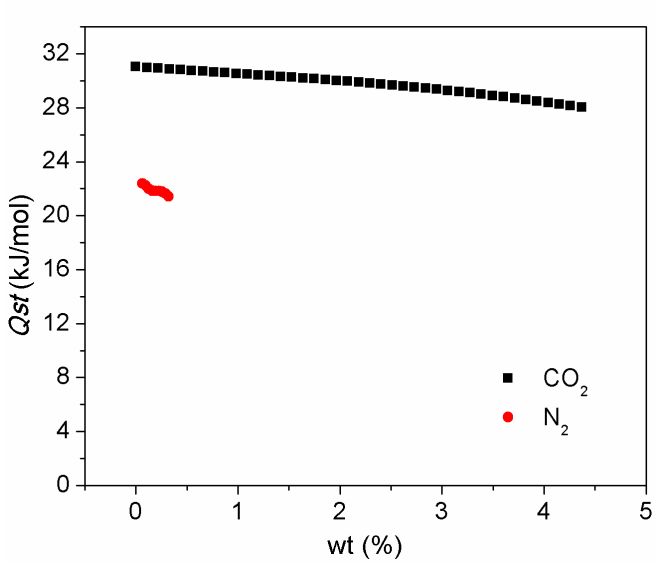

Figure 6.8. Heats of adsorption (Q_{st}) for CO_2 and N_2 of compound [6.1] calculated based on Virial method.

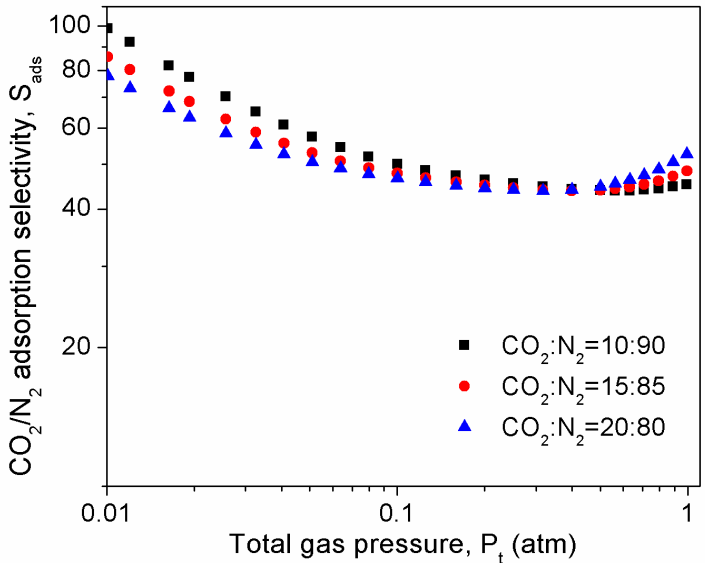

Figure 6.9. The room temperature CO_2/N_2 selectivity calculated by IAST method for three CO_2 concentrations (CO_2/N_2: 10:90 (10%), 15:85 (15%), and 20:80 (20%) in CO_2-N_2 binary mixtures.

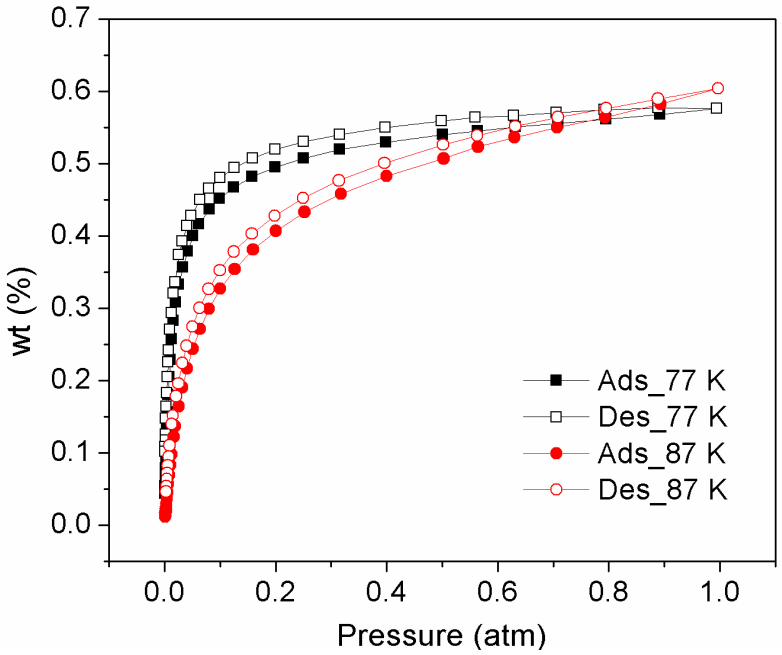

Figure 6.10. H_2 adsorption-desorption isotherms of compound [6.1] at 77 K and 87 K.

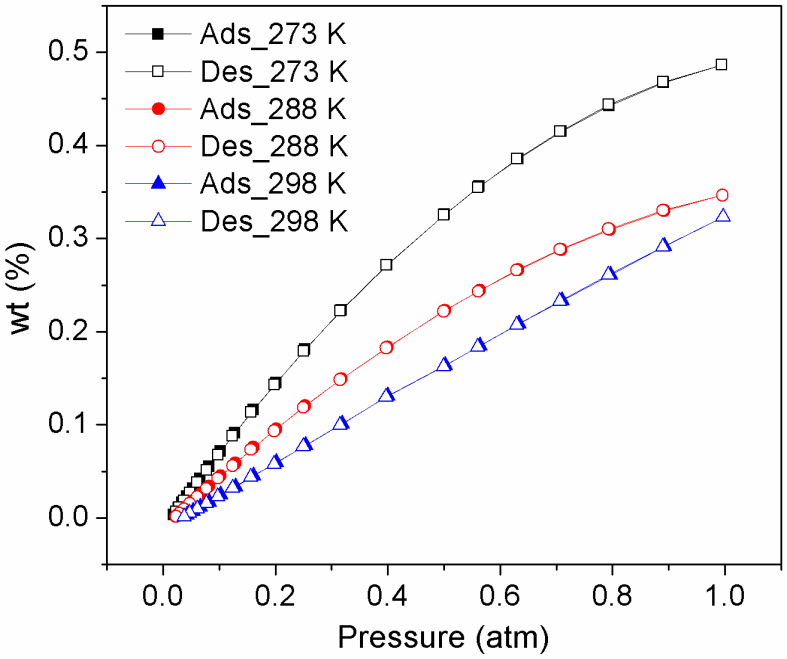

Figure 6.11. The N_2 adsorption-desorption isotherms of compound [6.1] at 273 K (black), 288K (red) and 298 K (blue).

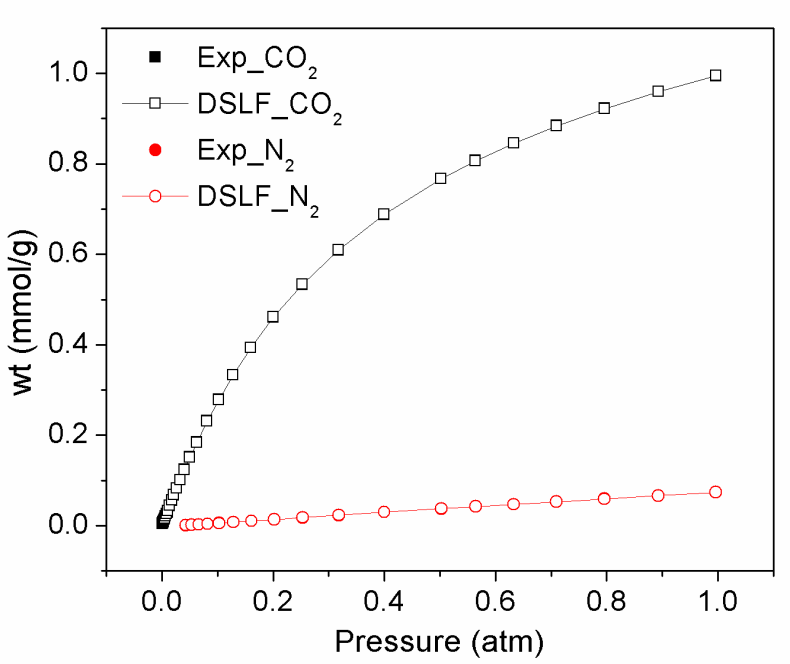

Figure 6.12. Experimental and fitted isotherms for CO_2 and N_2 at 298 K for compound [6.1].

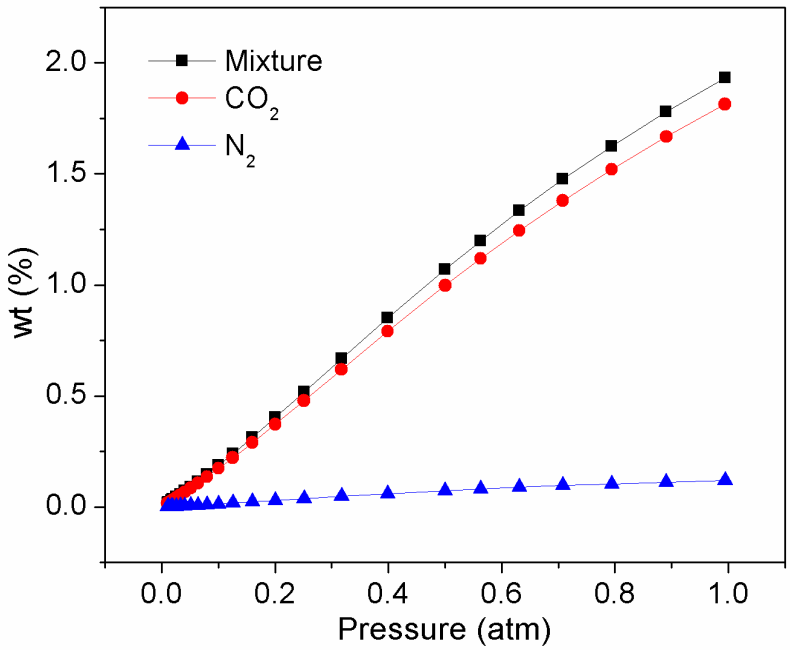

Figure 6.13. The IAST predicted isotherms of a binary mixture of CO_2 and N_2 (CO_2:N_2 = 15:85) at 298 K as a function of the total pressure.

6.4. Result and Discussion

6.4.1 Structure description of compound [6.1], Ca(4,4'-SDB)·H_2O

The reaction of metal salt $CaCl_2 \cdot xH_2O$ with the organic linker (SDB) under solvothermal conditions leads to the formation of needle shaped crystals of compound [6.1]. Single crystal structure analysis shows that [6.1] is a three-dimensional (3D) network, composed of corner-sharing calcium polyhedral chains along crystallographic [010] direction (Fig. 6.14). Calcium is present in octahedral coordination, with bonds to five-carboxylate groups and a sulfonyl oxygen atom. One of the sulfonyl oxygen atoms (O5) of the linker is uncoordinated. Each of the calcium polyhedral chains is connected with six other such chains in [100] and [001] directions by the linker molecules. Such a connectivity leads to the formation of a channel running in the [010] direction with a square-shaped cross section of average size 5.9 Å × 5.8 Å, based on the Van der Waal radii of the aromatic carbon atoms. Disordered water molecules are present within the channel. PLATON[138] indicates an accessible volume of 18.2 % (275 $Å^3$) upon solvent removal. The water molecules present within the channel are readily removed below 250 °C, as evident from the TG experiments (observed: 5.1%, calculated: 4.97%). The dehydrated network undergoes thermal decomposition at ~575°C (Fig. 6.4). Crystal analysis of the dehydrated network reveals that after activation compound [6.1] undergoes a structural transformation to a different, denser phase (denoted as [6.1a]). Compounds [6.1] and [6.1a] crystallize in the same space group ($P2_1/n$), with very similar unit cell dimensions (Table 6.1), but with different origin of the unit cell and different packing of organic linkers. The main observable change is the position of sulfur atoms, influencing how the linkers surrounding the same channel are facing each other. In compound [6.1], linkers of the same channel are packed in parallel manner, after activation they are turned by 45º from each other. As a consequence, the volume of the channel

is smaller, changing the overall porosity of compound [6.1a] from 18.2 % (calculated for [6.1]) to 16%. The change in linker packing pattern results in the reorganization of calcium coordination sphere. The M-O-M connectivity of compound [6.1] changes from corner sharing chains to edge sharing dimer in compound [6.1a] (Fig. 6.17).

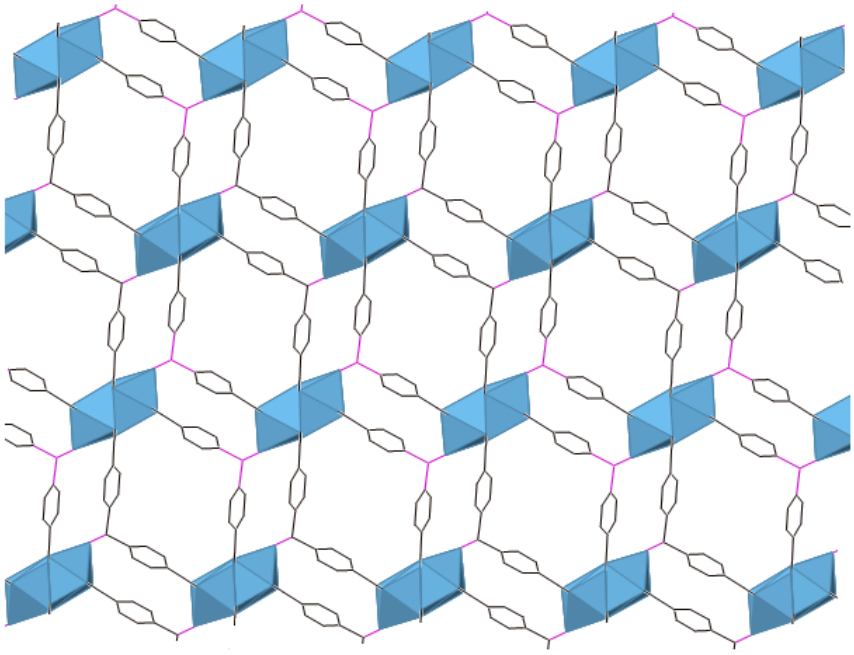

Figure 6.14. View of compound [6.1] along the [010] direction. Hydrogen and solvent (water) molecules are omitted for clarity.

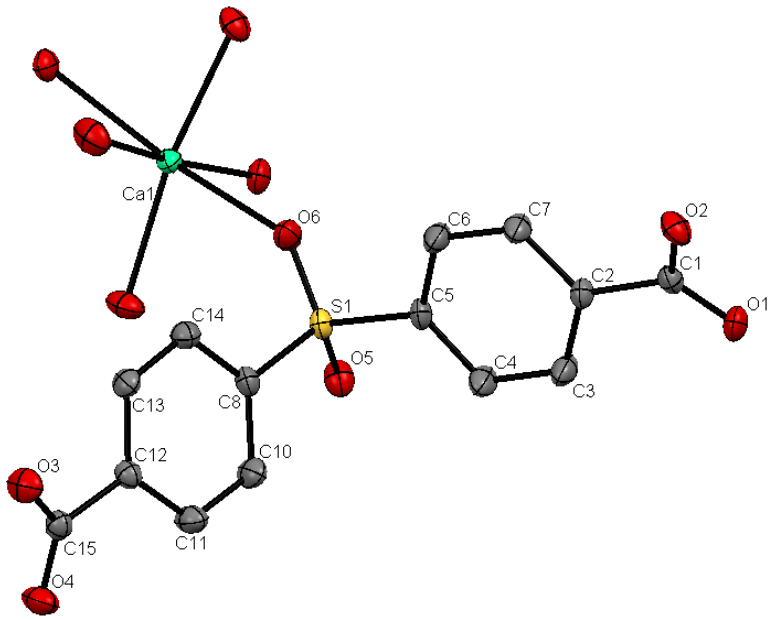

Figure 6.15. ORTEP view of compound [6.1], illustrating the numbering scheme. Ellipsoids are shown at 50% probability level. Hydrogen atoms are omitted for clarity. Symmetry related oxygen atoms are shown to complete the coordination sphere of the calcium center.

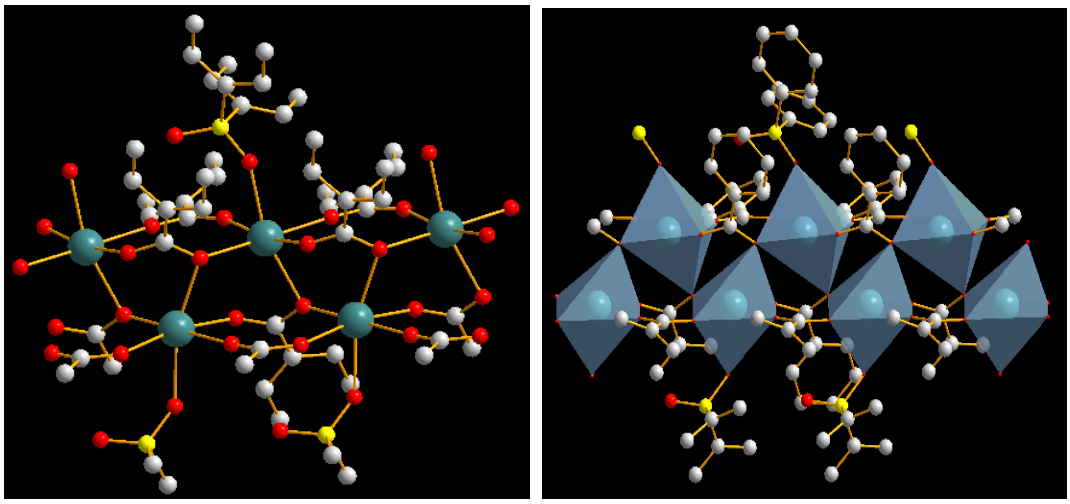

Figure 6.16. View of a single chain in ball-and-stick (left) and polyhedra (right) form of compound [6.1].

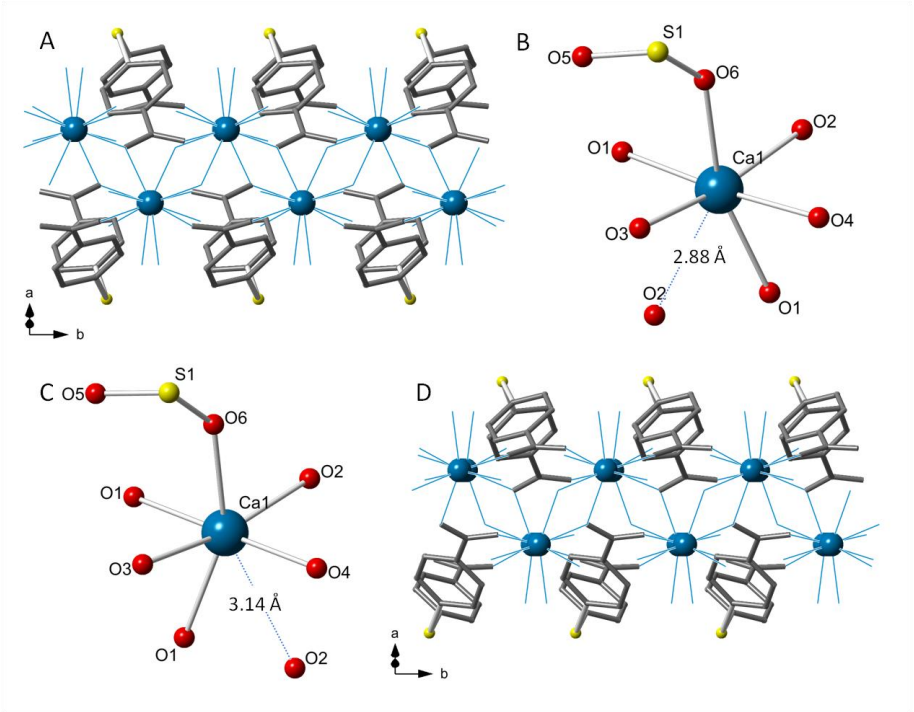

Figure 6.17. Structural differences between compounds [6.1] and [6.1a]. **A**: cross-section of the channel, showing parallel organization of organic linkers in compound [6.1]. **B**: Ca coordination sphere in [6.1], **C**: Ca coordination sphere in [6.1a], **D**: cross-section of the channel showing tilted organization of SDB linkers in [6.1a]

Table 6.2. Selected bond lengths (Å) and angles (°) for compound [6.1]

Ca(1)-O(1)#4	2.3739(11)	O(4)#1-Ca(1)-O(3)#2	95.68(4)
Ca(1)-O(2)#3	2.3565(10)	O(4)#1-Ca(1)-O(6)	90.38(4)
Ca(1)-O(3)#2	2.2954(11)	O(1)#4-Ca(1)-O(6)	87.67(4)
Ca(1)-O(4)#1	2.2951(11)	O(2)#3-Ca(1)-O(2)#5	117.36(2)
Ca(1)-O(6)	2.4621(10)	O(6)-Ca(1)-O(2)#5	147.76(3)

Symmetry code: #1 -x+1/2, y-1/2, -z+1/2. #2 -x+1/2, y+1/2, -z+1/2. #3 -x+1, -y+1, -z. #4 -x+1,-y+2, -z. #5 x+1/2, -y+3/2, z+1/2.

6.4.2. Discussion

The dehydrated compound [6.1a] maintains its topology after gas-adsorption experiments and when exposed to air for 2 days as observed from PXRD patterns (Fig. 6.1). Further, the TGA data of compound [6.1a] shows no evidence of moisture adsorption upon exposure to air (Fig. 6.5). However, both compounds transform to a different phase when placed in liquid water.

The permanent porosity of the compound [6.1a] was confirmed by pore characterization and gas-adsorption studies. The N_2 adsorption isotherm at 77K displays a type I sorption behavior, verifying its microporous nature. The BET surface area was calculated to be 145.15 m^2/g. Experiments of H_2 adsorption reveal a moderate uptake of 0.55 wt% at 77K and 1 atm (Fig. 6.10). The isosteric heats of H_2 sorption, calculated by fitting the adsorption data at 77K and 87K to the Virial equation, were found to be between 7.41 and 8.92 kJ/mol in the loading range below 0.4 wt% (Fig. 6.6). The Q_{st} (H_2) is slightly lower than MOF-74(Mg), but considerably higher than other porous materials like MOF-5,[156] ZIF-8[157] and PCN-6.[158] Further, [6.1a] was tested for CO_2 adsorption at different temperatures and pressures. Compound [6.1a] shows a reversible uptake of 5.75 and 4.37 wt% at 273 and 298K and 1 atm pressure, respectively (Fig. 6.7). The heats of CO_2 adsorption at low loadings are ~28-31 kJ/mol, significantly higher than those of N_2 (~19-23 kJ/mol) in the same loading range (Fig. 6.8). The value of Q_{st} for CO_2 are lower than those of M-MOF-74 (M= Mg, Co, Ni) series under similar experimental conditions, [19] but are comparable to those of HKUST-1[159] and MOF-5.[76] The higher Q_{st} for M-MOF-74 (M= Mg, Co, Ni) series is due to the presence of open metal sites in the activated framework,[22] while **1** possesses no open metal sites (OMSs). For post-combustion CO_2 capture, OMSs are subject to water vapor and will lead to significantly reduced capture performance. The relatively high Q_{st} of

compound [6.1a] may be attributed to its small pore size[12] and the ionic nature of Ca-O bonding, which favors quadruple interactions with CO_2 molecules.[19,139]

The ideal adsorbed solution theory (IAST), developed by Myers and Prausnitz, [160] is a widely adopted method to predict multi-component isotherms from pure gas isotherms. It has been reported that it can accurately predict gas mixture adsorption in many zeolites[161-165] and more recently in MOF materials. [23,161,166-172] In the current case, IAST is employed to estimate the CO_2 and N_2 adsorption selectivity in compound [6.1a]. Adsorption isotherms predicted by IAST for mixtures of CO_2/N_2 (CO_2:N_2 = 15:85) in [6.1a] as a function of total bulk pressure are shown in Fig. 6.13. The predicted CO_2/N_2 selectivity at different pressures and mixture compositions for [6.1a] are shown in Fig. 6.9. The values are above 45. At 0.15 bar of CO_2 and 0.85 bar of N_2, a typical composition of flue gas mixture from power plants, the selectivity is in the range of 48 - 85 at 298 K. These values are comparable to Mg-MOF-74[23,139] and higher than Ni-MOF-74 (30), [139,173] HKUST-1 (20-22)[174] and a py-CF_3 modified MOF (25-45)[169] under similar conditions. In addition, they are considerably higher than those of experimental values reported for several carbon adsorbents and zeolites, such as MCM-41 (12-18),[175] MFI (20-30),[176] and NoritAC (14.18),[177] under similar conditions.

6.5. Conclusion

A thermally stable, microporous calcium based coordination network with sustainable and accessible pores has been synthesized and structurally characterized. The compound contains a robust 1D channel that remains intact upon solvent removal. It has a strong affinity toward CO_2, a high CO_2/N_2 selectivity and shows remarkable stability in air. The work shows that CNs built on calcium metal centers and appropriate organic linkers are capable of reversible gas-adsorption. Compound [6.1a] possesses high binding energy towards CO_2 despite the absence of open metal sites, and this is both desirable and interesting. The structural origins of selectivity, and the trade-offs between pore size and gases-framework interaction potentials in determining selectivity, will be priorities in future work.

Chapter 7

Anionic Gallium-Based Metal-Organic Frameworks and Its Sorption and Ion Exchange Properties

The content of this chapter is published in

An Anionic Gallium Based Metal Organic Framework and its Sorption and Ion Exchange Properties**.** Banerjee D., Kim, S. J.; Wu H.; Xu W. Q.; Borkowski L. A.; Li, J.; Parise, J. B;. *Inorg. Chem.* **2011**, 50 (1), 208-212

7.1 Abstract

A gallium based metal organic framework $Ga_6(C_9H_3O_6)_8\cdot(C_2H_8N)_6(C_3H_7NO)_3(H_2O)_{26}$ [Ga_6(1,3,5-BTC)$_8$·6DMA·3DMF·26H_2O] [7.1]; GaMOF-1, space group *I*-43d, a= 19.611(1) Å, V = 7953.4(6) $Å^3$ was synthesized using solvothermal techniques and characterized by synchrotron-based X-ray microcrystal diffraction. Compound [7.1] consists of isolated gallium tetrahedra connected by the organic linker (BTC), forming a (3,4)-connected anionic porous network. Disordered positively charged ions and solvent molecules are present in the pore compensating for the negative charge of the framework. These positively charged molecules could be exchanged with alkali metal ions as evident by ICP study. The H_2 storage capacity of the parent framework is moderate with a H_2 storage capacity of ~0.5 wt% at 77K and 1atm.

7.2. Introduction

A wide range of metal centers and multifunctional organic ligands are used to construct metal organic frameworks (MOFs) and coordination polymers (CPs),[1,7,73,178] which could be tailored for specific uses such as gas storage,[17,75-78,80,82] ion exchange,[85-87] separation,[92,93] catalysis,[88,89] sensing and detection.[179-181] One of the advantages of this particular class of materials is that the structural topologies and properties can be tuned by altering synthetic parameters such as solvents[130,132,133] and temperature,[33] in addition to the metal ions and organic linkers. Most of the coordination polymers synthesized to date combine aromatic polycarboxylates ligands[10,78] with first row divalent transition[76,79,82] or trivalent lanthanide metal centers,[116,182,183] while the use of s and p block metal centers is comparatively limited. Férey and others have reported a series of trivalent p-block (Al, [184-188] Ga, [189-195] In [196-198]) based coordination polymers containing interesting architectures and properties. As an example, indium based networks tend to form anionic porous framework materials, with tetrahedrally coordinated In(III) metal centers.[196,197] A porous anionic framework capable of ion exchange is a potential precursor for inserting alkali metal cations into the pores.[199] Recently Hupp[46-48] and Schroder[44,45,200] have reported, being able to "dope" alkali metal cations in the channels of pre-synthesized MOFs, as a way to increase the gravimetric storage capacity of the parent materials. The increase in the percentage of H_2 storage is attributed to the high enthalpy of adsorption of gas molecules on the bare metal center. The challenge underlying this strategy is to successfully insert the alkali metal center into the pore either in metallic or ionic form. The gravimetric advantage of a gallium based MOFs over its indium analogue encouraged us to investigate the formation of coordination networks, combining gallium metal centers with different organic linkers under solvothermal conditions. In the course of that investigation, an anionic gallium

framework with (3,4) net topology was isolated under solvothermal conditions. In this chapter, we describe the synthesis, structural characterization, ion exchange and gas storage studies of Ga_6(1,3,5-BTC)$_8$·6DMA·3DMF·26H_2O [7.1] based on isolated gallium tetrahedra and 1,3,5-benzenetricarboxylate as the linker.

7.3. Experimental Section

7.3.1. Synthesis

Compound [7.1] was synthesized under solvothermal conditions using Teflon –lined Parr stainless steel autoclaves. The starting materials include gallium nitrate hydrate ($Ga(NO_3)_3$·xH_2O, 99.9%, metal basis, Sigma-Aldrich) 1,3,5-benzenetricarboxylic acid ($C_9H_6O_6$, 95%, Sigma-Aldrich), ammonium fluoride (NH_4F, 98%, Sigma-Aldrich), N,N dimethylformamide (C_3H_7NO, DMF, 99%, Sigma-Aldrich) and ethanol (C_2H_5OH, 99%, Sigma-Aldrich) and were used without any further purification.

A typical synthesis involves using a mixture of 0.001 moles of $Ga(NO_3)_3$ (0.304 gram), 0.002 moles of 1,3,5-benzenetricarboxylic acid (0.490 gram), and 0.001 moles of NH_4F (0.048 gram). The mixture was dissolved in 14.9 gram of DMF and stirred for 4 hours to achieve homogeneity [molar ratio of metal salt: ligand: solvent =1:2:204]. The resultant solution was heated for 5 days at 180°C. The product was obtained as block shaped microcrystal (yield: 50% based on gallium) and was recovered by filtration and subsequently washed with ethanol. (Elemental analysis. Calcd. for compound [7.1]: C,36.74 ; N, 4.14; H, 4.75. Found C, 36.79; N, 4.08; H, 4.22 (Galbraith Laboratories Inc. Knoxville, TN).

7.3.2. X-ray crystallography

A suitable crystal of compound [7.1] was selected from the bulk and was mounted on a glass fiber using epoxy. Reflections for compound [7.1] were collected with 0.5° φ scans at ChemMatCars (Sector 15) at the Advanced Photon Source (APS) synchrotron X-ray storage ring (λ= 0.41328Å) using a three-circle Bruker D8 diffractometer equipped with an APEXII detector at 100 K. The raw intensity data were analyzed using the APEXII suite of software [69] and were corrected for absorption using SADABS.[67] The structure was solved using direct methods and refined using SHELXL.[67] The single gallium atom in the asymmetric unit was located first followed by the location of other atoms in the main framework (O, C) from the Fourier difference map. All non-hydrogen atoms were refined anisotropically. Hydrogen atoms were placed using geometrical constraints. Contained within the void spaces of the compound [7.1] was a combination of highly disordered neutral solvent molecules and charge compensating counter-cations. Thus, PLATON/SQUEEZE model was applied to remove the contributions of the scattering from the disordered species. [138] The discrepancy in simulated vs. experimental powder pattern originates because the contribution from the disordered extra-framework species is absent in the simulated pattern. The chemical formula of compound [7.1] was determined using a combination of TGA-DSC, elemental analysis, and single crystal XRD studies. The crystallographic details of compound [7.1] are summarized in Table 7.1.

Table 7.1. Crystallographic data and structural refinement details of compound [7.1] [a]

Empirical formula	$C_{12}H_4GaO_8$
Formula weight	345.87
Collection Temperature(K)	77(2)
Wavelength(Å)	0.41328
Space Group	*I*-43d
Crystal system	cubic
a (Å)	19.9611(9)
Volume ($Å^3$)	7953.4(6)
Z	12
Calculated Density(g/cm^3)	0.867
Absorption coefficient(mm^{-1})	0.223
F(000)	2052
Crystal size (mm)	0.11×0.12×0.03
Θ range of data collection	1.45-15.97
Index range	$-23 \leq h \leq 26$
	$-18 \leq k \leq 26$
	$-26 \leq l \leq 23$
Total reflections	40804
Independent reflections	1648 [R(int) = 0.0473]
Goodness of fit	1.07
Refinement method	Full matrix least squares on F^2
Data/ Restraints/parameter	1648 / 0 / 51
R1(*on* F_o^2, $I>2\sigma(I)$)	0.0263
wR2 (*on* F_o^2, $I> 2\sigma(I)$)	0.0598

[a] data based on the PLATON/SQUEEZE [50] model

7.3.3 Powder XRD and thermal Analysis

Bulk sample identification and confirmation of phase purity were determined using powder X-ray diffraction (XRD). Data within a range of $5° \leq 2\theta \leq 40°$ (step size: 0.02°, counting time: 1s/step) were collected using a Scintag Pad-X diffractometer equipped with Cu Kα (λ= 1.5405 Å) radiation. Comparison of the observed and calculated powder XRD for **7.**1 confirmed phase purity (Fig. 7.1)

A combined TGA-DSC experiment for compound [7.1] was performed using a Netzsch 449C Jupiter instrument. The sample was heated from room temperature to 750°C under a N_2 atmosphere with a heating rate of 5°C/minute. The thermal analyses of Li/Na-exchanged compound [7.1] were conducted in similar manner (Fig. 7.2)

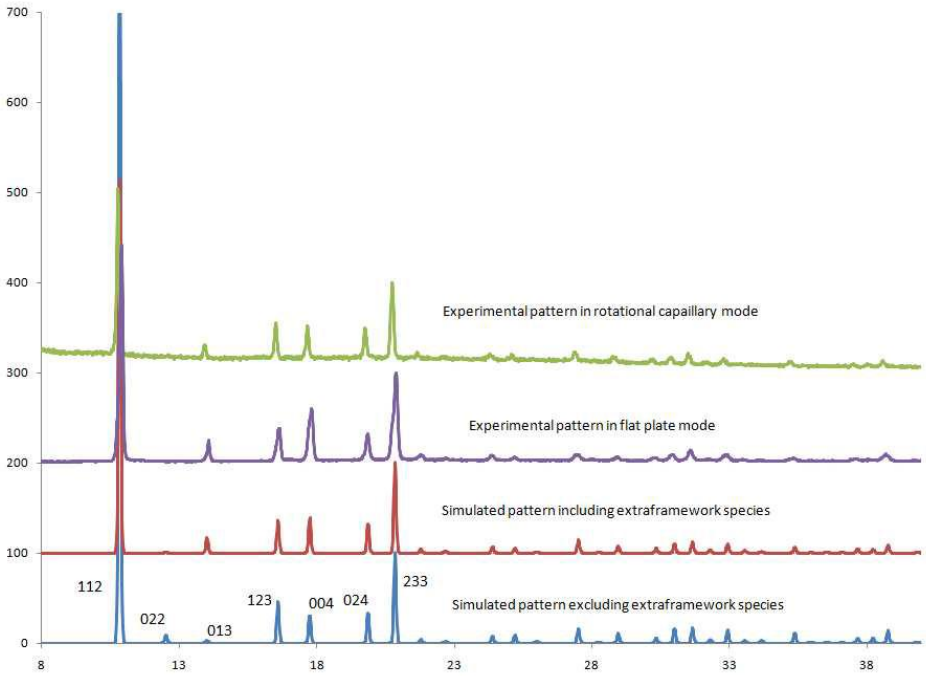

Figure 7.1. Simulated and experimental PXRD patterns of compound [7.1].

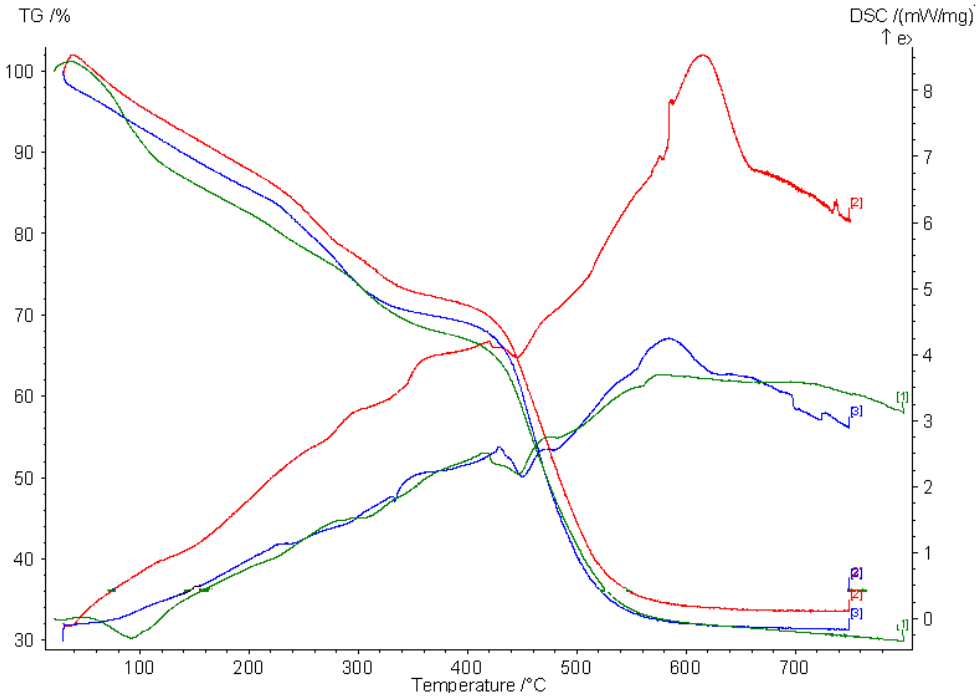

Figure 7.2. Combined TGA-DSC study of Li exchanged (red) and Na-exchanged (blue) and compound [7.1] (green)

7.3.4. Gas Sorption Measurements

All gas sorption experiments were performed on a volumetric gas sorption analyzer (Autosorb-1 MP, Quantachrome Instruments). Liquid nitrogen and liquid argon were used as coolant to achieve cryogenic temperatures (77 and 87K, respectively). The experiments were conducted using ultra high purity H_2, N_2 (99.999%) and CO_2 (99.998%). The N_2 sorption isotherms were collected using a pressure range of 10^{-6} to 1 atmosphere at 77K. The CO_2 sorption isotherm was performed at 273K, using a pressure range of 10^{-3} to 1 atmosphere. The H_2 sorption isotherms were carried out at 77K and 87K, respectively, with pressures ranging from 10^{-3} to 1 atm. The initial outgassing process for each sample was carried out at 448K overnight (under vacuum). An outgassed sample of 176 mg was used in the gas sorption measurements with the sample weight recorded before and after outgassing to confirm the removal of guest molecules. The outgassing procedure was repeated on the same sample between experiments for approximately 30 minutes to 1 hour. Pore properties (e.g. pore volume, pore size, and surface area) were analyzed using Autosorb v1.50 software (Fig. 7.3).

7.3.5. Ion Exchange Experiments

Saturated solutions of $LiNO_3$, $NaNO_3$ in DMF were separately added to the as-synthesized compound [7.1] (80-90 mg in each vial). The saturated salt solutions were decanted and replaced by fresh solution every 24 hours for 5 days. The ion exchanged samples were filtered and washed with DMF before being stored under fresh DMF for 3 days. At this time they were once again filtered and washed prior to being tested for their metal content using ICP techniques (Galbraith Laboratories Inc. Knoxville, TN, USA) (Fig. 7.4)

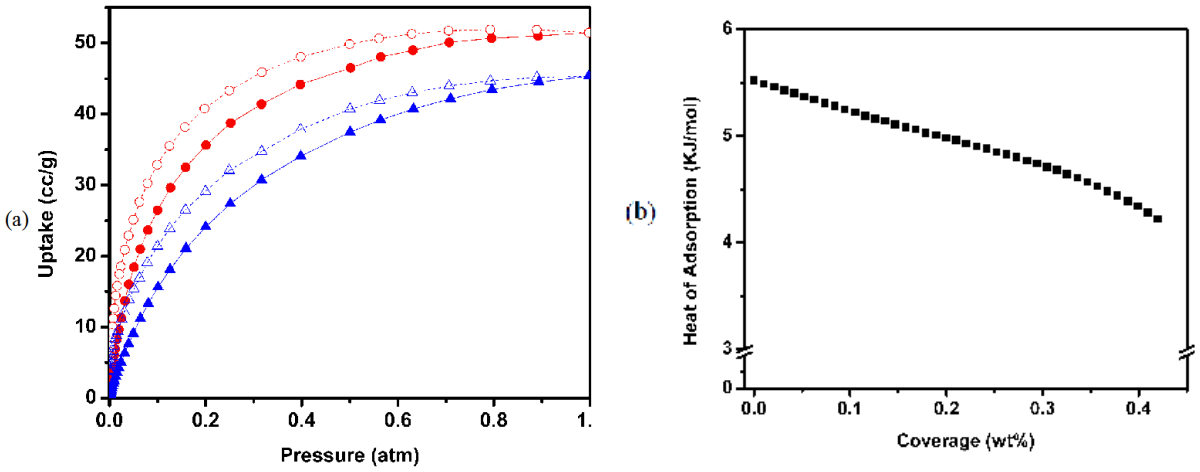

Figure 7.3. (a) Hydrogen isotherms at 77K (Red) and 87K (Blue). Adsorption and Desorption data are denoted as filled and open symbols, respectively. (b) Hydrogen Heats of Adsorption (Qst) calculated based on 77K and 87K isotherms using Virial method.

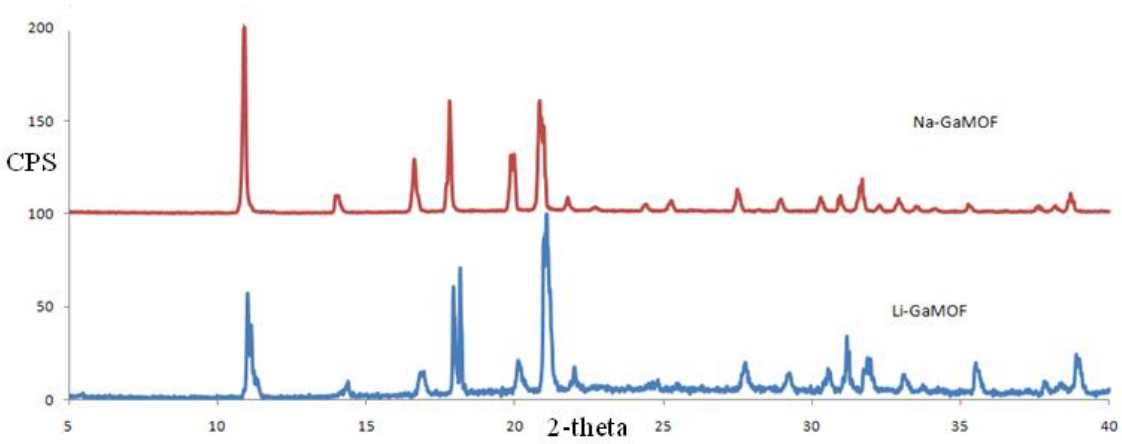

Figure 7.4. PXRD pattern of ion-exchanged compound [7.1] with alkali metal cations.

Table 7.2. The ICP-MS data for the Li and Na exchanged compound [7.1]

Sample Name	% Gallium	% Alkali Metal
Li exchanged [7.1]	12.2%	0.9195(Li)
Na-exchanged [7.1]	12.0%	1.86% (Na)

7.4. Results and Discussion

7.4.1 Structural Description of [7.1], $Ga_6(1,3,5\text{-}BTC)_8 \cdot 6DMA \cdot 3DMF \cdot 26H_2O$

Compound [7.1] consists of isolated gallium tetrahedra connected by the organic ligands forming an overall 3-D network (Fig. 7.5a). The asymmetric unit of compound [7.1] consists of one crystallographically independent gallium metal center (Ga1), and 1/3 of the organic linker including one carboxylate group (Fig. 7.5b). The gallium metal center is present in distorted tetrahedral coordination environment, with an average distance between the gallium center and the carboxylate oxygen atoms (O1 and its symmetry equivalent positions) of 1.832 Å. The tetrahedral coordination of gallium with carboxylate oxygen atoms is not common. A number of tetrahedrally coordinated GaO4 are reported in the case of open-framework gallium phosphates.[201,202] The coordination number of gallium(III) is strongly influenced by the symmetry, steric requirements, and mode of coordination of the linker. The nature of the solvent and structure-directing agent also plays a major role in the gallium coordination behavior. The bond valence sum of the gallium center is 3.03 v. u. (v. u. = valance unit), matching well with the expected value of +3.[109]

Each gallium center is connected with four organic linkers (BTC) through their carboxylate oxygen atom. Interestingly only one oxygen (O1) of each carboxylate group participates in a bonding interaction with the gallium metal center. The other oxygen center (O2) remains uncoordinated. The distance between carboxylate carbon (C1) and the two carboxylate oxygen atoms (O1, O2) are 1.310(2) and 1.201(3) Å respectively, confirming O2 remains uncoordinated. Each organic linker is bonded to three gallium centers through each of its carboxylate moieties. Each gallium center is thus connected with eight other gallium centers though four intervening organic linkers. The organic linkers function as the trigonal node, while

the gallium center is present as the tetrahedral node in the structure forming a C_3N_4 type (3,4)-connected framework. Compound [7.1] does not have straight channels, although a large void with at diameter of approximately 8 Å is present within the structure. PLATON calculates a solvent accessible volume of 5056.2 $Å^3$ per unit cell, equivalent to a pore volume ratio of 63.57% per unit cell. Disordered counter-ions and solvent molecules occupy the large void space.[138]

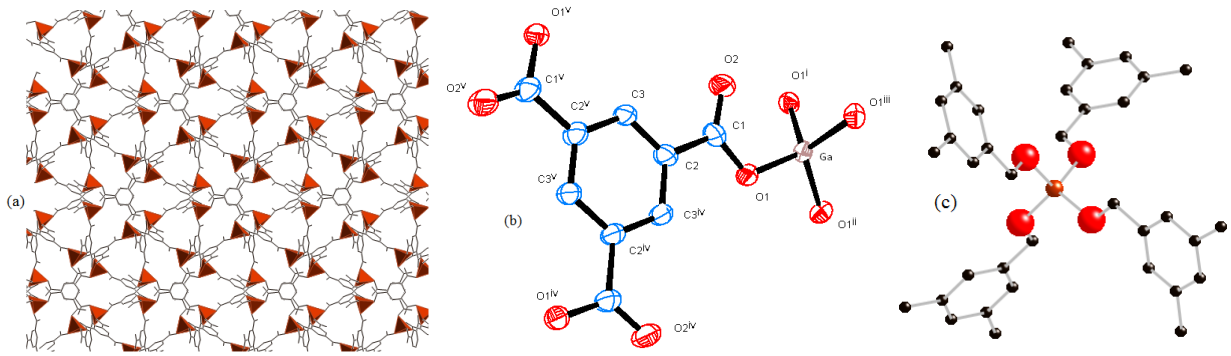

Figure.7.5. (a). View of compound [7.1] from [111] direction showing the connectivity of metal ion with the organic linkers. (b) Ellipsoidal plot of the asymmetric unit of compound [7.1]. Ellipsoids are shown at the 50% probability level. Hydrogen atoms have been omitted for clarity. Symmetry related atoms are shown to complete the coordination sphere of the gallium center and organic ligand. Symmetry operators: i (x, y, z), ii (-x+1/2, -y, z+1/2), iii (-x, y+1/2, -z+1/2), iv (x+1/2, -y+1/2, -z), v (z, x, y). (c) Local environment of gallium metal center in compound [7.1]

Table 7.3. Selected bond lengths and angles of compound [7.1].

Ga(1)-O(1)	1.8317(12)	O(1)#1-Ga(1)-O(1)	103.99(4)
Ga(1)-O(1)#1	1.8317(12)	O(1)-Ga(1)-O(1)#2	121.09(8)
Ga(1)-O(1)#2	1.8317(13)	O(1)#1-Ga(1)-O(1)#2	103.99(4)
Ga(1)-O(1)#3	1.8317(12)	O(1)#1-Ga(1)-O(1)#3	121.09(8)
C(1)-C(2)	1.496(2)	O(1)-C(1)-C(2)	114.13(17)
O(1)-C(1)	1.310(2)	C(3)-C(2)-C(1)	120.81(17)
O(2)-C(1)	1.201(3)	O(2)-C(1)-C(2)	123.01(18)

Symmetry codes: #1 y-1/4, -x+1/4, -z+7/4, #2 -x+0, -y+1/2, z+0, #3 -y+1/4, x+1/4, -z+7/4

7.4.2 Discussion

The microcrystalline nature and weak scattering from the sample makes single crystal XRD data collected on a laboratory based diffractometer unsuitable for the precise determination of even the framework structure of compound [7.1]. While high quality synchrotron XRD data collected at the APS does allow precise determination of structural parameters for the framework, characterization of the chemical nature of disordered extra-framework species could not be determined unambiguously from these data alone. The overall formula of compound [7.1] can be inferred by considering a combination of the empirical framework formula given in Table 7.1, the elemental analysis in section 7.2 and the analysis of the TGA-DSC results shown in Fig. 7.2. The TGA-DSC shows an almost continuous weight loss of 37.5 wt% up to 425°C. We assume this weight loss is due to disordered extra-framework species alone, which were not crystallographically identified. The TGA-DSC data thus indicates that the empirical framework formula weight of 345.87 g/mole, calculated based on the single crystal XRD, accounts for 62.5% of the empirical formula weight of compound [7.1]**.** The empirical formula weight of compound [7.1], including extra-framework species is calculated to be 553.392 g/mole. The weight percent of C, H, N within the empirical formula was calculated based on the elemental analysis value discussed in section 7.2. The number of formula units in the molecular formula of compound [7.1] is determined as 6, since this provides a chemically reasonable charge balanced formula. The possibility of charge balancing cations under the synthetic condition of compound [7.1] is limited to NH_4^+, H_3O^+ and protonated dimethyl amine (DMA), formed by decomposition of DMF at high temperature and in the presence of water. The possibility of NH_4^+ as a counter cation was ruled out in the calculation, as the synthesis of compound [7.1] can be achieved without the use of NH_4F in the starting reaction mixture. The higher weight percent of nitrogen

in the empirical formula derived from the experimental elemental analysis favors the possibility of the presence of positively charged DMA as an extra-framework species. Positively charged DMA probably formed due to the decomposition of DMF. On the basis of the above arguments solvent DMF and water molecules are assigned as the plausible extra-framework species in compound [7.1]. Although it was not possible to specifically determine the order of loss of chemical species during TGA-DSC measurement, due to the continuous nature of the weight loss, we believe the order to be water > DMF> protonated DMA primarily based on their size and charge. This step is followed by the decomposition of the framework between 425°C to 540°C. The end product is recovered as black poorly crystalline powder. No further characterization was done on this recovered material.

The properties of compound [7.1] were investigated using N_2, and H_2 adsorption isotherms. The BET and Langmuir surface areas were estimated based on N_2 adsorption isotherms measured at 77K. The sorption behavior reveals a Type I isotherm indicating a microporous material.[72] The BET surface area of compound [7.1] based on N_2 adsorption isotherm is 204.9m^2/g (Langmuir surface area: 236.2 m^2/g). The pore volume is calculated as 0.11cm^3/g using the HK method which uses the N_2 adsorption isotherm.

The hydrogen adsorption isotherms for compound [7.1] show an uptake of 0.47wt% and 0.41wt% of H_2 at 77K and 87K, respectively (Fig. 7.3a). The isosteric heats of H_2 adsorption for sample [7.1] are calculated by the Virial method to be between 4.2-5.5 KJ/mol in the loading range of 0 ~ 0.4wt% (Fig. 7.3b). It is worth noting that the activation of compound [7.1] is strongly dependent on the positively charged cation. The interaction between the positively charged amine cation with the negatively charged framework hinders complete removal of all extra-framework species. The attempts to remove the positively charged cations, by activating at

either a higher temperature or for a longer time, results in the loss of crystallinity of compound [7.1]. Therefore, the adsorption data were collected on samples, where the extra-framework counter ions were only partially evacuated from the pore.

The presence of the cationic species within the pore makes compound [7.1] a suitable candidate for ion exchange studies with alkali metal cations. Compound [7.1] undergoes partial ion exchange with alkali metal cations like Li^+ (Ga/Li: 13) and Na^+ (Ga/Na: 6.45) as evident by ICP studies (Table S7). The powder XRD pattern of ion exchanged materials reveals similar unit cell with respect to synthesized compound [7.1] (Fig. 3). The TGA-DSC curve of ion-exchange compound [7.1] showed similar thermal stability as the parent compound.

7.5. Conclusion

A three-dimensional gallium-based anionic framework was synthesized using solvothermal techniques. Compound [7.1] consists of isolated gallium tetrahedra and 1,3,5-BTC as nodes forming a 3,4-type network encompassing large pores, which contain solvent molecules and counter ions. Compound [7.1] shows a moderate H_2 storage capacity of ~ 0.5 wt% at 77 K and 1 atm. It also undergoes partial ion exchange with alkali-metal cations (lithium and sodium), as is evident by ICP-MS studies. Currently, we are exploring similar gallium-based frameworks using different solvothermal conditions.

Chapter 8

Conclusion

The aim of the project was to carry out exploratory syntheses of main group metal based coordination networks under solvothermal reaction conditions. Alkali and alkaline earth metal centers were used mainly to construct the extended networks, while trivalent gallium metal was used as a representative of p-block metal center to form porous networks. Networks of different topologies and properties were formed based on the synthetic conditions. The variation of synthesis temperature leads to variation of network dimensionality, with the general trend being that the dimensionality of the networks increases with increase in synthetic temperature. Solvents on the other hand, were found to exert a profound effect on the network topologies. The dimensionality and physical properties of the as-synthesized networks depends on the coordination behavior of the solvent molecules with the metal center. The presence of extra-framework solvent molecules can also influence the physical properties, by their degree of interaction with the network. The as-synthesized compounds were characterized using single crystal X-ray diffraction and thermal methods. The porosity of the activated materials was determined by conventional gas-adsorption methods.

The high charge density and low atomic weight of lithium make it, in principle, an ideal metal center for the construction of lightweight networks, tailored toward gas storage applications. Further, the choice of lithium as the charge carrier in many new generation batteries suggests lithium-carboxylate based networks may be more eco-friendly alternatives to other inorganic materials. A number of novel lithium based networks were synthesized under solvothermal conditions using aromatic polycarboxylate linkers - 2,6-NDC, 4,4'-BPDC and 4,4'-

SDB. The use of 2,6-NDC and 4,4'-BPDC leads to the formation of 3-D dense isostructural networks (ULMOF-1 and ULMOF-2), formed by antifluorite type LiO layers, connected by the organic linker moieties. On the other hand, network formed by V-shaped 4,4'-SDB linker, where the functional carboxylate groups are present at a mutual angle of 104°, forms tetrameric clusters of lithium tetrahedra, connected by the organic linkers. Clearly, the mutual orientation of the functional carboxylate groups plays the major role in determining the network topology. These networks (ULMOF-1-3, compounds [1.1] – [1.3]) exhibit exceptional thermal stability of over 500°C under N_2 atmosphere. In particular, ULMOF-1 (compound [1.1]) shows the highest thermal stability (~ 610°C) of all inorganic-organic hybrid material reported to date.

The chemistry of lithium based coordination networks were further explored using different structural isomers of pyridinedicarboxylates. A range of reaction conditions and various isomers (2,6-, 3,5-, 2,5-) of pyridinedicarboxylates were used to synthesize novel networks of diverse dimensionalities and properties. It was found that the mutual orientation of the carboxylate groups with respect to the pyridyl nitrogen largely controls the topologies of the networks so formed. The close proximity of carboxylate groups with the pyridyl nitrogen in the 2,6-isomer leads to the formation of layered networks with chelating carboxylate groups. While, in case of 3,5-, 2,5- isomers, formation of 3-D networks of different topologies were observed. The 2,5-isomer based network ULMOF-5 (compound [4.4]) is particularly interesting, as the coordination environment of the lithium metal centers undergoes rearrangement upon desolvation, as monitored by ^{6}Li solid state NMR. Further, the desolvated network reverts back to its original form upon exposure to the DMF solvent showing dynamic structural behavior. All the networks formed based on pyridinedicarboxylate linkers show moderate thermal stability under N_2 atmosphere.

The role of solvent in the formation of coordination networks was explored using the model system based on magnesium-3,5-PDC. A total of four coordination networks were formed based on the nature of solvents used when all other synthesis conditions were intentionally held constant. The dimensionality and the physical properties of the networks depend on the coordination environment of the magnesium metal center, which is largely controlled by the synthesis solvent. It was found that water has the highest affinity to coordinate with the magnesium metal center, followed by DMF, ethanol and methanol. Ethanol and methanol tend not to coordinate with the metal centers in presence of water and DMF.

The synthesis of alkaline-earth metal based coordination networks were further investigated using calcium as the metal center and 4,4'-SDB as the organic linker, forming the first example of robust, porous calcium based network. Upon removal of solvent water molecules from the channel, the as-synthesized network undergoes structural changes as a result of different stacking pattern of the aromatic rings in the activated state. The activated network shows a moderate H_2 uptake of ~0.6wt% at 77K and 1atm pressure. It shows a moderate CO_2 uptake of 4.75wt% at room temperature and 1 atm pressure. Further, the activated network shows remarkable (85 ×) CO_2/N_2 selectivity, crucially important for any post-combustion capture applications. The activated network is stable in air and under high relative humidity (> 85% RH) showing remarkable structural integrity, most probably due to the absence of open metal sites in the activated state.

The exploratory synthetic effort was extended to obtain novel gallium based porous network material. A 3-D anionic framework of (3,4)- topology was synthesized under solvothermal conditions using trimesic acid as the linker. Highly disordered solvent molecules and DMA cations were present within the void space, as confirmed by IR and elemental analysis

study. These positively charged ions can be exchanged with alkali metal ions, as evident by ICP-MS study. The activated framework shows a moderate 0.5wt% H_2 uptake at 77K and 1atm pressure, confirming permanent porosity after guest molecule removal.

Even though a number of reports claim the possibility of rational design of microporous solids, the synthesis of main group metal based coordination networks remains a difficult task, particularly because of the absence of pre-formed secondary building units under applied synthetic conditions. However, careful systematic studies using appropriate organic linkers and metal centers, in combination with *in-situ* techniques like time-resolved X-ray diffraction and theoretical studies can further help us understand and possibly design microporous networks with desirable properties.

References

(1) Cheetham, A. K.; Rao, C. N. R.; Feller, R. K. *Chem. Commun.* **2006**, 4780.

(2) Fromm, K. M. *Coord. Chem. Rev.* **2008**, *252*, 856.

(3) Murray, L. J.; Dinca, M.; Long, J. R. *Chem. Soc. Rev.* **2009**, *38*, 1294.

(4) Li, J. R.; Kuppler, R. J.; Zhou, H. C. *Chem. Soc. Rev.* **2009**, *38*, 1477.

(5) Ma, L. Q.; Abney, C.; Lin, W. B. *Chem. Soc. Rev.* **2009**, *38*, 1248.

(6) Allendorf, M. D.; Bauer, C. A.; Bhakta, R. K.; Houk, R. J. T. *Chem. Soc. Rev.* **2009**, *38*, 1330.

(7) James, S. L. *Chem. Soc. Rev.* **2003**, *32*, 276.

(8) Tranchemontagne, D. J.; Mendoza-Cortes, J. L.; O'Keeffe, M.; Yaghi, O. M. *Chem. Soc. Rev.* **2009**, *38*, 1257.

(9) Perry, J. J.; Perman, J. A.; Zaworotko, M. J. *Chem. Soc. Rev.* **2009**, *38*, 1400.

(10) Park, H.; Britten, J. F.; Mueller, U.; Lee, J.; Li, J.; Parise, J. B. *Chem. Mater.* **2007**, *19*, 1302.

(11) Lee, J. D. *Concise Inorganic Chemistry*; Fourth Edition ed.; Chapman & Hall: New York, 1991.

(12) Abrahams, B. F.; Grannas, M. J.; Hudson, T. A.; Robson, R. *Angew Chem.; Int Ed.* **2010**, *49*, 1087.

(13) Porter, W. W.; Wong-Foy, A.; Dailly, A.; Matzger, A. J. *J. Mat. Chem.* **2009**, *19*, 6489.

(14) Hausdorf, S.; Baitalow, F.; Bohle, T.; Rafaja, D.; Mertens, F. O. R. L. *J. Am. Chem. Soc.* **2010**, *132*, 10978.

(15) Serre, C.; Millange, F.; Surble, S.; Ferey, G. *Angew Chem.; Int Ed.* **2004**, *43*, 6286.

(16) Sumida, K.; Hill, M. R.; Horike, S.; Dailly, A.; Long, J. R. *J. Am. Chem. Soc.* **2009**, *131*, 15120.

(17) Dinca, M.; Long, J. R. *J. Am. Chem. Soc.* **2005**, *127*, 9376.

(18) Dietzel, P. D. C.; Blom, R.; Fjellvag, H. *Eur. J. Inorg. Chem.* **2008**, 3624.

(19) Caskey, S. R.; Wong-Foy, A. G.; Matzger, A. J. *J. Am. Chem. Soc.* **2008**, *130*, 10870.

(20) Sumida, K.; Brown, C. M.; Herm, Z. R.; Chavan, S.; Bordiga, S.; Long, J. R. *Chem. Commun.* **2011**, *47*, 1157.

(21) Wu, H.; Zhou, W.; Yildirim, T. *J. Am. Chem. Soc.* **2009**, *131*, 4995.

(22) Britt, D.; Furukawa, H.; Wang, B.; Glover, T. G.; Yaghi, O. M. *Proc. Natl. acad. sci. U. S. A.* **2009**, *106*, 20637.

(23) Mason, J. A.; Sumida, K.; Herm, Z. R.; Krishna, R.; Long, J. R. *Energy Environ. Sci.* **2011**, *4*, 3030.

(24) Kizzie, A. C.; Wong-Foy, A. G.; Matzger, A. J. *Langmuir* **2011**, *27*, 6368.

(25) Clegg, W.; Russo, L. *Cryst. Growth Des.* **2009**, *9*, 1158.

(26) Falcao, E. H. L.; Naraso; Feller, R. K.; Wu, G.; Wudl, F.; Cheetham, A. K. *Inorg. Chem.* **2008**, *47*, 8336.

(27) Appelhans, L. N.; Kosa, M.; Radha, A. V.; Simoncic, P.; Navrotsky, A.; Parrinello, M.; Cheetham, A. K. *J. Am. Chem. Soc.* **2009**, *131*, 15375.

(28) Kam, K. C.; Young, K. L. M.; Cheetham, A. K. *Cryst. Growth Des.* **2007**, *7*, 1522.

(29) Banerjee, D.; Kim, S. J.; Borkowski, L. A.; Xu, W. Q.; Parise, J. B. *Cryst. Growth Des.* **2010**, *10*, 709.

(30) Banerjee, D.; Kim, S. J.; Li, W.; Wu, H. H.; Li, J.; Borkowski, L. A.; Philips, B. L.; Parise, J. B. *Cryst. Growth Des.* **2010**, *10*, 2801.

(31) Banerjee, D.; Finkelstein, J.; Smirnov, A.; Forster, P. M.; Borkowski, L. A.; Teat, S. J.; Parise, J. B. *Cryst. Growth Des.* **2011**, *11*, 2572.

(32) Gurunatha, K. L.; Uemura, K.; Maji, T. K. *Inorg. Chem.* **2008**, *47*, 6578.

(33) Forster, P. M.; Burbank, A. R.; Livage, C.; Ferey, G.; Cheetham, A. K. *Chem. Commun.* **2004**, 368.

(34) Pan, L.; Frydel, T.; Sander, M. B.; Huang, X. Y.; Li, J. *Inorg. Chem.* **2001**, *40*, 1271.

(35) Zhang, J. P.; Ghosh, S. K.; Lin, J. B.; Kitagawa, S. *Inorg. Chem.* **2009**, *48*, 7970.

(36) Humphrey, S. M.; Mole, R. A.; Thompson, R. I.; Wood, P. T. *Inorg. Chem.* **2010**, *49*, 3441.

(37) Xie, L. H.; Lin, J. B.; Liu, X. M.; Wang, Y.; Zhang, W. X.; Zhang, J. P.; Chen, X. M. *Inorg. Chem.* **2010**, *49*, 1158.

(38) Zou, R. Q.; Zhong, R. Q.; Han, S. B.; Xu, H. W.; Burrell, A. K.; Henson, N.; Cape, J. L.; Hickmott, D. D.; Timofeeva, T. V.; Larson, T. E.; Zhao, Y. S. *J. Am. Chem. Soc.* **2010**, *132*, 17996.

(39) Thirumurugan, A.; Tan, J. C.; Cheetham, A. K. *Cryst. Growth Des.* **2010**, *10*, 1736.

(40) Wu, T.; Zhang, J.; Bu, X. H.; Feng, P. Y. *Chem. Mater.* **2009**, *21*, 3830.

(41) Zhang, H.; Wu, T.; Zhou, C.; Chen, S. M.; Feng, P. Y.; Bu, X. H. *Angew Chem.; Int Ed.* **2009**, *48*, 2542.

(42) Calderone, P. J.; Banerjee, D.; Borkowski, L. A.; Parise, J. B. *Inorg. Chem. Commun.* **2011**, *14*, 741.

(43) Zheng, S. T.; Li, Y. F.; Wu, T.; Nieto, R. A.; Feng, P. Y.; Bu, X. H. *Chem-Eur. J.* **2010**, *16*, 13035.

(44) Yang, S.; Lin, X.; Blake, A. J.; Thomas, K. M.; Hubberstey, P.; Champness, N. R.; Schroder, M. *Chem. Commun.* **2008**, 6108.

(45) Yang, S. H.; Lin, X.; Blake, A. J.; Walker, G. S.; Hubberstey, P.; Champness, N. R.; Schroder, M. *Nat. Chem.* **2009**, *1*, 487.

(46) Mulfort, K. L.; Hupp, J. T. *J. Am. Chem. Soc.* **2007**, *129*, 9604.

(47) Mulfort, K. L.; Hupp, J. T. *Inorg. Chem.* **2008**, *47*, 7936.

(48) Mulfort, K. L.; Wilson, T. M.; Wasielewski, M. R.; Hupp, J. T. *Langmuir* **2009**, *25*, 503.

(49) Baes, F. H. M., R.E. *The Hydrolysis of Cations*; John Wiley & Sons: New York, 1976.

(50) Nguyen, J. G.; Cohen, S. M. *J. Am. Chem. Soc.* **2010**, *132*, 4560.

(51) Ma, D. Y.; Li, Y. W.; Li, Z. *Chem. Commun.* **2011**, *47*, 7377.

(52) Pan, L.; Parker, B.; Huang, X. Y.; Olson, D. H.; Lee, J.; Li, J. *J. Am. Chem. Soc.* **2006**, *128*, 4180.

(53) Yoo, Y.; Varela-Guerrero, V.; Jeong, H. K. *Langmuir* **2011**, *27*, 2652.

(54) Imaz, I.; Rubio-Martinez, M.; An, J.; Sole-Font, I.; Rosi, N. L.; Maspoch, D. *Chem. Commun.* **2011**, *47*, 7287.

(55) Smaldone, R. A.; Forgan, R. S.; Furukawa, H.; Gassensmith, J. J.; Slawin, A. M. Z.; Yaghi, O. M.; Stoddart, J. F. *Angew Chem.; Int Ed.* **2010**, *49*, 8630.

(56) Banerjee, D.; Parise, J. B. *Cryst. Growth Des.* **2011**, *11*, 4704.

(57) Forster, P. M.; Thomas, P. M.; Cheetham, A. K. *Chem. Mater.* **2002**, *14*, 17.

(58) Banerjee, D.; Kim, S. J.; Parise, J. B. *Cryst. Growth Des.* **2009**, *9*, 2500.

(59) Cooper, E. R.; Andrews, C. D.; Wheatley, P. S.; Webb, P. B.; Wormald, P.; Morris, R. E. *Nature* **2004**, *430*, 1012.

(60) Parnham, E. R.; Morris, R. E. *Acc. Chem. Res.* **2007**, *40*, 1005.

(61) Morris, R. E. *Chem. Commun.* **2009**, 2990.

(62) Ma, Z.; Yu, J. H.; Dai, S. *Adv. Mat.* **2010**, *22*, 261.

(63) Torimoto, T.; Tsuda, T.; Okazaki, K.; Kuwabata, S. *Adv. Mat.* **2010**, *22*, 1196.

(64) Cheetham, A. K.; Forster, P. M.; Burbank, A. R.; Livage, C.; Ferey, G. *Chem. Commun.* **2004**, 368.

(65) *SMART 5.6, Bruker-AXS: Madison, WI* **2001**.

(66) *SAINT 5.1; Bruker-AXS: Madison, WI* **2000**.

(67) Sheldrick, G. M. *Acta Crystallogr. A.* **2008**, *64*, 112.

(68) *CrysAlis PRO. Verion 4.Oxford Diffraction Ltd. Yarnton, Oxfordshire, England* **2010**.

(69) *Apex II, v2009.3-0; Bruker AXS. Inc.: Madison, WI, 2009.*

(70) lowell, S. Ed. *Charecterization of Porous Solids and Powders : Surface Area, Pore Size and Density*; Kluwer Academic Publishers: Dordrecht, The Netherlands, 2004.

(71) Brunauer, S.; Emmett, P. H.; Teller, E. *J. Am. Chem. Soc.* **1938**, *60*, 309.

(72) Sing, K. S. W.; Everett, D. H.; Haul, R. A. W.; Moscou, L.; Pierotti, R. A.; Rouquerol, J.; Siemieniewska, T. *Pure Appl. Chem.* **1985**, *57*, 603.

(73) Eddaoudi, M.; Kim, J.; Rosi, N.; Vodak, D.; Wachter, J.; O'Keeffe, M.; Yaghi, O. M. *Science* **2002**, *295*, 469.

(74) Rowsell, J. L. C.; Yaghi, O. M. *Micorpor. Mesopor. Mat.* **2004**, *73*, 3.

(75) Han, S. S.; Furukawa, H.; Yaghi, O. M.; Goddard, W. A. *J. Am. Chem. Soc.* **2008**, *130*, 11580.

(76) Millward, A. R.; Yaghi, O. M. *J. Am. Chem. Soc.* **2005**, *127*, 17998.

(77) Sun, D. F.; Ma, S. Q.; Ke, Y. X.; Collins, D. J.; Zhou, H. C. *J. Am. Chem. Soc.* **2006**, *128*, 3896.

(78) Ma, S. Q.; Zhou, H. C. *J. Am. Chem. Soc.* **2006**, *128*, 11734.

(79) Dinca, M.; Dailly, A.; Liu, Y.; Brown, C. M.; Neumann, D. A.; Long, J. R. *J. Am. Chem. Soc.* **2006**, *128*, 16876.

(80) Dinca, M.; Yu, A. F.; Long, J. R. *J. Am. Chem. Soc.* **2006**, *128*, 8904.

(81) Rosi, N. L.; Eckert, J.; Eddaoudi, M.; Vodak, D. T.; Kim, J.; O'Keeffe, M.; Yaghi, O. M. *Science* **2003**, *300*, 1127.

(82) Rowsell, J. L. C.; Millward, A. R.; Park, K. S.; Yaghi, O. M. *J. Am. Chem. Soc.* **2004**, *126*, 5666.

(83) Rood, J. A.; Noll, B. C.; Henderson, K. W. *Inorg. Chem.* **2006**, *45*, 5521.

(84) Lee, J. Y.; Pan, L.; Kelly, S. R.; Jagiello, J.; Emge, T. J.; Li, J. *Adv. Mat.* **2005**, *17*, 2703.

(85) Lin, Z. Z.; Jiang, F. L.; Yuan, D. Q.; Chen, L.; Zhou, Y. F.; Hong, M. C. *Eur. J. Inorg. Chem.* **2005**, 1927.

(86) Fan, J.; Gan, L.; Kawaguchi, H.; Sun, W. Y.; Yu, K. B.; Tang, W. X. *Chem-Eur. J.* **2003**, *9*, 3965.

(87) Maji, T. K.; Matsuda, R.; Kitagawa, S. *Nat. Mat.* **2007**, *6*, 142.

(88) Wu, C. D.; Hu, A.; Zhang, L.; Lin, W. B. *J. Am. Chem. Soc.* **2005**, *127*, 8940.

(89) Lin, W. B. *J. Solid State Chem.* **2005**, *178*, 2486.

(90) Fujita, M.; Kwon, Y. J.; Washizu, S.; Ogura, K. *J. Am. Chem. Soc.* **1994**, *116*, 1151.

(91) Seo, J. S.; Whang, D.; Lee, H.; Jun, S. I.; Oh, J.; Jeon, Y. J.; Kim, K. *Nature* **2000**, *404*, 982.

(92) Bradshaw, D.; Prior, T. J.; Cussen, E. J.; Claridge, J. B.; Rosseinsky, M. J. *J. Am. Chem. Soc.* **2004**, *126*, 6106.

(93) Kepert, C. J.; Prior, T. J.; Rosseinsky, M. J. *J. Am. Chem. Soc.* **2000**, *122*, 5158.

(94) Senkovska, I.; Kaskel, S. *Eur. J. Inorg. Chem.* **2006**, 4564.

(95) Park, H.; Moureau, D. M.; Parise, J. B. *Chem. Mater.* **2006**, *18*, 525.

(96) Pan, L.; Finkel, B. S.; Huang, X. Y.; Li, J. *Chem. Commun.* **2001**, 105.

(97) Wang, Y. H.; Bredenkotter, B.; Rieger, B.; Volkmer, D. *Dalton Trans.* **2007**, 689.

(98) Ma, L.; Lin, W. *J Am. Chem. Soc* **2008**, *130*, 13834.

(99) Volkringer, C.; Loiseau, T.; Marrot, J.; Ferey, G. *Crystengcomm* **2009**, *11*, 58.

(100) Davies, R. P.; Less, R. J.; Lickiss, P. D.; White, A. J. P. *Dalton Trans.* **2007**, 2528.

(101) Liu, X.; Guo, G. C.; Liu, B.; Chen, W. T.; Huang, J. S. *Cryst. Growth Des.* **2005**, *5*, 841.

(102) Liu, X.; Guo, G. C.; Wu, A. Q.; Huang, J. S. *Inorg. Chem. Commun.* **2004**, *7*, 1261.

(103) Blomqvist, A.; Araujo, C. M.; Srepusharawoot, P.; Ahuja, R. *Proc. Natl. acad. sci. U. S. A* **2007**, *104*, 20173.

(104) Dalach, P.; Frost, H.; Snurr, R. Q.; Ellis, D. E. *J. Phys. Chem. C.* **2008**, *112*, 9278.

(105) Mavrandonakis, A.; Tylianakis, E.; Stubos, A. K.; Froudakis, G. E. *J. Phys. Chem. C.* **2008**, *112*, 7290.

(106) Klontzas, E.; Mavrandonakis, A.; Tylianakis, E.; Froudakis, G. E. *Nano Lett.* **2008**, *8*, 1572.

(107) Kolmann, S. J.; Chan, B.; Jordan, M. J. T. *Chem. Phys. Lett.* **2008**, *467*, 126.

(108) Sheldrick, G. M.; TWINABS, Bruker AXS: Madison WI: 2008.

(109) Brese, N. E.; O'Keeffe, M. *Acta Cryst. Sec B.* **1991**, *47*, 192.

(110) Zhuang, W. J.; Jin, L. P. *Appl. Organomet. Chem.* **2007**, *21*, 76.

(111) Zhuang, W. J.; Sun, C. Y.; Jin, L. P. *Polyhedron* **2007**, *26*, 1123.

(112) Wang, X. S.; Ma, S. Q.; Sun, D. F.; Parkin, S.; Zhou, H. C. *J. Am. Chem. Soc.* **2006**, *128*, 16474.

(113) Cote, A. P.; Benin, A. I.; Ockwig, N. W.; O'Keeffe, M.; Matzger, A. J.; Yaghi, O. M. *Science* **2005**, *310*, 1166.

(114) Cote, A. P.; El-Kaderi, H. M.; Furukawa, H.; Hunt, J. R.; Yaghi, O. M. *J. Am. Chem. Soc.* **2007**, *129*, 12914.

(115) Jia, J. H.; Lin, X.; Blake, A. J.; Champness, N. R.; Hubberstey, P.; Shao, L. M.; Walker, G.; Wilson, C.; Schroder, M. *Inorg. Chem.* **2006**, *45*, 8838.

(116) Ghosh, S. K.; Bharadwaj, P. K. *Inorg. Chem.* **2005**, *44*, 3156.

(117) Frisch, M.; Cahill, C. L. *Dalton Trans.* **2006**, 4679.

(118) Ghosh, S. K.; Bharadwaj, P. K. *Inorg. Chem.* **2004**, *43*, 2293.

(119) Banerjee, D.; Borkowski, L. A.; Kim, S. J.; Parise, J. B. *Cryst. Growth Des.* **2009**, *9*, 4922.

(120) Banerjee, D.; Kim, S. J.; Parise, J. B. *Cryst. Growth Des.* **2009**, *9*, 2500.

(121) Lin, X.; Telepeni, I.; Blake, A. J.; Dailly, A.; Brown, C. M.; Simmons, J. M.; Zoppi, M.; Walker, G. S.; Thomas, K. M.; Mays, T. J.; Hubberstey, P.; Champness, N. R.; Schroder, M. *J. Am. Chem. Soc.* **2009**, *131*, 2159.

(122) Vaidhyanathan, R.; Iremonger, S. S.; Dawson, K. W.; Shimizu, G. K. H. *Chem. Commun.* **2009**, 5230.

(123) Ingleson, M. J.; Barrio, J. P.; Bacsa, J.; Dickinson, C.; Park, H.; Rosseinsky, M. J. *Chem. Commun.* **2008**, 1287.

(124) Yamada, T.; Sadakiyo, M.; Kitagawa, H. *J. Am. Chem. Soc.* **2009**, *131*, 3144.

(125) Sadakiyo, M.; Yamada, T.; Kitagawa, H. *J. Am. Chem. Soc.* **2009**, *131*, 9906.

(126) Park, H.; Krigsfeld, G.; Parise, J. B. *Cryst. Growth Des.* **2007**, *7*, 736.

(127) Volkringer, C.; Loiseau, T.; Ferey, G.; Warren, J. E.; Wragg, D. S.; Morris, R. E. *Solid State Sci.* **2007**, *9*, 455.

(128) Mallick, A.; Saha, S.; Pachfule, P.; Roy, S.; Banerjee, R. *J. Mat. Chem.* **2010**, *20*, 9073.

(129) Moulton, B.; Zaworotko, M. J. *Chem. Rev.* **2001**, *101*, 1629.

(130) Chen, S. C.; Zhang, Z. H.; Huang, K. L.; Chen, Q.; He, M. Y.; Cui, A. J.; Li, C.; Liu, Q.; Du, M. *Cryst. Growth Des.* **2008**, *8*, 3437.

(131) Huang, X. C.; Li, D.; Chen, X. M. *Crystengcomm* **2006**, *8*, 351.

(132) Pedireddi, V. R.; Varughese, S. *Inorg. Chem.* **2004**, *43*, 450.

(133) Wang, F. K.; Yang, S. Y.; Huang, R. B.; Zheng, L. S.; Batten, S. R. *Crystengcomm* **2008**, *10*, 1211.

(134) Ma, L. F.; Wang, L. Y.; Lu, D. H.; Batten, S. R.; Wang, J. G. *Cryst. Growth Des.* **2009**, *9*, 1741.

(135) Ghosh, S. K.; Kitagawa, S. *Crystengcomm* **2008**, *10*, 1739.

(136) Wang, Z. Q.; Kravtsov, V. C.; Zaworotko, M. J. *Angew Chem.; Int Ed.* **2005**, *44*, 2877.

(137) Sheldrick, G. M. *CELL_NOW*; Bruker AXS: Madison, WI., 2008.

(138) Spek, A. L. *J. Appl. Crystallogr.* **2003**, *36*, 7.

(139) Sumida, K.; Rogow, D. L.; Mason, J. A.; McDonald, T. M.; Bloch, E. D.; Herm, Z. R.; Bae, T.-H.; Long, J. R. *Chem. Rev.* **2011**.

(140) Saha, D.; Bao, Z. B.; Jia, F.; Deng, S. G. *Environ. Sci. Technol.* **2010**, *44*, 1820.

(141) White, J. C.; Dutta, P. K.; Shqau, K.; Verweij, H. *Langmuir* **2010**, *26*, 10287.

(142) Liu, Q. L.; Mace, A.; Bacsik, Z.; Sun, J. L.; Laaksonen, A.; Hedin, N. *Chem. Commun.* **2010**, *46*, 4502.

(143) Ho, M. T.; Allinson, G. W.; Wiley, D. E. *Ind. Eng. Chem. Res.* **2008**, *47*, 1562.

(144) Caro, J.; Noack, M.; Kolsch, P.; Schafer, R. *Micorpor. Mesopor. Mat.* **2000**, *38*, 3.

(145) Breck, D. W. *Zeolite molecular sieves : structure, chemistry, and use*; R.E. Krieger: Malabar, Fla., 1984.

(146) Barrer, R. M. *Zeolite and Clay Minerals as Sorbents and Molecular Sieves*; 1st ed.; Academic Press: London, 1978.

(147) Long, J. R.; Yaghi, O. M. *Chem. Soc. Rev.* **2009**, *38*, 1213.

(148) Suh, M. P.; Park, H. J.; Prasad, T. K.; Lim, D.-W. *Chem. Rev.* **2012,** 112, 782.

(149) Wu, H.; Gong, Q.; Olson, D. H.; Li, J. *Chem. Rev.* **2012**, 112, 836.

(150) Li, J.-R.; Sculley, J.; Zhou, H.-C. *Chem. Rev.* **2012,** 112, 869.

(151) Yoon, M.; Srirambalaji, R.; Kim, K. *Chem. Rev.* **2012,** 112, 1196.

(152) Volkringer, C.; Marrot, J.; Ferey, G.; Loiseau, T. *Cryst. Growth Des.* **2008**, *8*, 685.

(153) Miller, S. R.; Horcajada, P.; Serre, C. *Crystengcomm* **2011**, *13*, 1894.

(154) Platero-Prats, A. E.; de la Pena-O'Shea, V. A.; Snejko, N.; Monge, A.; Gutierrez-Puebla, E. *Chem-Eur. J.* **2010**, *16*, 11632.

(155) Liang, P. C.; Liu, H. K.; Yeh, C. T.; Lin, C. H.; Zima, V. *Cryst. Growth Des.* **2011**, *11*, 699.

(156) Rowsell, J. L. C.; Yaghi, O. M. *J. Am. Chem. Soc.* **2006**, *128*, 1304.

(157) Zhou, W.; Wu, H.; Hartman, M. R.; Yildirim, T. *J. Phys. Chem. C.* **2007**, *111*, 16131.

(158) Ma, S. Q.; Eckert, J.; Forster, P. M.; Yoon, J. W.; Hwang, Y. K.; Chang, J. S.; Collier, C. D.; Parise, J. B.; Zhou, H. C. *J. Am. Chem. Soc.* **2008**, *130*, 15896.

(159) Wang, Q. M.; Shen, D. M.; Bulow, M.; Lau, M. L.; Deng, S. G.; Fitch, F. R.; Lemcoff, N. O.; Semanscin, J. *Micorpor. Mesopor. Mat.* **2002**, *55*, 217.

(160) Myers, A. L.; Prausnitz, J. M. *AIChE J.* **1965**, *11*, 121.

(161) Babarao, R.; Hu, Z.; Jiang, J.; Chempath, S.; Sandler, S. I. *Langmuir* **2006**, *23*, 659.

(162) Krishna, R.; Baur, R. *Sep. Purifi. Tech.* **2003**, *33*, 213.

(163) Goj, A.; Sholl, D. S.; Akten, E. D.; Kohen, D. *J. Phys. Chem. B.* **2002**, *106*, 8367.

(164) Challa, S. R.; Sholl, D. S.; Johnson, J. K. *J. Chem. Phys.* **2002**, *116*, 814.

(165) Peng, J.; Ban, H.; Zhang, X.; Song, L.; Sun, Z. *Chem. Phys. Lett.* **2005**, *401*, 94.

(166) Babarao, R.; Jiang, J.; Sandler, S. I. *Langmuir* **2009**, *25*, 5239.

(167) Bae, Y.-S.; Mulfort, K. L.; Frost, H.; Ryan, P.; Punnathanam, S.; Broadbelt, L. J.; Hupp, J. T.; Snurr, R. Q. *Langmuir* **2008**, *24*, 8592.

(168) Bae, Y.-S.; Farha, O. K.; Spokoyny, A. M.; Mirkin, C. A.; Hupp, J. T.; Snurr, R. Q. *Chem. Commun.* **2008**, 4135.

(169) Bae, Y.-S.; Farha, O. K.; Hupp, J. T.; Snurr, R. Q. *J. Mat. Chem.* **2009**, *19*, 2131.

(170) Li, B.; Zhang, Z.; Li, Y.; Yao, K.; Zhu, Y.; Deng, Z.; Yang, F.; Zhou, X.; Li, G.; Wu, H.; Nijem, N.; Chabal, Y. J.; Lai, Z.; Han, Y.; Shi, Z.; Feng, S.; Li, J. *Angew Chem.; Int Ed***, 2012,** 51, 1412.

(171) Krishna, R.; van Baten, J. M. *Phys. Chem. Chem. Phys.* **2011**, *13*, 10593.

(172) Yang, Q.; Zhong, C. *J. Phys. Chem. B.* **2006**, *110*, 17776.

(173) Dietzel, P. D. C.; Besikiotis, V.; Blom, R. *J. Mat. Chem.* **2009**, *19*, 7362.

(174) Yang, Q.; Xue, C.; Zhong, C.; Chen, J.-F. *AIChE J.* **2007**, *53*, 2832.

(175) Belmabkhout, Y.; Sayari, A. *Chem. Eng. Sci.* **2009**, *64*, 3729.

(176) Liu, B.; Smit, B. *Langmuir* **2009**, *25*, 5918.

(177) Dreisbach, F.; Staudt, R.; Keller, J. U. *Adsorpt.-J. Int. Adsorpt. Soc.* **1999**, *5*, 215.

(178) Janiak, C. *Dalton Trans.* **2003**, 2781.

(179) Lu, W. G.; Jiang, L.; Feng, X. L.; Lu, T. B. *Inorg. Chem.* **2009**, *48*, 6997.

(180) Fang, Q. R.; Zhu, G. S.; Xue, M.; Sun, J. Y.; Sun, F. X.; Qiu, S. L. *Inorg. Chem.* **2006**, *45*, 3582.

(181) Lan, A. J.; Li, K. H.; Wu, H. H.; Olson, D. H.; Emge, T. J.; Ki, W.; Hong, M. C.; Li, J. *Angew Chem Int Ed.* **2009**, *48*, 2334.

(182) de Lill, D. T.; Cahill, C. L. *Chem. Commun.* **2006**, 4946.

(183) Guo, X. D.; Zhu, G. S.; Li, Z. Y.; Sun, F. X.; Yang, Z. H.; Qiu, S. L. *Chem. Commun.* **2006**, 3172.

(184) Loiseau, T.; Lecroq, L.; Volkringer, C.; Marrot, J.; Ferey, G.; Haouas, M.; Taulelle, F.; Bourrelly, S.; Llewellyn, P. L.; Latroche, M. *J. Am. Chem. Soc.* **2006**, *128*, 10223.

(185) Loiseau, T.; Serre, C.; Huguenard, C.; Fink, G.; Taulelle, F.; Henry, M.; Bataille, T.; Ferey, G. *Chem-Eur. J.* **2004**, *10*, 1373.

(186) Volkringer, C.; Popov, D.; Loiseau, T.; Guillou, N.; Ferey, G.; Haouas, M.; Taulelle, F.; Mellot-Draznieks, C.; Burghammer, M.; Riekel, C. *Nat. Mat.* **2007**, *6*, 760.

(187) Comotti, A.; Bracco, S.; Sozzani, P.; Horike, S.; Matsuda, R.; Chen, J.; Takata, M.; Kubota, Y.; Kitagawa, S. *J. Am. Chem. Soc.* **2008**, *130*, 13664.

(188) Volkringer, C.; Loiseau, T.; Guillou, N.; Ferey, G.; Haouas, M.; Taulelle, F.; Audebrand, N.; Margiolaki, I.; Popov, D.; Burghammer, M.; Riekel, C. *Cryst. Growth Des.* **2009**, *9*, 2927.

(189) Volkringer, C.; Loiseau, T.; Ferey, G.; Morais, C. M.; Taulelle, F.; Montouillout, V.; Massiot, D. *Micorpor. Mesopor. Mat.* **2007**, *105*, 111.

(190) Volkringer, C.; Loiseau, T.; Guillou, N.; Ferey, G.; Elkaim, E.; Vimont, A. *Dalton Transactions* **2009**, 2241.

(191) Volkringer, C.; Meddouri, M.; Loiseau, T.; Guillou, N.; Marrot, J.; Ferey, G.; Haouas, M.; Taulelle, F.; Audebrand, N.; Latroche, M. *Inorg. Chem.* **2008**, *47*, 11892.

(192) Vougo-Zanda, M.; Huang, J.; Anokhina, E.; Wang, X. Q.; Jacobson, A. J. *Inorg. Chem.* **2008**, *47*, 11535.

(193) Mensinger, Z. L.; Zakharov, L. N.; Johnson, D. W. *Inorg. Chem.* **2009**, *48*, 3505.

(194) Loiseau, T.; Muguerra, H.; Haouas, M.; Taulelle, F.; Ferey, G. *Solid State Sci.* **2005**, *7*, 603.

(195) Chaplais, G.; Simon-Masseron, A.; Porcher, F.; Lecomte, C.; Bazer-Bachi, D.; Bats, N.; Patarina, J. *Phys. Chem. Chem. Phys.* **2009**, *11*, 5241.

(196) Lin, Z. Z.; Jiang, F. L.; Chen, L.; Yue, C. Y.; Yuan, D. Q.; Lan, A. J.; Hong, M. C. *Cryst. Growth Des.* **2007**, *7*, 1712.

(197) Chen, S. M.; Zhang, J.; Wu, T.; Feng, P. Y.; Bu, X. H. *J. Am. Chem. Soc.* **2009**, *131*, 16027.

(198) Volkringer, C.; Loiseau, T. *Mater. Res. Bull.* **2006**, *41*, 948.

(199) Breck, D. W. *Zeolite Molecular Sieves: Structure, Chemistry and Use*; Krieger Publishing Company: Malabar, Florida, 1984.

(200) Yaghi, O. M. *Nat. Mat.* **2007**, *6*, 92.

(201) Estermann, M.; Mccusker, L. B.; Baerlocher, C.; Merrouche, A.; Kessler, H. *Nature* **1991**, *352*, 320.

(202) Stalder, S. M.; Wilkinson, A. P. *Chem. Mater.* **1997**, *9*, 2168.